University of California
Santa Barbara

Compactifying Real Polynomials via Non-Crossing Combinatorics

A dissertation submitted in partial satisfaction
of the requirements for the degree

Doctor of Philosophy
in
Mathematics

by

Sam Sehayek

Committee in charge:

Professor Jon McCammond, Chair
Professor Stephen Bigelow
Professor Daryl Cooper
Professor Fedya Manin

September 2024

The Dissertation of Sam Sehayek is approved.

Professor Stephen Bigelow

Professor Daryl Cooper

Professor Fedya Manin

Professor Jon McCammond, Committee Chair

June 2024

Compactifying Real Polynomials via Non-Crossing Combinatorics

by

Sam Sehayek

Dedicated to my mother who always encouraged me and my grandmother who always expected excellence.

Acknowledgements

Earning my doctorate was a very challenging task and I would like to acknowledge those in my professional and personal life that have aided me in this endeavor. Firstly, to my advisor Jon McCammond, thanks for your care and attention to my work. I feel very lucky to have such a supportive mentor. Also, thanks to the rest of my committee: Stephen Bigelow, Daryl Cooper, and Fedya Manin. Almost everything I know about topology was learned in your classes, and I greatly appreciate your notes and feedback on this dissertation. In addition, I would like to acknowledge some of the other professors at this and other institutions that have helped train, advise, and mentor me to this point, including Pamela Harris, Dustin Ross, Matthias Beck, Ken Goodearl, Katy Craig, Peter Garfield, Gordon Kirby, Susanna Fishel, and Kim Seashore. The UC Santa Barbara Mathematics Department staff also deserve acknowledgment, especially Medina Price, Rachel Zaragoza, and David Brodbeck, for helping me whenever I needed tech support, administrative support, or any help navigating graduate school. I will not forget the friends I made in academia who have been instrumental in getting me to this stage: Greg McGrath, Elizabeth Crow, Alan Raydan, Andrés Vindas Meléndez, Timmy Chan, Jennifer Elder, Carlos Martínez Mori, and many others. Finally, I would not be where I am without my family's love and support, especially from my mom and sister.

Curriculum Vitæ

Sam Sehayek

Education

2024	Ph.D. in Mathematics, University of California, Santa Barbara.
2018	M.A. in Mathematics, San Francisco State University.
2014	B.S. in Mathematics, minor in Philosophy, University of California, Davis.

Publications

Unit-Interval Parking Functions and the Permutohedron
Joint with L. Chavez-Meyles, P.E. Harris, G. Kirby, R. Jordaan, E. Spingarn
To appear in Journal of Combinatorics

Abstract

Compactifying Real Polynomials via Non-Crossing Combinatorics

by

Sam Sehayek

The space of monic polynomials of degree d with distinct roots is a well-known classifying space for the braid group on d strands. Recently, Dougherty and McCammond have defined a compactification of this space using the Lyashko-Looijenga map, giving it a piece-wise Euclidean cell structure indexed by pairs of non-crossing partitions. The compactified space retracts onto another well-known classifying space of the braid group. Both the compactification and its spine are conjectured to be CAT(0).

In this dissertation, I investigate the subspaces and subcomplexes that result when attention is restricted to real polynomials. These subspaces have multiple components with well-known fundamental groups and I explicitly describe the corresponding subcomplexes for small values of d. The non-crossing partitions used to index the cells in the complexes for real polynomials belong two specific classes of non-crossing partition chains: reflection symmetric chains and palindromic chains. Although reflection symmetric non-crossing partitions have previously been defined, the streamlined techniques introduced here clarify many aspects of their structure. Palindromic non-crossing partition chains are defined here for the first time.

Contents

Chapter 1

Introduction

The space of monic polynomials of degree d with distinct roots is a well-known classifying space for the braid group on d strands. Recent work of Dougherty and McCammond compactifies the space of monic polynomials using the Lyashko-Looijenga map and gives it a piece-wise Euclidean cell structure indexed by compatible pairs of non-crossing partitions. The compactified space, which they call the Branched Rectangle Complex, can be given face identifications to form what they call the Branched Annulus Complex, which in turn retracts onto a spine which is another well-known classifying space of the braid group called the Dual Braid Complex. Both the Branched Rectangle Complex and the Dual Braid Complex are conjectured to be CAT(0). The goal of this dissertation is to understand the portions of both the Branched Rectangle Complex and the Branched Annulus Complex that come from a restriction to polynomials with real coefficients.

In Part I, we lay out all of the relevant work needed to understand this process to compactify monic complex polynomials culminating in Chapters 6 and 7 where we lay out the outline of this research program initiated by Michael Dougherty and Jon McCammond in [10, 11]. The part begins in Chapter 2 with a brief discussion about the braid groups and classifying spaces. In Chapters 3 and 4, we highlight examples of classifying spaces

and their constructions: Configuration spaces and complex polynomials, and the Salvetti complex, respectively.

In Chapter 5, we illuminate the work done by Brady and McCammond in [7], who designed a well-behaved metric on the cell complex associated to the dual presentation of the braid group introduced in [4], called the Dual Braid Complex. That construction relies heavily on the combinatorics of non-crossing partitions, which are featured throughout this dissertation.

In Part II, we turn our attention from complex polynomials to those that are fixed by the action of complex conjugation: the real polynomials. In Chapter 8, we investigate the specialized non-crossing combinatorics that appear for these polynomials. The non-crossing partitions used to index the cells in the complexes for monic real polynomials belong to two specific classes of non-crossing partition chains: reflection symmetric and palindromic non-crossing partition chains—an investigation into their combinatorial features makes up the content of Chapter 8. Although reflection symmetric non-crossing partitions have previously been defined in [9], the streamlined techniques introduced in Chapter 8 clarify many aspects of their structure. We also introduce palindromic chains of non-crossing partitions in Section 8.8, along with combinatorial techniques to produce and recognize them efficiently.

Then in Chapter 9, we show how these combinatorics inform the construction of the analog for what is called the Branched Rectangle Complex for real polynomials. Finally, in Chapter 10, we turn our attention towards the cell complex for real monic polynomials with distinct roots. This complex has several complicated features and is the setting for several still open problems. It has multiple components with well-known fundamental groups as expressed in the main theorems in Section 10.1 of Chapter 10. In Section 10.2 of that chapter, we explicitly describe the corresponding subcomplexes for degrees up to 5.

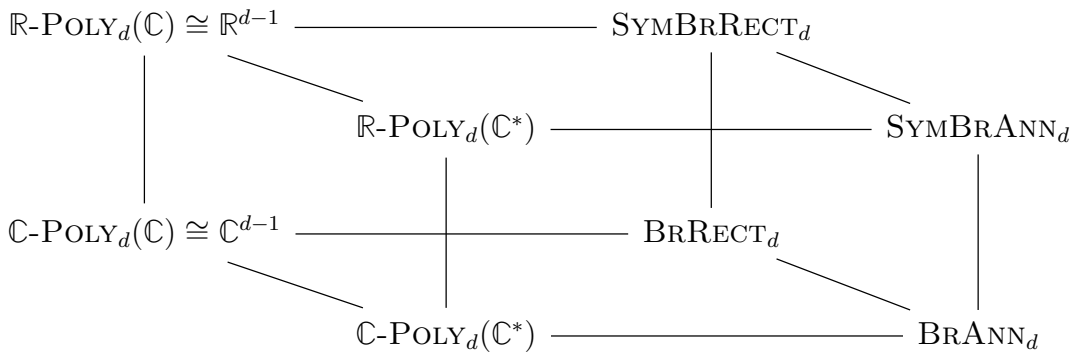

Figure 1.1: The division of related spaces that are discussed in this dissertation.

When discussing polynomials, we make three binary distinctions throughout this dissertation: Are the coefficients of the polynomial real or complex? Are the roots distinct or not (equivalently, is 0 a critical value or not)? And in terms of the associated spaces, are we considering the space from the point of view of algebraic geometry or as piece-wise Euclidean cell complexes? These distinctions and their connections are described in Figure 1.1. The distinction of $\mathbb{R}$ versus $\mathbb{C}$ coefficients is marked by the top and bottom, respectively. In the bottom level, the four spaces are all dealing with complex coefficients whereas all the spaces in the top come from real coefficients, which imbue more restrictive symmetries. The distinction of algebraic geometry versus cell complex is marked in the left and right sides. On the left are the polynomial spaces as we think of them in algebraic geometry, the space $\mathbb{R}$-Poly$_d(\mathbb{C}^*)$ for example is the space of monic, centered, polynomials with real coefficients whose critical values are in $\mathbb{C}^*$. On the right, the compactified associated cell complexes—for complex coefficients the Branched Rectangle Complex, BrRect and the Branched Annulus Complex, BrAnn identified and studied by Michael Dougherty and Jon McCammond in [12], and for real coefficients, the symmetric versions introduced in this dissertation. Whether we are talking about

any set of roots or distinct roots is marked in the back and front, respectively, as that feature for distinct roots is equivalent to the set of critical values being entirely in $\mathbb{C}^*$. For the cell complexes, on the bottom level $\textsc{BrAnn}_d$ is obtained from $\textsc{BrRect}_d$ via side identifications. For real coefficients the situation is more complicated.

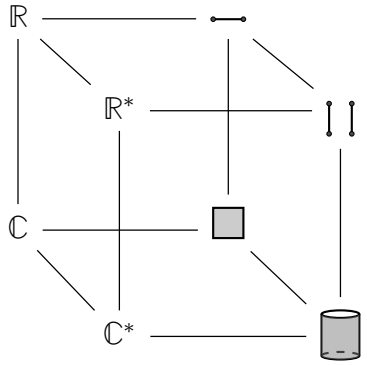

Figure 1.2: A version of the diagram in Figure 1.1 for the quadratic polynomial case when $d = 2$.

We conclude this introduction by clarifying these distinctions for the case of a quadratic polynomial, where the degree is low enough so that there is no branching. Figure 1.2 is the analog of Figure 1.1 for this degree. Because the polynomials we study are centered and monic, every quadratic polynomial simply appears as $z^2 + c$. If the value of $c \in \mathbb{C}$ or $c \in \mathbb{R}$ we see that we get that set back as the algebraic geometric point of view for this degree. Just as easily, we can understand these quadratics using the image of critical point at 0, its image c is the only critical value of $z^2 + c$. By compactifying, for $\mathbb{R}$ we obtain a closed segment and for $\mathbb{C}$ we get a closed square or disk as the possible critical values. Once we restrict our viewpoint towards distinct roots, we no longer can have 0 as a critical value, so in particular, $c \neq 0$. This breaks the closed segment into two closed segments (after another compactification) in the case of $\mathbb{R}$ or results in a closed annulus in the case of $\mathbb{C}$.

Part I

Complex Polynomials and their Associated Cell Complexes

The chapters in Part I focus on braid groups, complex polynomials, and their associated cell complexes. The first and second chapters review the definition of the braid groups and their realization as fundamental groups of quotients of complex hyperplane complements, as well as the interpretation of these spaces and the collection of complex polynomials with distinct roots. The third and fourth chapters build up cell complexes that are classifying spaces for the braid groups. The last chapters of this part deal with constructions of cell complexes for monic and centered complex polynomials. If the roots of those polynomials are distinct, the associated cell complex is also a classifying space for the braid group.

Chapter 2

Braid Groups and Classifying Spaces

This short chapter reviews braid groups and classifying spaces. First recall the standard presentation of the braid group on d strands.

Definition 2.0.1 (Braid Groups)**.** The *standard presentation* for the braid group on d strands is

$$\textsc{Braid}_d = \langle \sigma_1, \ldots, \sigma_{d-1} \mid \sigma_i\sigma_j = \sigma_j\sigma_i \text{ for } |i-j| \geq 2, \quad \sigma_i\sigma_{i+1}\sigma_i = \sigma_{i+1}\sigma_i\sigma_{i+1} \rangle$$

The relations $\sigma_i\sigma_j = \sigma_j\sigma_i$ for $|i-j| \geq 2$ are called *commuting relations* and the relations $\sigma_i\sigma_{i+1}\sigma_i = \sigma_{i+1}\sigma_i\sigma_{i+1}$ are called *braid relations*.

Next, recall the definition of a classifying space.

Definition 2.0.2 (Classifying Spaces)**.** A *classifying space* for a group G is a connected topological space X with a contractible universal cover and with fundamental group $G = \pi_1(X)$. Note that all topological spaces in this dissertation are cell complexes and/or manifolds, and they all have universal covers. Such a space is also known as an Eilenberg-Mac Lane space or a $K(G, 1)$.

Classifying spaces have several nice properties.

Remark 2.0.3 (Properties of Classifying Space)**.** Every group admits a classifying space. In fact, every group has a simplicial classifying space via a classical construction due to von Neumann. Moreover, the classifying space for a group G is essentially unique in that all classifying spaces for G are homotopy equivalent. Any group G with a finite dimensional classifying space must be torsion-free. See [17].

Many classifying spaces for the braid groups have been constructed. The other chapters in this part discuss four of these. The configuration space of d unlabeled points in $\mathbb{C}$, which corresponds to monic polynomials of degree d with distinct roots is discussed in Chapter 3 [15].

The Salvetti complex of the braid arrangement [25] is discussed in Chapter 4. The complex derived from the dual Garside structure introduced by Birman, Ko and Lee [4, 6] is discussed in Chapter 5. And the "thickened" version of the dual complex constructed by Dougherty and McCammond [11, 12] is discussed in Chapter 7. All classifying spaces for the braid group are homotopy equivalent. However, concrete connections between them are murky due to their varied motivations and constructions. One motivation for the work outlined in Chapter 7 is that it bridges some of these murky connections.

Chapter 3

Configuration spaces and Complex Polynomials

The first classifying space for the braid group comes from the natural action of the symmetric group SYM_d on the complex vector space $\mathbb{C}^d$ which simply permutes the coordinates. This action is not free. For example, the tuple $(1, \ldots, 1)$ is fixed by any permutation. The subset of $\mathbb{C}^d$ where the action is not free is a union of hyperplanes called the (complex) *braid arrangement*.

Definition 3.0.1 (Braid Arrangement)**.** Let $\mathbb{C}^d$ be a d-dimensional complex vector space with a fixed coordinate system and let $\vec{z} = (z_1, \ldots, z_d)$ be a vector in $\mathbb{C}^d$. Let $H_{ij} = \{\vec{z} \in \mathbb{C}^d \mid z_i = z_j\}$ be the hyperplane were the i-th and j-th coordinates are equal, and let $\mathscr{H}_d$ be union of hyperplanes where there exists two equal coordinates. The set $\mathscr{H}_d$ is called the (complex)*braid arrangement*. By construction,

$$\mathscr{H}_d := \bigcup_{i \neq j} H_{ij} = \{\vec{z} \in \mathbb{C}^d \mid z_i = z_j \text{ for some } i \neq j\}.$$

Definition 3.0.2 (Configuration Spaces)**.** The complement of the hyperplanes $\mathscr{H}_d$ is a

domain for which the symmetric group action is free called the (ordered) *configuration space* of points in $\mathbb{C}$, $\mathrm{Conf}_n(\mathbb{C}) := \mathbb{C}^n \setminus \mathscr{H}$. It is is path-connected and its fundamental group is PBRAID_d, the d-string pure braid group. The *unordered configuration space* $\mathrm{UConf}_d(\mathbb{C})$ is the quotient of $\mathrm{Conf}_d(\mathbb{C})$ by the free action of SYM_d.

Proposition 3.0.3. *The fundamental group of the ordered and unordered configuration spaces of points in* $\mathbb{C}$ *are the pure braid group and braid group, respectively. I.e.* $\pi_1(\mathrm{Conf}_d(\mathbb{C})) = \mathrm{PBRAID}_d$ *and* $\pi_1(\mathrm{UConf}_d(\mathbb{C})) = \mathrm{BRAID}_d$. *There is also a short exact sequence:*

$$0 \to \mathrm{PBRAID}_d \hookrightarrow \mathrm{BRAID}_d \twoheadrightarrow \mathrm{SYM}_d \to 0$$

Remark 3.0.4. The proof of Proposition 3.0.3 is not too hard to see by using a clever trick to visualize $\mathrm{Conf}_d(\mathbb{C})$. By definition, this configuration space lives inside a space with $2d$ real dimensions, however, since each coordinate is distinct, we can associate to each element of configuration space a labeled collection of complex numbers on the plane. Now, a loop in this space is a continuous path with the same start and end point. In particular, since at each point in time, the coordinates (the labeled points in $\mathbb{C}$) are distinct, and the result of a continuous deformation of the original coordinate, the loop can be visualized as the path each labeled point takes in $\mathbb{C}$ back unto itself, never crossing the other strands, or paths of the other points. If we quotient $\mathrm{Conf}_d(\mathbb{C})$ by the symmetric group action, the effect is to remove the labels of our distribution of points in $\mathbb{C}$. Now, points can end at a different point as long as it was one of the ones in the original configuration. So, after the quotient, the fundamental group is the braid group BRAID_d.

Not as obviously, the universal cover of $\mathrm{UConf}_d(\mathbb{C})$ is contractible, and as such, we have the following proposition proven by Fadell and Neuwirth in 1962 [15].

Proposition 3.0.5. *The topological space* $\mathrm{UConf}_d(\mathbb{C})$ *is a classifying space for* BRAID_d.

Definition 3.0.6 (Multisets of Complex Points)**.** If instead of considering the quotient of the symmetric group on $\mathrm{Conf}_k(\mathbb{C})$ we considered it on $\mathbb{C}^k$, the set we obtain consists of all unordered sets of k points in $\mathbb{C}$ which we call $\textsc{Mult}_k(\mathbb{C})$ (for multisets) or $\textsc{Mult}_k(U)$ for $U \subseteq \mathbb{C}$.

Remark 3.0.7. The elements of $\textsc{Mult}_k(\mathbb{C})$ are in natural bijection with the vectors $(z_1, \ldots, z_k) \in \mathbb{C}^k$ whose components are in lexicographic order, i.e $z_1 = a_1 + b_1 i$ is ordered before $z_2 = a_2 + b_2 i$ when $a_1 < a_2$ or when $a_1 = a_2$ and $b_1 < b_2$. The map $\mathbf{lex} : \mathbb{C}^k \to \textsc{Mult}_k(\mathbb{C})$ that rearranges the input vectors components into lexicographic order is a $k!$ to 1 map away from the Braid Arrangement. To simplify notation, when referring to elements in $\textsc{Mult}_k(\mathbb{C})$ we will often borrow the notation of vectors and identify a multiset with its image under the **lex** map.

Definition 3.0.8 (Polynomial Spaces)**.** For each $d \in \mathbb{N}$, let $\mathbb{C}\text{-}\textsc{Poly}_d \subset \mathbb{C}[z]$ be the collection of complex polynomials of degree d. For any given $p \in \mathbb{C}\text{-}\textsc{Poly}_d$, we write $p(z) = a_d z^d + a_{d-1} z^{d-1} + \cdots + a_1 z + a_0$ with $a_d \in \mathbb{C} \setminus \{0\}$ and $a_i \in \mathbb{C}$ for all $i \in \{0, \ldots, d-1\}$. The polynomial p is *monic* if $a_d = 1$ and *centered* if $a_{d-1} = 0$ which, for monic polynomials, occurs whenever the sum of the roots of p is zero. Let $\mathbb{C}\text{-}\textsc{Poly}_d^m$ be the subspace of monic polynomials over $\mathbb{C}$ and $\mathbb{C}\text{-}\textsc{Poly}_d^{mc}$ be the subspace of monic, centered polynomials. Similarly, we define $\mathbb{R}\text{-}\textsc{Poly}_d^m \subset \mathbb{C}[z]$ as the set of monic polynomials over $\mathbb{C}$ that have real coefficients and $\mathbb{R}\text{-}\textsc{Poly}_d^{mc}$ as the monic, centered polynomials over $\mathbb{C}$ that have real coefficients.

In addition, we add the extra argument in $\mathbb{C}\text{-}\textsc{Poly}_d(U)$ or any of the other similarly defined spaces to be the polynomials in that space whose *critical values* lie in U. We may use the argument of $\mathbb{C}$ to emphasize situations in which there are no restrictions on the critical values

Remark 3.0.9 (Centered)**.** When we consider the symmetric group action on a d di-

mensional space, it is point-wise fixing the vectors where all the coordinates are equal, which is a copy of $\mathbb{C}$. To rectify this, we can either quotient by that subspace or restrict to where the coordinate sum is zero. The complement of the braid arrangement has a decomposition as its intersection with the hyperplane with coordinate sum zero and a copy of $\mathbb{C}$. In $\mathrm{UConf}_d(\mathbb{C})$, any element has a unique "centered" representative via translating in the $(1, \ldots, 1)$ direction.

Geometrically, centering a polynomial makes the average of the roots at the origin. Precomposing a polynomial with a translation translates the roots (in the opposite direction) and the critical values don't change. A centered polynomial is a canonical representative for the equivalence class under precomposition with a translation that preserves the critical values of the polynomial. Precomposing a monic polynomial with a translation establishes a homeomorphism $\mathbb{C}\text{-}\textsc{Poly}_d^{mc}(U) \times \mathbb{C} \cong \mathbb{C}\text{-}\textsc{Poly}_d^{m}(U)$ which justifies our use of the space $\mathbb{C}\text{-}\textsc{Poly}_d^{mc}(U)$ as a convenient space of representatives with the same topology.

Definition 3.0.10 (Three Maps from Polynomials to Multisets)**.** Let $n = d - 1$ and define the following three maps that relate polynomials with multisets:

1. $\mathbf{rts} : \mathbb{C}\text{-}\textsc{Poly}_d^m \to \textsc{Mult}_d(\mathbb{C})$ that sends a polynomial p to its multiset of roots, the solutions of $p(z) = 0$.

2. $\mathbf{cpt} : \mathbb{C}\text{-}\textsc{Poly}_d^m \to \textsc{Mult}_n(\mathbb{C})$ that sends a polynomial to its multiset of critical points, the roots of its derivative: $\mathbf{rts}(p')$.

3. $\mathbf{cvl} : \mathbb{C}\text{-}\textsc{Poly}_d^m \to \textsc{Mult}_n(\mathbb{C})$ that sends a polynomial to its multiset of critical values, the image of its critical points: $\{p(z) \mid z \in \mathbf{cpt}(p)\}$.

Remark 3.0.11 (Roots as Multisets)**.** By the fundamental theorem of algebra, we can identify any monic polynomial over $\mathbb{C}$ to the unordered set of d points in $\mathbb{C}$ that are roots

of p. In other words the map **rts** is a homeomorphism from $\mathbb{C}$-$\textsc{Poly}_d^m$ to $\textsc{Mult}_d(\mathbb{C})$. We note that this identification when restricted to $\mathbb{R}$-$\textsc{Poly}_d^m$ still requires as a target space $\textsc{Mult}_d(\mathbb{C})$ since the roots of real polynomials can often be complex numbers. In particular,

$$\mathbb{R}\text{-}\textsc{Poly}_d^m = \{p(z) \in \mathbb{C}\text{-}\textsc{Poly}_d^m \mid p(z) = p(\overline{z}) \text{ for all } z \in \mathbb{C}\}$$

and can be identified with $\overline{\textsc{Mult}_d(\mathbb{C})} := \{\vec{z} \in \textsc{Mult}_d(\mathbb{C}) \mid \vec{z} = \mathbf{lex}(\overline{\vec{z}})\}$.

Finally, we also note that since $\text{UConf}_d(\mathbb{C})$ naturally lives in $\textsc{Mult}_d(\mathbb{C})$, and similarly $\overline{\text{UConf}_d(\mathbb{C})} \subset \overline{\textsc{Mult}_d(\mathbb{C})}$, we can identify $\text{UConf}_d(\mathbb{C})$ (respectively $\overline{\text{UConf}_d(\mathbb{C})}$) with $\mathbb{C}$-$\textsc{Poly}_d^m(\mathbb{C}^*)$ (respectively $\mathbb{R}$-$\textsc{Poly}_d^m(\mathbb{C}^*)$) by using the following easy to prove lemma.

Lemma 3.0.12. *A polynomial $p \in \mathbb{C}$-$\textsc{Poly}_d^m$ has distinct roots if and only if $\mathbf{rts}(p) \cap \mathbf{cpt}(p) = \emptyset$ if and only if zero is not a critical value, i.e. $\mathbf{cvl}(p) \subset \mathbb{C}^*$.*

Corollary 3.0.13. *The space of monic and centered complex polynomials of degree d with distinct roots, $\mathbb{C}$-$\textsc{Poly}_d^{mc}(\mathbb{C}^*)$, is a classifying space for the braid group $\textsc{Braid}_d$.*

Proof: Using the homeomorphism from Remark 3.0.11 along with Proposition 3.0.5 establishes the corollary, since $\mathbb{C}$-$\textsc{Poly}_d^m(\mathbb{C}^*)$ deformation retracts onto $\mathbb{C}$-$\textsc{Poly}_d^{mc}(\mathbb{C}^*)$. □

There is a natural homeomorphism between the unlabeled configuration space and monic polynomials over $\mathbb{C}$ with distinct roots. Thus, that is another classifying space for the Braid Group.

Chapter 4

Polytopes and the Salvetti Complex

This chapter outlines the construction a cell complex called the Davis complex, that can be created for any Coxeter group. For each Davis complex, there is an associated Salvetti complex, which is a classifying space for the corresponding Artin group. Due to the way in which these complexes are formed, via *polytopes*, we begin by laying the framework for these flat-sided shapes, which generalize polygons or polyhedrons into arbitrary dimensions. For the braid group, the Salvetti complex is constructed from a single polytope called the permutohedron.

4.1 Polytopes

The n-dimensional analogue to a polygon or polyhedron is called a *polytope*. It is simply a (convex) shape with flat sides. There are two regularly used ways to describe a polytope: The convex hull of a finite set of points; The bounded intersection of halfspaces.

Definition 4.1.1.

- A domain $D \subset \mathbb{R}^n$ is called *convex* if for any pair $x, y \in D$, the straight line segment

$$tx + (1-t)y \in D$$

for all $t \in [0, 1]$.

- The *convex hull* of a set of points S, denoted $\text{conv}(S)$, is the intersection of all convex domains that contain the set of points.

Definition 4.1.2.

- A *hyperplane* in $\mathbb{R}^n$ is an affine subspace of codimension 1. It is the solution set of a single linear equation.

- A hyperplane cuts $\mathbb{R}^n$ into two *halfspaces*.

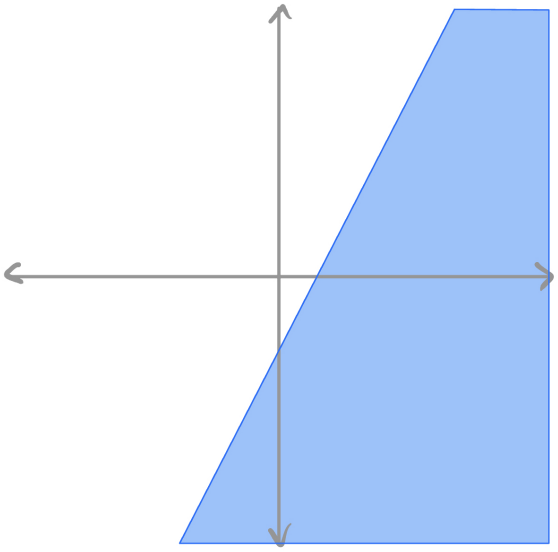

Figure 4.1: The halfspace $2x - y - 1 \leq 0$.

Proposition 4.1.3. *The intersection of any number of halfspaces is convex.*

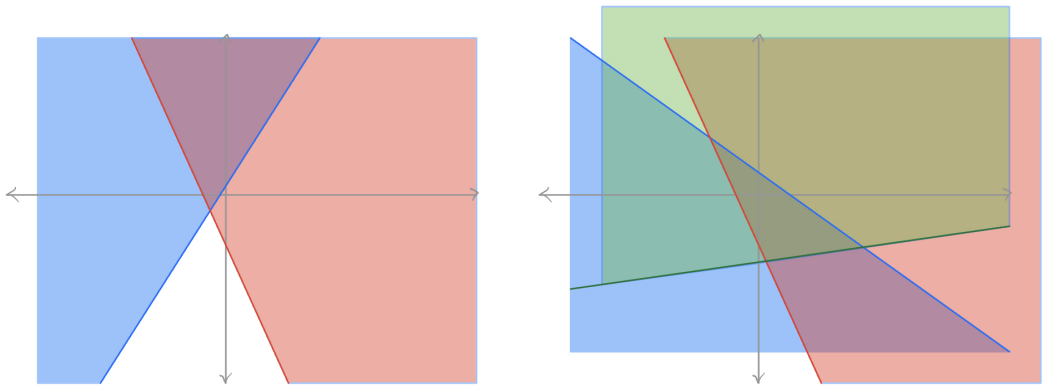

Figure 4.2: Some intersecting halfspaces.

Definition 4.1.4. If the common intersection of finitely many halfspaces is bounded, then that region is called a *polytope*. Equivalently, if for some finite $V \subseteq S$, $\text{conv}(V) = \text{conv}(S)$, then $\text{conv}(S)$ is a polytope.

Theorem 4.1.5.

- *Any polytope can be described in terms of its halfspaces*

$$P = \{\vec{x} \in \mathbb{R}^n \mid A\vec{x} \leq \vec{b}\}$$

where A is an $m \times n$ matrix where n is the dimension of the ambient space and m is the number of defining halfspaces.

- *Any polytope can be describe as the convex hull of a finite set of points. Concretely,*

$$P = \text{conv}(x_1, \ldots, x_n)$$

where $\{x_1, \ldots, x_n\} \in P$ contains the vertices of P.

Definition 4.1.6. (Faces of a Polytope)

- The (nontrivial) intersection of a hyperplane with a polytope defines a *face of the polytope* whenever the polytope is entirely contained in a halfspace of the hyperplane.

- Equivalently, a convex subset $F \subset P$ is a *face of* P if for all $z \in F$, $tx+(1-t)y = z$ for some $x, y \in P$ and $t \in (0,1)$ implies $x, y \in F$.

Remark 4.1.7. For a k dimensional polytope, the $(k-1)$-dimensional faces are called *facets*, the 0-dimensional *vertices*, and the 1-dimensional faces called *edges*. Every face of a polytope is again a polytope, and all of its faces are faces of the original polytope. In particular, the set of all faces for a polytope P are naturally ordered by containment, giving the set a poset structure.

Definition 4.1.8 (The Face Lattice)**.** The *face lattice* for a polytope P is the poset whose elements are the faces of P, and the partial order is set containment.

Definition 4.1.9.

- If two polytopes P and P' have face lattices that are isomorphic as posets, then P and P' are *combinatorially equivalent*.

- If there is an invertible affine map between P and P', they are *linearly equivalent*.

- If they have matching side lengths, angles, etc. they are *metrically equivalent*.

Definition 4.1.10. There is a unique $n-1$ dimensional polytope with n vertices (up to combinatorial equivalence), any polytope in this class is called a *simplex*.

Let $\{e_i\}$ be a standard orthonormal basis for $\mathbb{R}^n$.

Example 4.1.11 (Regular simplices)**.** The *standard simplex* is an example of a regular simplex and is defined as $P = \text{conv}(e_i \mid i \in [n])$. For example, the standard 3-simplex is the convex hull of the tips of the standard basis vectors $\{e_1, e_2, e_3, e_4\}$ in $\mathbb{R}^4$.

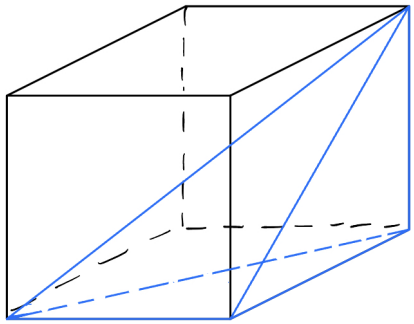

Figure 4.3: A 3-dimensional orthoscheme Θ_3 inscribed in a 3-cube.

Definition 4.1.12 (Orthoschemes)**.** The metric simplex resulting from quotienting a unit d-dimensional cube by natural $\textsc{Sym}_d$ group action fixing a vertex is called a *(standard) orthoscheme* Θ_d, which can also be described in terms of the convex hull

$$\Theta_d = \text{conv}\left(0, e_1, e_1 + e_2, e_1 + e_2 + e_3, \ldots, \sum_{i=1}^{d} e_i\right).$$

There is also a more general definition of an orthoscheme, which is any polytope obtained as the convex hull of a piece-wise linear path where the set of direction vectors for the linear pieces are pairwise orthogonal. The facets of a standard orthoscheme are orthoschemes of this more general type.

4.2 Permutohedra

To construct the Davis and Salvetti complexes, the most important example of a polytope is the permutohedron.

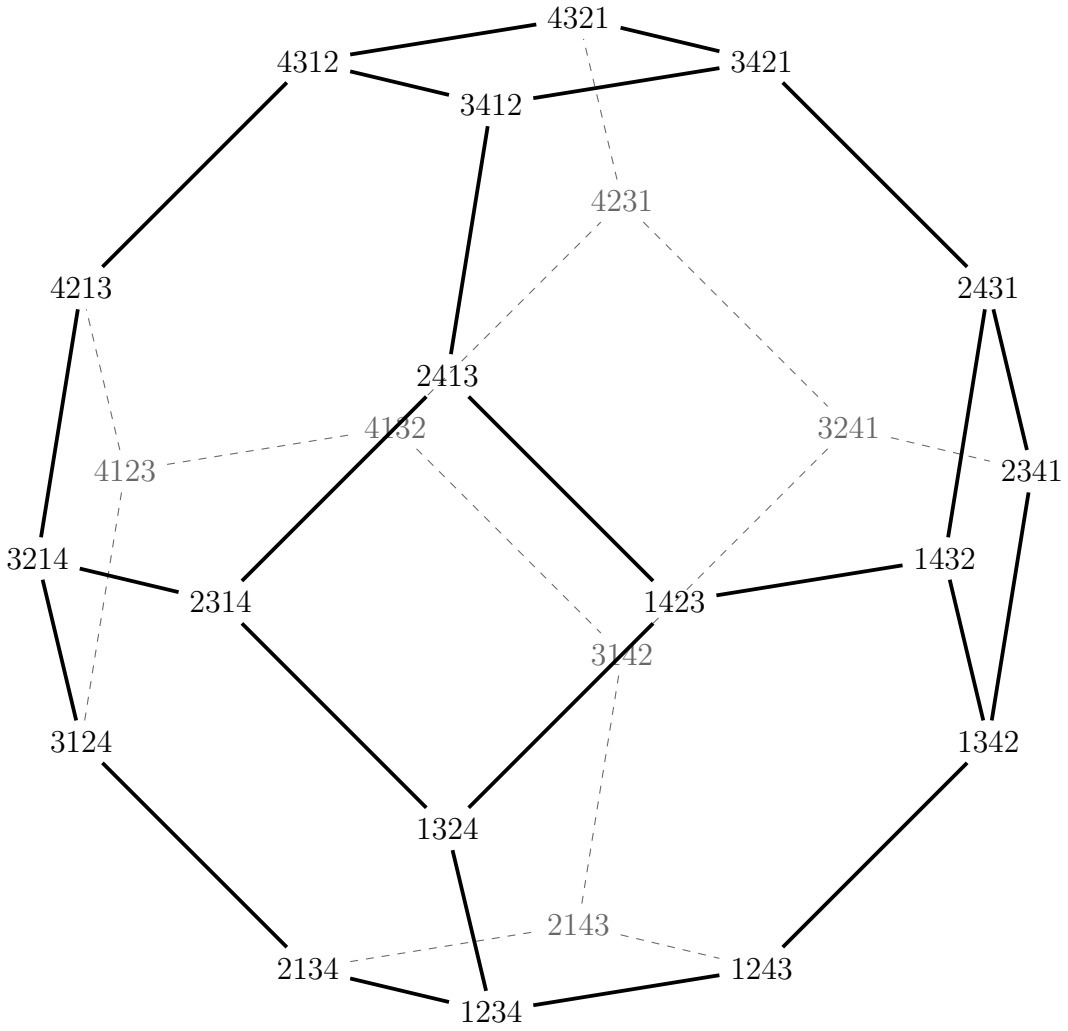

Figure 4.4: The permutohedron of dimension 3, denoted Π_3, a three dimensional polytope in $\mathbb{R}^4$.

Example 4.2.1 (Permutohedron)**.** Another classic family of polytopes is called the *permutohedron* Π_{d-1} which is the convex hull of the orbit of $(1, 2, \ldots, d)$ under the action of the symmetric group $\textsc{Sym}_d$. In other words

$$\Pi_{d-1} = \text{conv}(\sigma(1, 2, \ldots, d) \mid \sigma \in \textsc{Sym}_d).$$

The permutohedron of dimension $d-1$, Π_{d-1} is an $(d-1)$-dimensional polytope with $d!$

vertices. For $d = 3$ the permutohedron Π_2 is a regular hexagon in $\mathbb{R}^3$. Figure 4.4 is the 3-dimensional permutohedron for $d = 4$, Π_3, which naturally lives in $\mathbb{R}^4$.

Definition 4.2.2. Let $A, B \subset \mathbb{R}^n$. We define the *Minkowski sum* of A and B to be

$$A + B = \{a + b \mid a \in A \quad b \in B\}.$$

For example, the Minkowski sum of n orthonormal line segments is the unit n-cube.

Definition 4.2.3. For a Coxeter group W generated by reflections, the root system is the collection of normal vectors to the hyperplanes that define the reflections. The Minkowski sum of the (normalized) root system is the *W-permutohedron.*

Remark 4.2.4 (Davis complex)**.** For any Coxeter group W, there is a general construction of an associated cell complex called the *Davis complex* which is obtained by gluing W'-permutohedrons onto the (right) Cayley graph of W on the associated vertices of the cosets of the finite parabolic subgroups $W' \leq W$. For a finite Coxeter group, the Davis complex is the W-permutohedron.

The 1-skeleton of the permutohedron is the (right) Cayley graph of the symmetric group with respect to the minimal standard generating set (adjacent transpositions). In particular, the Minkowski sum of the two unit normal vectors perpendicular to the hyperplanes in the Braid Arrangement is the permutohedron and the W-permutohedron for $W = \textsc{Sym}_d = \textsc{Cox}(A_{d-1})$ is Π_{d-1} (up to scaling). In other words, the permutohedron, with a suitable cell structure, is the Davis complex for the symmetric group.

4.3 The Salvetti Complex

Via the Davis complex, which for our purposes is a permutohedron, we can construct another classic classifying space for the braid group called the Salvetti complex.

Definition 4.3.1 (Oriented Davis Complex and Salvetti Complex)**.** Any W-permutohedron has a well defined 'antipodal' map on its vertices. For a finite Coxeter group $\textsc{Cox}(\Gamma)$, we can orient the Davis complex, which is just a $\textsc{Cox}(\Gamma)$-permutohedron, from any vertex to its antipode and label each edge in the 1-skeleton according to the Cayley graph. Gluing the Davis complex with respect to these labeled edges and orientations results in a 1-vertex complex, called the *Salvetti complex*, whose fundamental group is the associated Artin group $\textsc{Art}(\Gamma)$. More generally, the Salvetti complex is the quotient of the oriented Davis complex by the free action of $\textsc{Cox}(\Gamma)$.

Example 4.3.2. As a key example, we can orient the edges of the permutohedron to flow positively from a vertex to the antipodal vertex and label the edges to correspond to the (right) Cayley graph of the symmetric group, by labeling each edge with the transposition that relates the connected vertices. If we identify edges with the same transposition label, we obtain the Salvetti complex for the braid group. It is homotopy equivalent to the hyperplane compliment quotient, and it is a classifying space for the braid group [23].

Recalling the presentation for $\textsc{Braid}_3$,

$$\textsc{Braid}_3 = \langle a, b \mid aba = bab \rangle,$$

where we use a and b to be the generators σ_1 and σ_2 for convenience. The 2-complex of this presentation is shown schematically in Figure 4.5. The hexagon with oriented labeled edges shown on the right is attached to the 1-skeleton shown on the left. This is the Salvetti complex for $\textsc{Braid}_3$. In Figure 4.6, we see the identifications for $\textsc{Braid}_4$ to obtain its Salvetti complex.

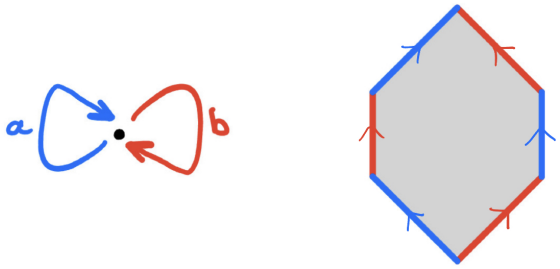

Figure 4.5: Visulaizing the presentation of $\textsc{Braid}_3$ topologically. Oriented upwards. Identifications via color.

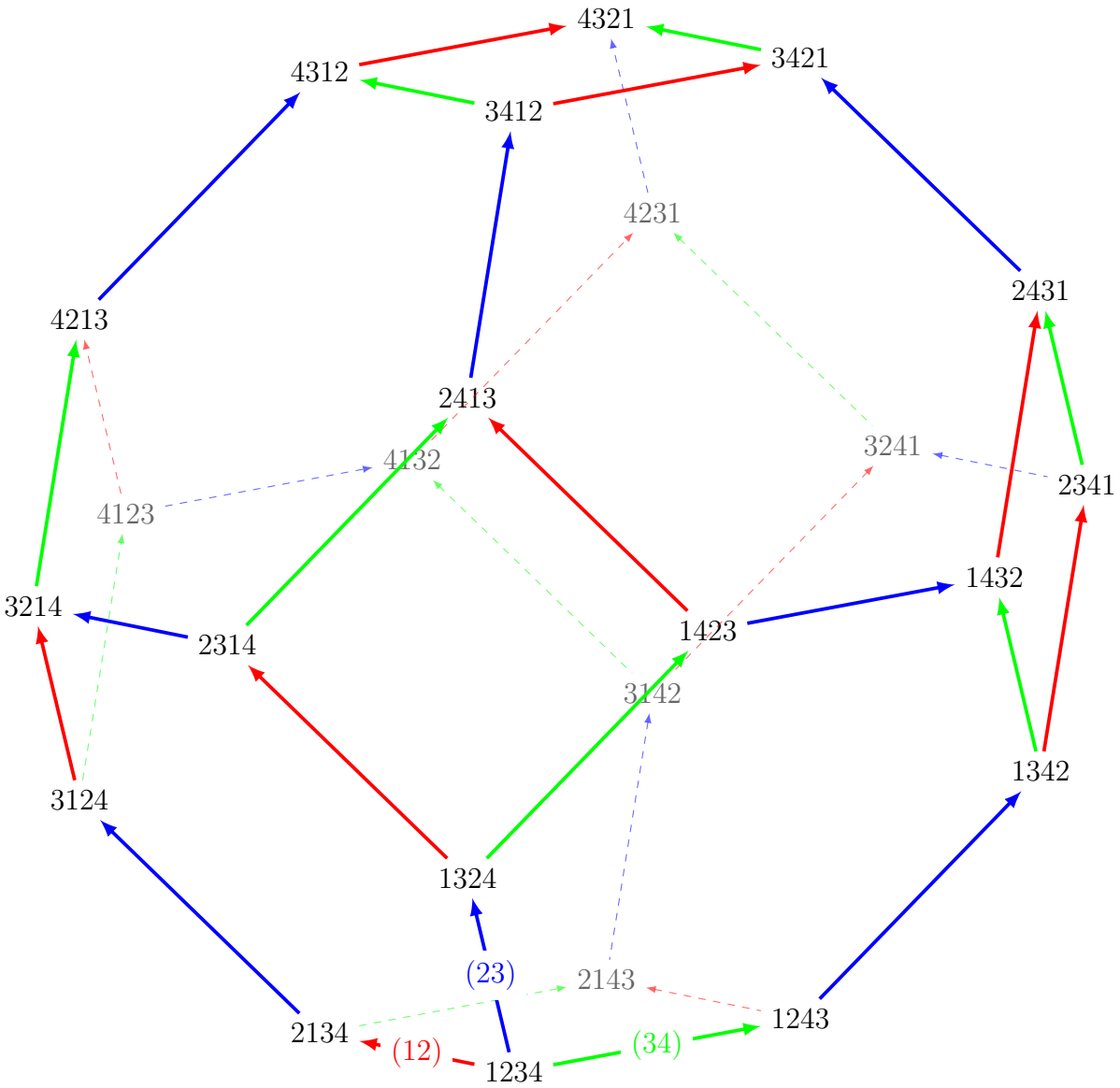

Figure 4.6: Visualizing the identifications for the Salvetti complex for $\textsc{Braid}_4$.

Chapter 5

Non-Crossing Partitions and the Dual Braid Complex

This chapter discusses an alternative type of presentation for the braid groups and a corresponding classifying space called the Dual Braid Complex. We begin with a primer on partially ordered sets, to highlight some properties that are leveraged in the construction of the Dual Braid Complex, another classifying space for the braid group. In Section 5.2, we discuss the particular partially ordered set underpinning this construction, the non-crossing partitions lattice. In Section 5.3 and 5.4, we develop the presentation of the braid groups introduced by Birman, Ko, and Lee [4] and in Section 5.5, we discuss the Dual Braid Complex and highlight some of its important aspects.

The Dual Braid Complex is known to be homotopy equivalent to monic, centered complex polynomials with critical values in $\mathbb{C}^*$, and recent work by Dougherty and McCammond [12] actually realizes it as the spine of this polynomial space.

Remark 5.0.1 (History of Dual Braid Complex)**.** The standard presentation for the braid group was introduced by Artin in 1925, where he also solves the word problem. His solution was exponential in word length, and therefore not the most efficient. Another

shortcoming was that it left unresolved the related conjugacy problem.

Improvements came in dissertation of Garside in 1969, who adapted Artin's approach and presented another solution to the word problem, with similar efficiency issues, but with a flexible enough construction to resolve the conjugacy problem as well. Garside left a large impact with his ideas that inspired 'Garside Theory' developed in the 1990s.

The first more efficient solution to the word problem came from Thurston in 1992, championing the Garside approach with modifications leading to a considerable increase in efficiency on the order of $\mathcal{O}(|W|^2 n \log n)$, and to date this is the most efficient solution that relies on the standard presentation of the braid group. [14]

However, in 1998 Birman, Ko, Lee introduce what became known as the dual presentation of the Braid group and used the new presentation to offer an even more efficient solution to the word problem, roughly in $\mathcal{O}(|W|^2 n)$ time [4].

The Dual Braid Complex which comes from this presentation, introduced by Tom Brady [6] and independently by David Bessis [3] and it was metricized by Brady and McCammond in 2010 [7], who proved the complex is CAT(0) for $n \leq 5$. This result was extended to $n = 6$ by Haettel-Kielak-Schwer [16], and to $n = 7$ by Jeong in [18].

5.1 Partially Ordered Sets

This section reviews basic definitions and conventions for partially ordered sets.

Definition 5.1.1. A set, P, along with a relation $\leq$, is called a *partially ordered set* or *poset* if for $a, b, c \in P$:

- (Reflexivity) $a \leq a$.
- (Anti-symmetry) If $a \leq b$ and $b \leq a$, then $a = b$.
- (Transitivity) If $a \leq b$ and $b \leq c$ then $a \leq c$.

If $a \leq b$ for some $a, b \in P$, we says that a and b are *comparable*. Otherwise, they are *incomparable*. Without the transitivity, we call P *locally ordered*.

Definition 5.1.2. For two comparable elements in a poset $x \leq y$, if there is no $z \neq x, y$ such that $x \leq z \leq y$, we say that y *covers* x or y is a cover of x. We may also call it a covering relation.

Remark 5.1.3 (Visualizing Posets)**.** The *Hasse Diagram* for a poset is a visualization graph for the poset in which each element is denoted by a vertex, and there is an edge between two vertices if the corresponding poset elements share a covering relation. As a convention, if $x \leq y$ in the poset, then the vertex labeled x will be below the element y in the Hasse diagram.

Example 5.1.4. The Boolean Lattice: $\textsc{Bool}_n = (2^{[n]}, \subseteq)$ is a classic example of a poset. Its Hasse diagram encodes the 1-skeleton of an n-cube.

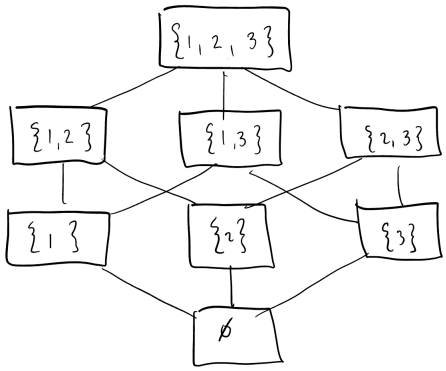

Figure 5.1: The Hasse Diagram for the Boolean Lattice for $n = 3$.

Remark 5.1.5. If there is an element that is "greater than" all the others in the poset we refer to this element as $\widehat{1}$, if an element is "less than" all others we will denote it as $\widehat{0}$. These maximum and minimum elements may not exist.

Definition 5.1.6. (Meets and Joins) If there is a unique least upper bound for two elements in a poset a, b, we refer to this poset element as the *join* denoted as $a \vee b$. Dually, if there is a greatest lower bound, we refer to this as the *meet* denoted $a \wedge b$. Again these need not exist.

Definition 5.1.7. A poset $(P, \leq)$ is a *lattice* if $p \vee q$ and $p \wedge q$ exists for any pair of elements $p, q \in P$.

Figure 5.2 shows the Hasse diagrams of three finite posets. Only the left most is a lattice. In the center poset, the minimal elements do not admit a meet. In the right most, the upper bounds for the elements on the lower level are not unique. Similarly, there is no uniqueness for the lower bounds of the elements on the upper level.

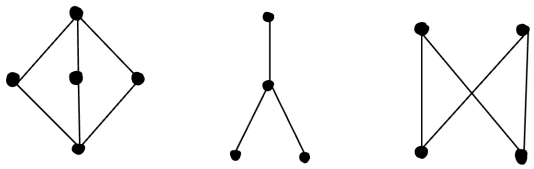

Figure 5.2: Hasse diagrams for a lattice on the left. The Hasse diagrams of posets that are not lattices in the center and on the right.

We end this section with a few other definitions that are used in subsequent sections/chapters.

Definition 5.1.8 (Chains)**.** A totally ordered subset of a poset, $C \subseteq P$, is called a *chain*. The chain's *length* is $|C| - 1$. If there is no element $x \in P \setminus C$ so that $x \sqcup C$ is a chain, we call C a *maximal chain*.

Definition 5.1.9. A poset is *graded* if there exists a well-defined rank function $\rho : P \to \mathbb{N}$ such that

- The rank function respects the partial ordering, i.e. $x <_P y$ implies $\rho(x) < \rho(y)$.

- The rank function respects covers, i.e. if y covers x, then $\rho(y) = \rho(x) + 1$.

Definition 5.1.10 (Intervals)**.** For elements $p \leq q \in P$, the *interval* $[p, q]$ is the set

$$[p, q] := \{x \in P \mid p \leq x \leq q\}$$

Definition 5.1.11. For two posets $(P, \leq_P)$ and $(Q, \leq_Q)$ we may define the *product* poset $P \times Q$ to be the collection of pairs (x, y) for $x \in P$ and $y \in Q$ along with the relation

$$(x_1, y_1) \leq (x_2, y_2) \text{ if and only if } x_1 \leq_P x_2 \text{ and } y_1 \leq_Q y_2.$$

Remark 5.1.12. Using the orthoscheme metric on the geometric realization of graded poset respects direct product. In other words, the orthoscheme realization of the poset direct product is equivalent to the metric direct product of each factor's orthoscheme realization. This is one way to see how the Boolean lattice connects with the n-cube. The orthoscheme realization glues together orthoschemes to form an n-cube.

Definition 5.1.13. A *poset isomorphism* is a bijective map $\varphi : P \to Q$ that respects the partial order, i.e $x \leq_P y$ if and only if $\varphi(x) \leq_Q \varphi(y)$ for all $x, y \in P$. A *poset anti-isomorphism* is the same notion except that it reverses the order, i.e. $x \leq_P y$ if and only if $\varphi(y) \leq_Q \varphi(x)$.

Definition 5.1.14 (Duality)**.** Every poset admits a *dual poset* which for our purposes is any poset in the anti-isomorphism class of P. We say it is *self-dual* if P itself is in the anti-isomorphism class.

Remark 5.1.15. It is easy to recognize duality in finite posets by investigating their Hasse diagrams, since the Hasse diagrams of dual posets are vertically flipped versions of each other.

5.2 Non-Crossing Partitions

The main poset of interest here is the lattice of non-crossing partitions.

Definition 5.2.1 (Combinatorial Non-Crossing Partitions)**.** Given a partition of $[n]$ with the usual total order, $\pi = (A_1, \ldots, A_k)$ where $\sqcup A_i = [n]$ is *non-crossing* if for every quadruple $a < b < c < d \in [n]$, if $\{a, c\} \subset A_i$ and $\{b, d\} \subset A_j$, then $i = j$.

The metric version explains the "non-crossing" title and provides a simple and evocative way to visualize a non-crossing partition.

Definition 5.2.2 (Metric Non-Crossing Partitions)**.** Suppose we have an embedding of a regular n-gon in the complex plane with labeled vertices according to some cyclic ordering. A partition π is *non-crossing* if the convex hulls of the vertices labeled by the numbers in each block of π form pairwise disjoint subspaces of $\mathbb{C}$.

The topological version avoids any mention of a metric.

Definition 5.2.3 (Topological Non-Crossing Partitions)**.** Let U be a closed topological disk, let $S \subset \partial U$ be a subset of its boundary with n path components and fix a bijective labeling of the components of S by the numbers in $[n]$ in the order they occur in the boundary of U. For every subspace V with $S \subset V \subset U$ we define a set partition $NCP(V)$ where i and j are in the same block of $NCP(V)$ if and only if the path components of S labeled i and j are in the same path component of V . A set partition π is a *(topological) non-crossing partition* if there exists a subspace V with $S \subset V \subset U$ such that $NCP(V) = \pi$. Note that if we view the subspaces of U containing S as a poset under inclusion, then the map to $NCP(n)$ is order-preserving. In other words, if $S \subset V \subset V' \subset U$ as subspaces, then $NCP(V) \leq NCP(V')$ as set partitions.

Remark 5.2.4. In this document, when we illustrate non-crossing partitions, we will typically use the metric version, but we may exaggerate the convex hulls using curved arcs

for clarity, since metric non-crossing partitions are topological non-crossing partitions, whether we use arcs or straight lines we retain all consistency.

Remark 5.2.5. The set of combinatorial non-crossing partitions on n form a partially ordered set under the refinement relation: $\pi \leq \tau$ if and only if for every i, $A_i \subseteq B_j$ for some j, where $\{A_1, \ldots, A_k\}$ and $\{B_1, \ldots, B_\ell\}$ are the parts of π and τ, respectively.

The following enumerative theorem is known for non-crossing partitions, which categorizes them as Catalan objects (objects enumerated by the Catalan number sequence). They share this designation with myriad other combinatorial objects, such as the number of closed parenthetical words, rooted trees, Dyck Paths, weakly-increasing parking functions, and many more. See [27] for many other examples.

Proposition 5.2.6.

$$|NCP(n)| = C_n = \frac{1}{n+1}\binom{2n}{n}$$

Remark 5.2.7 (Kreweras Complements)**.** There is a family of maps called *Kreweras complements* on $NCP(n)$ that can be used to create a complementary non-crossing partition. One way to construct it is to establish an ordering on the regions between the nodes in the circular diagram version of the non-crossing partition, and maximally extend the regions between these new nodes so as not to intersect the original partition. Figure 5.3 illustrates this process. There is a reasonable large amount of choice on what labels to pick for the new nodes, with the only really restriction is to select a consistent cyclic ordering. That choice is not very important except for in a few cases throughout this dissertation, when we will make a particular distinction for the Kreweras complement to simplify some methods or ideas.

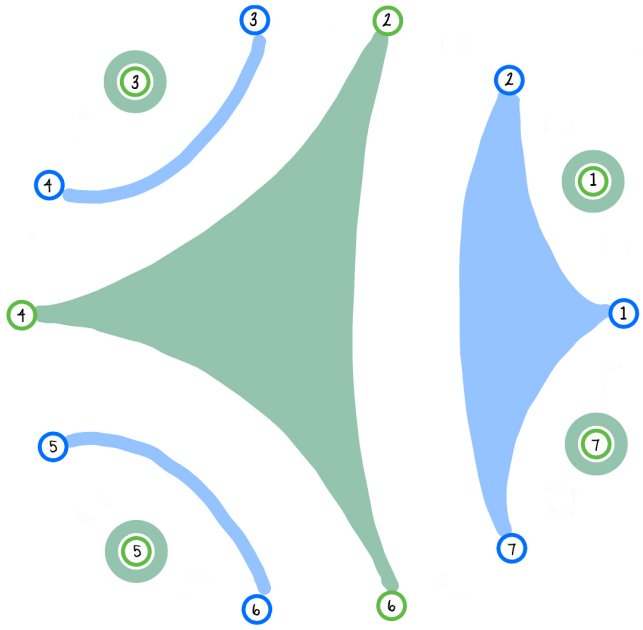

Figure 5.3: The partition $\pi = \{\{1, 2, 7\}, \{3, 4\}, \{5, 6\}\}$ and the Kreweras complement $\tau = \{\{1\}, \{2, 4, 6\}, \{3\}, \{5\}, \{7\}\}$ according to the given labelling.

Remark 5.2.8. Here are some properties that are well-known for the poset of non-crossing Partitions under the refinement relation (in this viewpoint, $NCP(n)$ is a sub-poset of the Partition Lattice)

- $(NCP(n), \text{refinement})$ is a lattice.
- It is self-dual under the Kreweras complement map [20].
- All of its maximal chains are of the same length, which implies the existence of a well-defined rank function—the number of blocks. Thus, $NCP(n)$ is graded.
- Maximal chains are in bijection with parking functions of length $n-1$ (Integer sequences $(b_1, \ldots, b_{n-1})$ satisfying $b_i \leq i$ and all of their permutations—there are n^{n-2} of these [19].)

- Each interval has the structure of direct products of smaller non-crossing partition lattices.

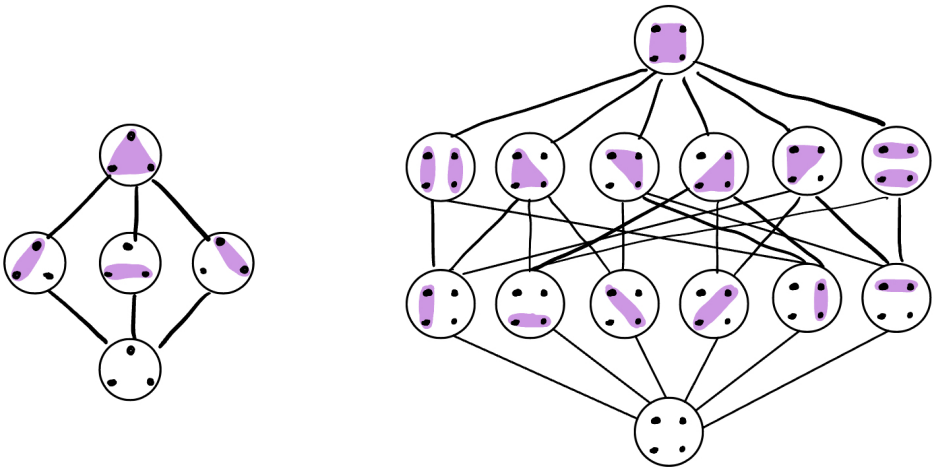

Figure 5.4: The Hasse Diagrams for the non-crossing Partition Lattices for $n = 3$ (left) and $n = 4$ (right).

5.3 Dual Simple Braids

We know turn our attention towards a particular set of braids in $\textsc{Braid}_n$ that generate the braid group called *dual simple braids* drawing from [13]. The braid group naturally surjects into the symmetric group by considering (without crossing information) the final position of each strand.

Concretely, we may define the map

$$\varphi : \textsc{Braid}_n \to \textsc{Sym}_n$$

that sends $\sigma_i \mapsto (i, i+1)$. To insert some non-crossing data into this system we can precompose this map with $\gamma : NCP(n) \to \textsc{Braid}_n$ which sends non-crossing partitions to compositions of what are called rotation braids.

Definition 5.3.1 (Rotation Braids)**.**

- Let $A \subseteq [n]$, the *rotation braid* δ_A rotates counterclockwise the vertices of A and fixes the other strands.
- If $|A| = 2$, δ_A is called a *positive half twist.*

Definition 5.3.2 (Dual Simple Braids)**.** For each $\pi \in NCP(n)$ of the form $\pi = (A_1, \ldots, A_k)$, the *dual simple braid* δ_π is the product of rotation braids $\delta_{A_1} \cdot \delta_{A_2} \cdots \delta_{A_k}$.

Note, since the underlying partition is non-crossing, the order of the multiplication is immaterial.

Altogether we have an injection into both the braid group and the symmetric group.

$$NCP(n) \hookrightarrow \textsc{Braid}_n \twoheadrightarrow \textsc{Sym}_n$$

$$\pi \mapsto \delta_\pi \mapsto \sigma_\pi$$

Consider the set DS_n of all dual simple braids. Its image in the symmetric group is called the set of non-crossing permutations. Both the set of dual simple braids and the set of non-crossing permutations inherit via the above injection, the poset structure of $NCP(n)$.

Proposition 5.3.3. *The map that sends $\pi \mapsto \delta_\pi$ gives an embedding of the Hasse Diagram of $NCP(n)$ into the (right) Cayley Graph of* $\textsc{Braid}_n$*. Similarly, $\pi \mapsto \sigma_\pi$ embeds the Hasse diagram into the (right) Cayley Graph of* $\textsc{Sym}_n$ *with respect to the set of transpositions.*

Theorem 5.3.4 (Geodesic Intervals)**.** *The Hasse Diagram of $NCP(n)$ is isomorphic to the subgraph of the Cayley graphs consisting of length minimizing (geodesic) paths from the identity braid/identity permutation to $\delta_{[n]}$/the cycle $(1, \ldots, n)$, respectively.*

Theorem 5.3.5. *For $\pi, \tau \in NCP(n)$:*

- *$\pi \leq \tau$ if and only if $\delta_\pi^{-1}\delta_\tau$ is a dual simple braid.*
- *$\pi < \tau$ is a cover if and only if $\delta_\pi^{-1}\delta_\tau$ is a positive half twist.*

Corollary 5.3.6. *Maximal chains are in bijective correspondence with minimum length factorizations of $(1, \ldots, n)$. A such, the number of minimum length factorizations of the n-cycle into transpositions is*

$$n^{n-2}$$

Remark 5.3.7. The bijection in the above corollary essentially labels every covering relation with a transposition that includes a number from each of the two blocks that merge. There are rules to follow, but rather than describe them, we illustrate this bijection is a few examples in Figure 5.5.

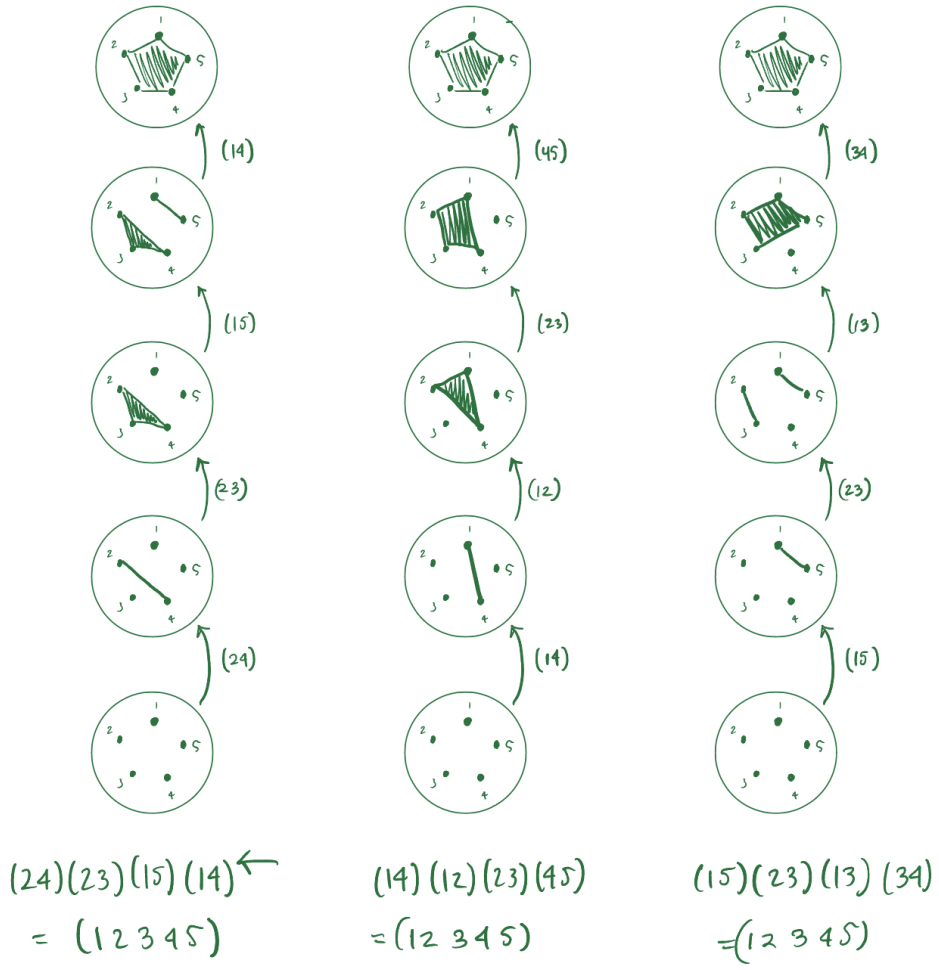

Figure 5.5: A few examples of the bijection between maximal non-crossing partition chains and factoring the n-cycle.

5.4 Dual Braid Presentation

With the machinery built up, we can introduce the different presentation for the Braid group conceived by Birman, Ko, and Lee [4] call the *Dual Presentation,* though the way it is presented below more closely resembles the version of the same from Tom Brady [6].

$$\textsc{Braid}_n = \langle DS_n^* \mid \delta_\pi \delta_\tau = \delta_{\pi \vee \tau} \text{ if } (\pi, \tau) \text{ is properly ordered} \rangle$$

Note, the set of generators DS_n^* is the set of dual simple braids excluding the trivial ones.

Example 5.4.1. We can compare this presentation to the standard presentation in the case of $n = 3$ as such

$$\langle a, b \mid aba = bab \rangle = \textsc{Braid}_3 = \langle a, b, c, d \mid ab = bc = ca = d \rangle.$$

Notice that the two standard generators appear in both presentations. However, in the dual presentation we have a few more generators and a different flavor of relations coming from the poset of non-crossing partitions.

Definition 5.4.2 (Order Complex)**.** Let L be a locally ordered set. The *order complex* $\Delta(L)$. is the ordered simplicial complex with vertices labeled by elements of L and an ordered k-simplex on the vertices

$$v_{\ell_0}, v_{\ell_1}, \ldots, v_{\ell_k}$$

in $\Delta(L)$ whenever

$$\ell_0 < \ell_1 < \cdots < \ell_k$$

is a k-chain in L.

Remark 5.4.3. An ordered simplicial complex is just a simplicial complex with orders on the vertices.

5.5 The Dual Braid Complex

We may assign a local order on $\textsc{Braid}_n$ by the rule that $\beta_1 \leq \beta_2$ if $\beta_1^{-1}\beta_2$ is a dual simple braid. Each dual simple braid can be written as a product of positive half twists,

so it follows that each relation in this local order appears in the absolute order, but not vice versa.

Definition 5.5.1. The $(n-1)$ -dimensional order complex for this local order with the orthoscheme metric is the *dual braid complex*, denoted $\mathcal{D}_n$.

Remark 5.5.2. Equivalently, the dual braid complex is the flag complex of the Cayley graph for $\textsc{Braid}_n$ with respect to the set of dual simple braids (the generating set of $\textsc{Braid}_n$ in the dual presentation).

Remark 5.5.3 (Properties of the Dual Braid Complex)**.** Here we collect a few well known properties for the Dual Braid Complex. See [7] and [21] for details.

- $\mathcal{D}_n$ is contractible.
- The 1-skeleton of $\mathcal{D}_n$ is the (right) Cayley graph for $\textsc{Braid}_n$ with respect to the dual generators.
- $\textsc{Braid}_n$ acts freely on itself by left multiplication and this induces a simplicial action on $\mathcal{D}_n$ with the order complex $\Delta(NCP(n))$ as a fundamental domain. The k-simplices in $\mathcal{D}_n$ are:

  $$\mathrm{conv}(\beta\delta_{\pi_0}, \beta\delta_{\pi_1}, \ldots, \beta\delta_{\pi_k})$$

  where $\delta_{\pi_0} < \delta_{\pi_1} < \cdots < \delta_{\pi_k}$ is a chain of dual simple braids and $\beta \in \textsc{Braid}_n$.
- The quotient of this action is a single-vertex Δ-complex which is a quotient of $\Delta(NCP(n))$.

Example 5.5.4. $\mathcal{D}_3$ is a topologically the product of trivalent tree and the real line.

Consider the 3 string braid group with the dual presentation

$$B_3 = \langle a, b, c, d \mid ab = bc = ca = d \rangle.$$

The orthoscheme realization of the associated non-crossing partition lattice consists of three right triangles glued along the common hypotenuse. The dual braid complex is topologically the product of a trivalent tree with the real line. Each column exactly matches with the column in the $\mathbb{Z}^2$ generated by $(1,0),(0,1),(1,1)$ which is built up by orthoschemes. The thing to notice is that the dual braid complex for $d = 3$ is simply the $\mathbb{Z}^2$ from the discussion of buildings except with branching at each of the trivalent vertices.

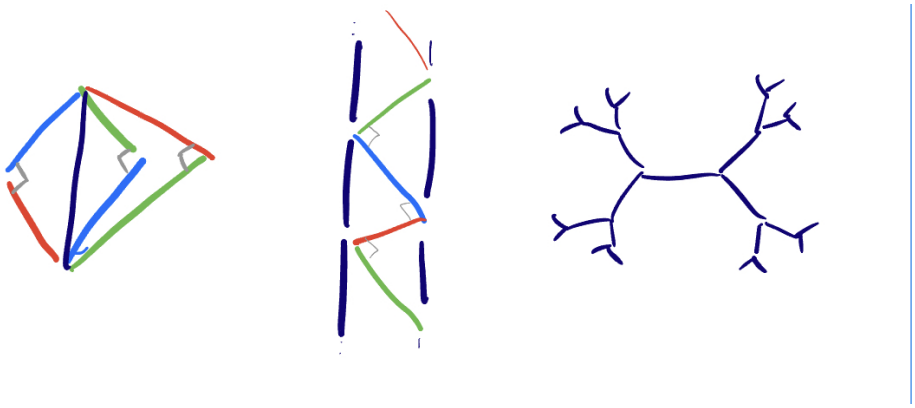

Figure 5.6: From left to right: The orthoscheme realization of NC_3, a column in the dual braid complex for $d = 3$, a portion of the trivalent tree cross-section of the dual braid complex.

In the figure above, the colors red, blue, and green match the generators a, b, and c with the common hypotenuse corresponding to the generator d. The dual braid complex whose quotient is that orthoscheme realization is topologically a trivalent tree crossed with the reals. Metrically, each of the interval edges seen in the cross-section looks like the tiling of a column with orthoschemes like in the middle picture. In total we obtain something whose skeleton is the Cayley graph for $\textsc{Braid}_3$ (with respect to the dual presentation).

For the 4 string version, the non-crossing partition lattice for $d = 4$ has 16 maximal chains, so the orthoscheme realization consists of 16 copies of 3-dimensional orthoschemes

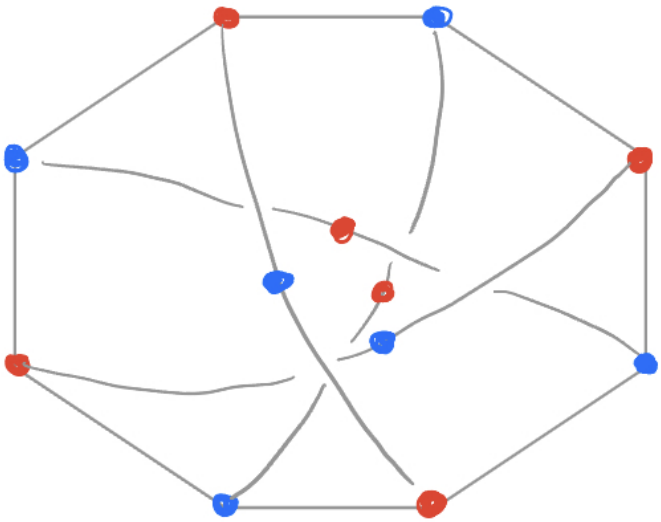

Figure 5.7: The graph corresponding to the link of the long edge in the orthoscheme realization for the Non-crossing partition lattice for $n = 4$.

all glued along the long diagonal which we can encode in a graph. The graph in Figure 5.7 is the small neighborhood to a point in the long edge. Perpendicular to long edge, taking an ε neighborhood we have $\pi/3$ arcs— 16 of them. Figure 5.7 is a visual representation of this long edge link. More reading on this subject in [7].

Chapter 6

Extracting Combinatorial Data From a Polynomial

This chapter aims to summarize a connection between a monic, complex polynomial and the combinatorial objects, non-crossing partitions, that was developed by Michael Dougherty and Jon McCammond in [12]. In particular, through a close examination of some examples, they establish that all polynomials of this type can be associated to two chains in the non-crossing partitions lattice that start at the discrete partition and end at the trivial partition. The figures contained in this chapter are copied from [12] with permission from the authors.

6.1 Monic Complex Polynomials Combinatorially

In this section, we aim to understand what specific combinatorial data we can associate with a monic complex polynomial. We will be especially interested what can be gleaned from the critical values of a polynomial.

Example 6.1.1 (Running Example)**.** Let p be the unique monic complex polynomial of

degree 5 with $p(0) = 0$ and critical points

$$\mathbf{cpt}(p) = \left\{-\frac{2}{5}, \frac{2}{5}, \frac{7-7i}{5}, \frac{10+i}{5}\right\}.$$

Concretely, $p(z)$ is the polynomial

$$p(z) = z^5 + \left(\frac{-17+6i}{4}\right) z^4 + \left(\frac{73-63i}{15}\right) z^3 + \left(\frac{34-12i}{25}\right) z^2 + \left(\frac{-308+252i}{125}\right) z.$$

The (rounded) critical values are

$$\mathbf{cvl}(p) = \{.8 - .6i, -6 + .5i, -8.5 - 4.3i, 3.6 - 6.9i\}.$$

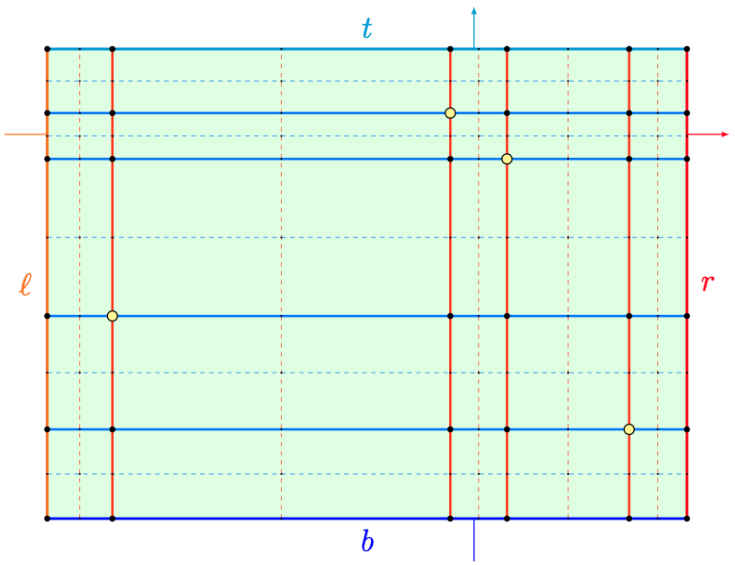

Figure 6.1: A subdivided rectangular complex R containing $\mathbf{cvl}(p)$ (they are the points in yellow).

We may obtain a subdivided rectangle as follows: bound all the critical values of p by a rectangle in $\mathbb{C}$. Using lines through each critical value in the horizontal and vertical

directions, we break it up into 25 rectangles.

Remark 6.1.2. We pay attention to critical points and critical values because, away from those, polynomials are local homeomorphisms (a quick consequence of the Inverse Mapping Theorem). If we remove the critical values and their preimages, what is left is a covering space. Because it is a covering space, an open rectangle that avoids critical values will pull back as open rectangles – evenly covered. So for p, each of the open rectangles pull back to 5 open rectangles in the domain.

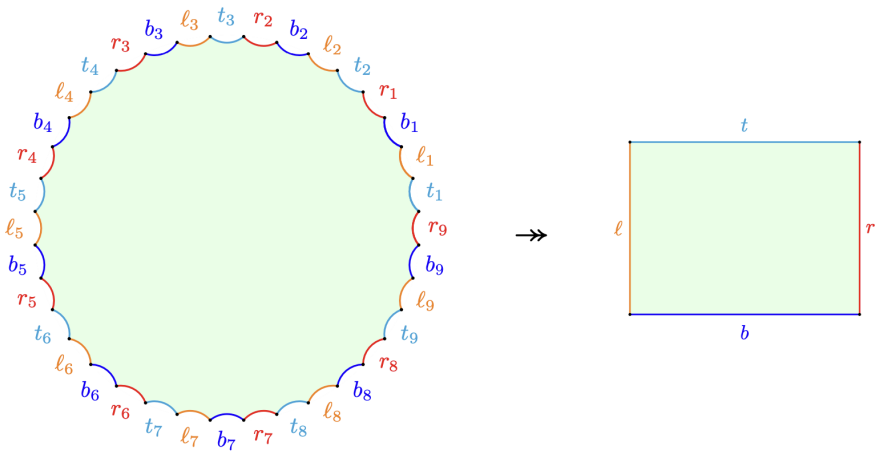

Figure 6.2: A d-sheeted branched rectangle, with the pullback metric, is a right-angled $4d$-gon.

Remark 6.1.3 (Polynomials exhibit branching)**.** A polynomial map $p : \mathbb{C} \to \mathbb{C}$ is a local homeomorphism away from its critical points and its a covering map once you remove the critical values and their preimages (the preimages are potentially a bigger set than just the critical points). There is finite branching at the critical points. It makes the domain behave like covering space except there are branched points—the critical points/other preimages of the critical values—where it looks more complicated.

Abstractly, given some map from a $4d$-gon to a rectangle, it must have some branching.

We can imbue the planar $4d$-gon with the pullback metric from the rectangle, discussion of which we push to Chapter 7. Except for isolated points, it is a local homeomorphism.

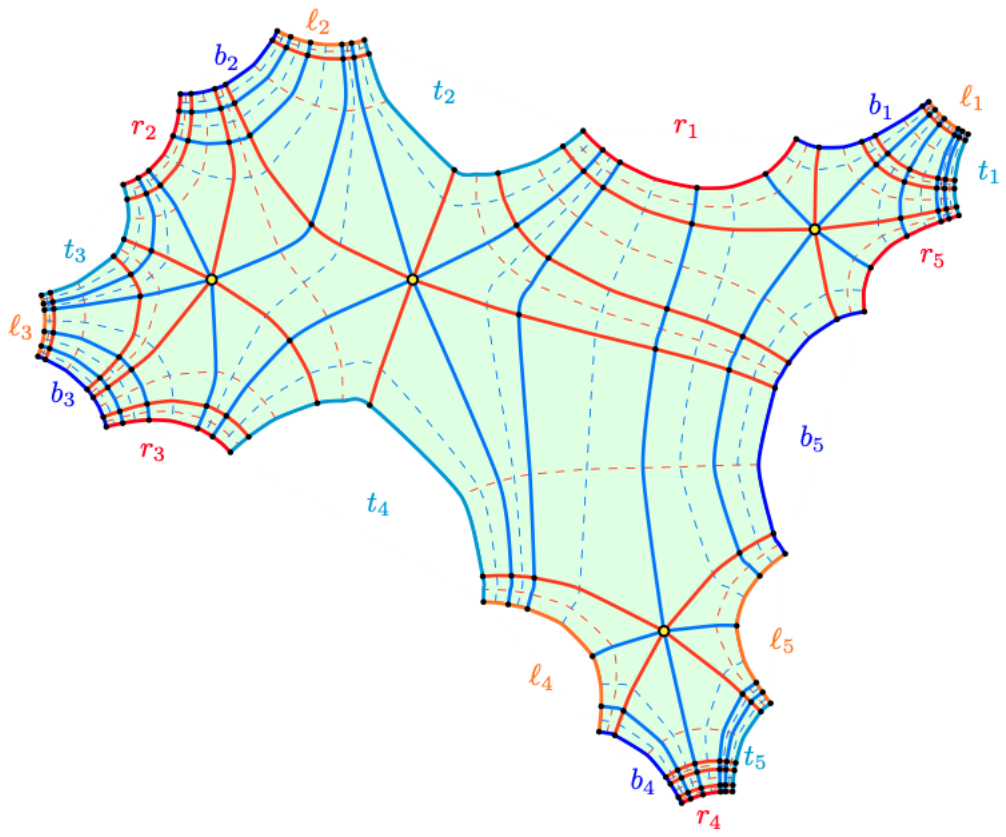

Figure 6.3: The preimage $p^{-1}(R)$ is a branched rectangular complex.

In the polynomial case of Example 6.1.1 where we had rectangles pulling back to 125 rectangles, we can use the metric on the output side to understand the metric on the preimage. It will no longer lie flat (isometrically embed) in the Euclidean plane with its usual metric, but it will enjoy some nice properties, namely it will be non-positively curved. It will look like a metric, piece-wise rectangular complex (even though the preimages look curved, it has the metric of a euclidean rectangle). At every vertex there

are either 4 corners meeting at 2π angle or 8 or 16, giving some multiple of 2π. Figure 6.3 exhibits the rectangular cell structure that encodes the 125 open rectangle preimages for our running example. The four distinguished points in yellow look like they have eight corners around them— they are the critical points.

In order to highlight the combinatorial information from a diagram like Figure 6.3, we may suppress the metric information. Consider the rectangle from Figure 6.1, but stylized so that all the rectangles are equal sizes.

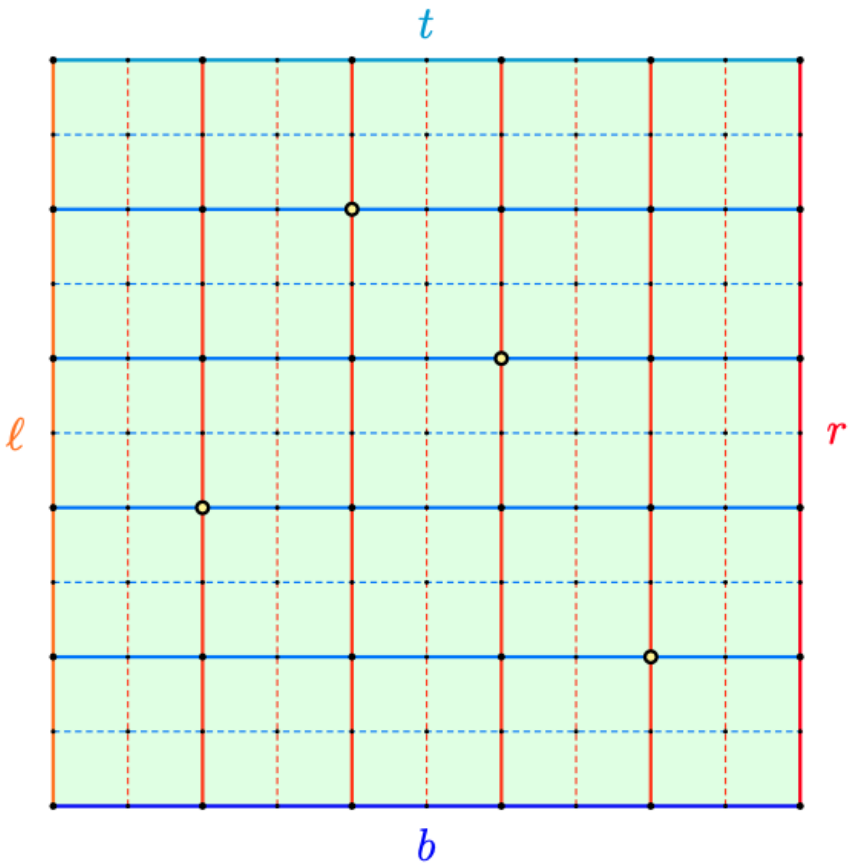

Figure 6.4: This stylized version of Figure 6.1 suppresses the metric information to highlight the combinatorial structure.

The boundary of this rectangle is regular, and far from the critical values, this polynomial behaves like $z \mapsto z^d$ (wrapping around a large circle on itself d times. When we

pull back the regular rectangle we would get a 20-gon, and ignoring metric information for the preimage in Figure 6.3 we obtain the content of Figure 6.5.

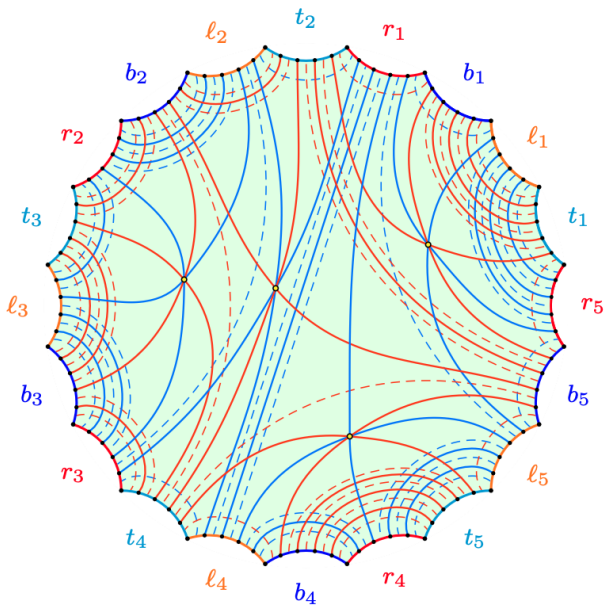

Figure 6.5: The stylized version of Figure 6.3.

Remark 6.1.4 (Regular points)**.** To understand the combinatorics, instead of considering the lines that runs through critical values, lines through the rectangle consisting of only regular points are more useful. In Figures 6.4 and 6.5, this will correspond to removing the solid lines and instead focusing on the dotted lines as in Figure 6.6.

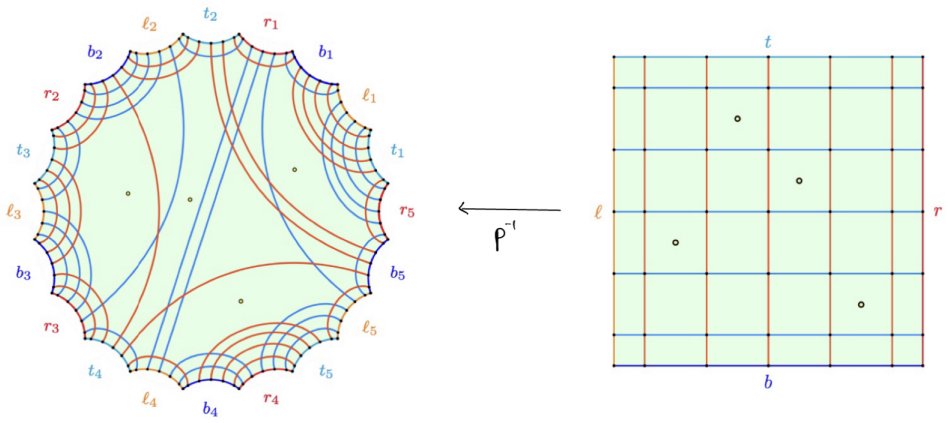

Figure 6.6: The same rectangle and branched rectangle from Figures 6.4 and 6.5, now with regular horizontal and vertical lines in the pullback.

The regular lines being pulled back do not branch. Since the lines avoid the critical values on the range side, their preimages are unions of disjoint unbranched arcs. In order to highlight the combinatorics, we can 2-color a regular top-bottom split, and pull it back to obtain this pair of figures:

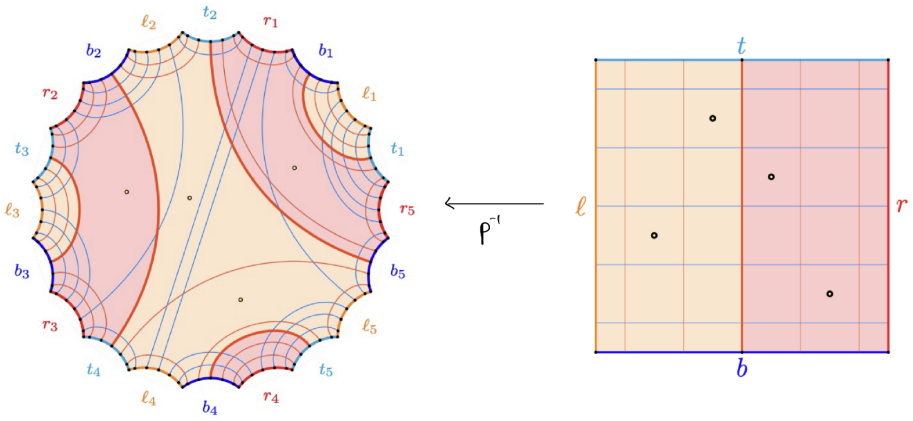

Figure 6.7: A vertically separated 2-coloring that avoids $\mathbf{cvl}(p)$ and its pullback.

At this point, we can start to see the non-crossing partitions that can arise from this example. In all these figures, we are using rectangular coordinates on the output, pulling

back horizontal and vertical lines and getting nice and regular curves, and they uncover non-crossing combinatorics.

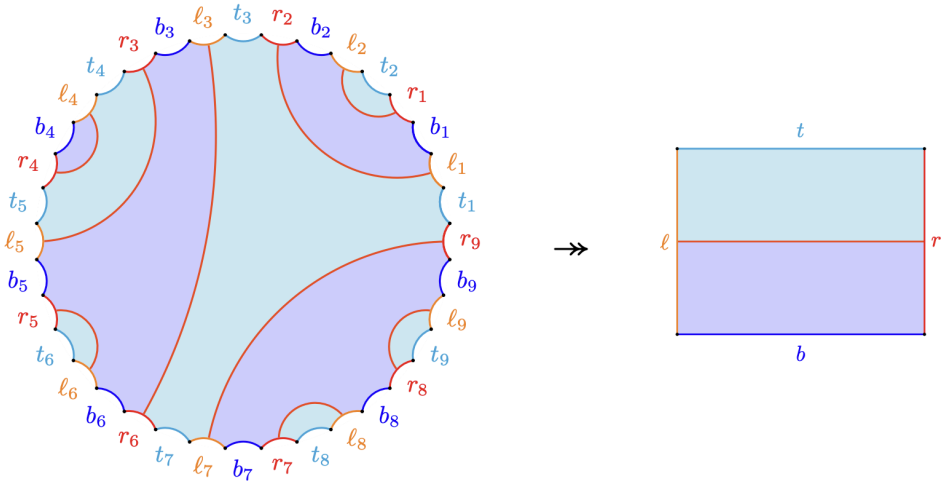

Figure 6.8: Preimages of regular lines are non-crossing matchings.

Example 6.1.5. On Figure 6.8, we see an example of a general phenomenon. As an important note, this figure relates more closely to a degree 9 polynomial, not our running example. The degree increased so that the non-crossing data is more prominent. In this example, if you have a horizontal line the connects left and right side and avoids all critical values, the preimage will have to be things that start at the 9 left sides, travel along non-branched arcs, to the 9 right sides. Further, they can never cross because they are all regular preimages, so it pulls back like a covering space. The result is what is called a *non-crossing matching* of the 9 "left" and "right" sides. And this phenomenon stays true, some potential matchings are prohibited if they have a crossing. So, non-crossing phenomenon are appearing.

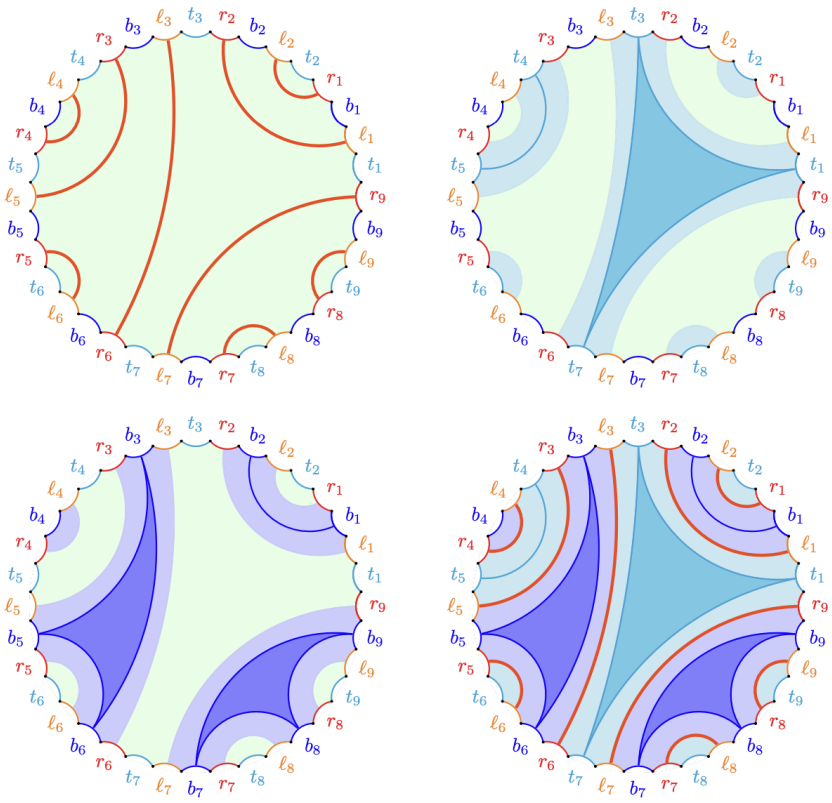

Figure 6.9: non-crossing matchings equivalently induce non-crossing partitions.

Remark 6.1.6 (Non-crossing matchings induce non-crossing partitions)**.** Intuitively, non-crossing matchings give non-crossing partitions.

In Figure 6.9, the matching in the top left connects "left" and "right" sides. It induces a non-crossing partition of the "top" sides (the top right diagram) by considering the largest such partition that doesn't cross the arcs in the matching. Dually, it also defines a non-crossing partition of the "bottom" sides (the bottom left diagram) in the same way. Equivalently, given a non-crossing partition of the "tops" or of the "bottoms," we can recover the non-crossing matching. The dual non-crossing partitions and the non-crossing matching are superimposed in the bottom left diagram.

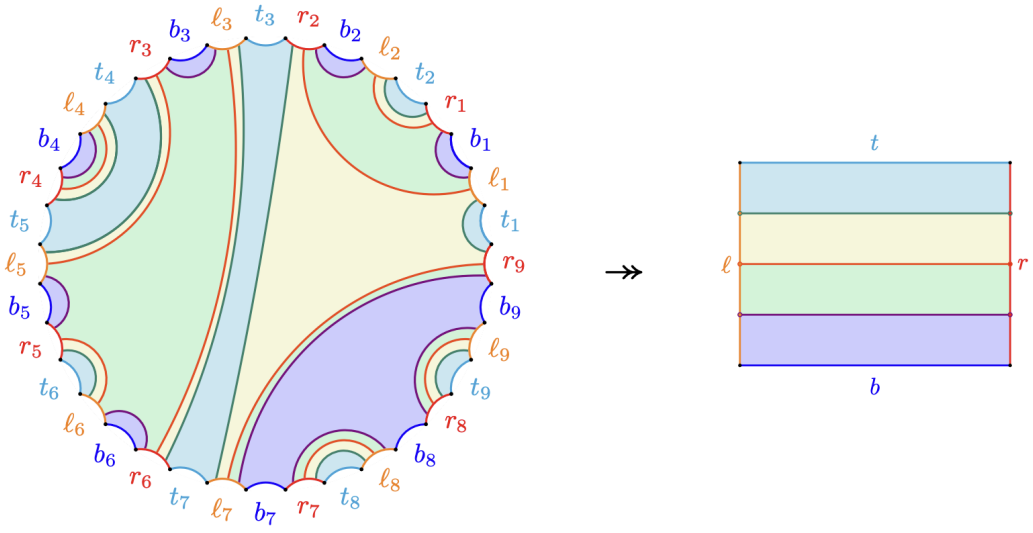

Figure 6.10: Parallel line preimages determine chains of non-crossing partitions.

Remark 6.1.7 (Morse theory gives chains)**.** Using the real and imaginary directions, we obtain height functions and can effectively use Morse theory on the preimage. Pulling back the purple region in Figure 6.10 determines a non-crossing partition. Pulling back the green and purple together gives another non-crossing partition, which covers (in the poset sense) the previous non-crossing partition. Continuing like this, the bottom to top Morse theory on this preimage determines a chain in the non-crossing partition lattice, starting at the discrete partition, and ending at the trivial partition. Note that this chain need not be maximal.

A similar thing is happening in Figure 6.7 with a left-right Morse theory. Another thing to note is that the partition changes to a larger one exactly after passing through critical values on the output.

To help visualize the non-crossing partitions and chains, below is the non-crossing partition lattice for $d = 4$ using these diagrams.

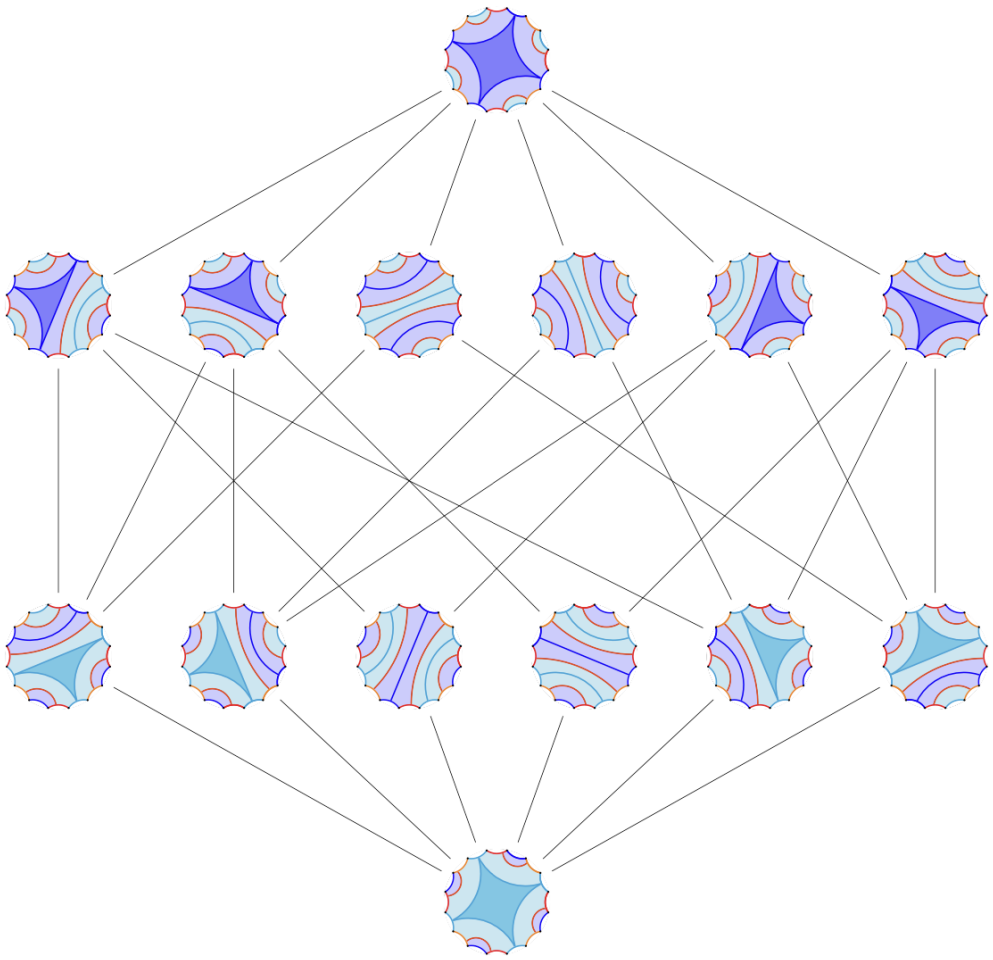

Figure 6.11: The non-crossing partition lattice for $d = 4$, in the point of view of branched rectangle diagrams.

Remark 6.1.8 (Two chains for every polynomial)**.** Effectively, every polynomial determines not one, but two chains in the non-crossing partition lattice, one from bottom-top Morse theory, and one from left-right Morse theory. The length of the chain from the bottom-top is given by the number of distinct latitudes (horizontal cuts) of critical values and the length for the left-right Morse theory is the number of distinct longitudes (vertical cuts) for the critical values.

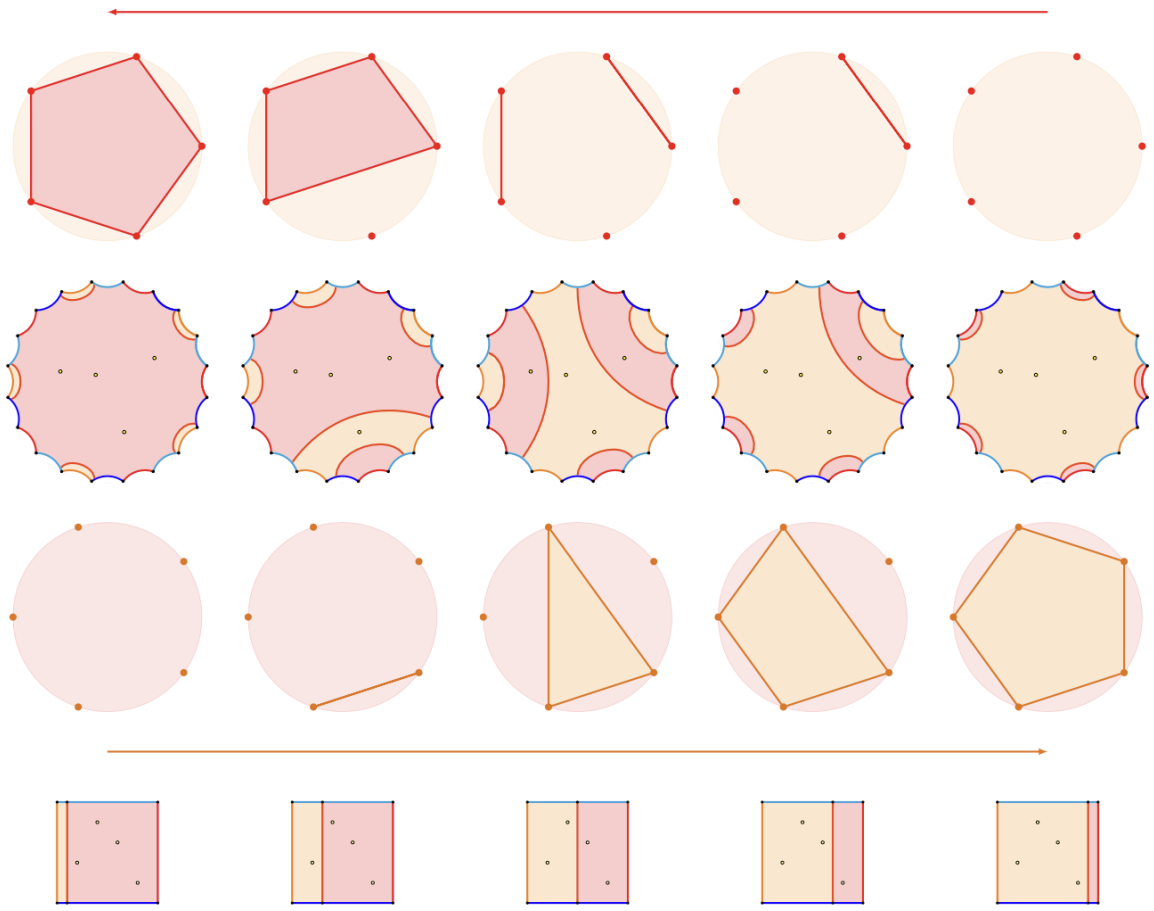

Figure 6.12: Left (or right) non-crossing partition chains determined by left-right, (or right-left) Morse Theory on the preimage.

To really drive this point home, Figure 6.12 illustrates: on the top level, a chain in the non-crossing partition lattice; on the next level, a series of branched rectangle diagrams determining that chain; on the 2nd level from the bottom, another non-crossing chain which is the dual chain to the top level (with respect to Kreweras compliment); on the bottom level, the rectangle diagrams that determine these chains. In Figure 6.13, is the same idea on the vertical Morse theory for this example rectangle diagram.

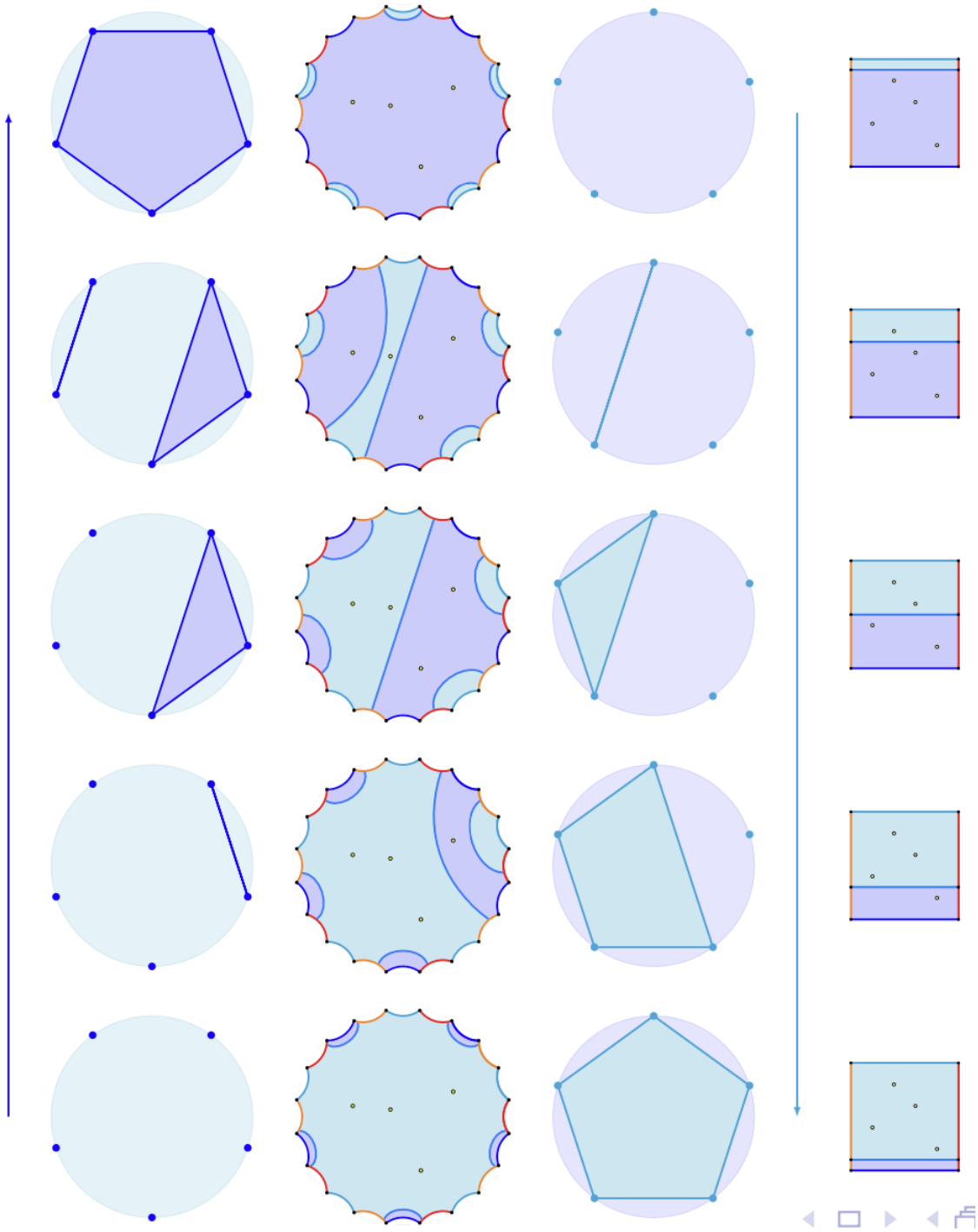

Figure 6.13: Morse theory in the vertical direction on the same example and the corresponding non-crossing partition chains.

In 1799, Gauss tried to prove the Fundamental Theorem of Algebra by focusing on the pullback of the real and imaginary axes. Given a complex polynomial with no critical values on the real or imaginary axis, Gauss noted that the pullback of the real and imaginary axis consisted of $4d$ rays. Moreover, every real axis preimage intersects exactly one imaginary axis preimage. The pull back of the intersection determines a root.

A few centuries later in 2007, Martin, Savitt, and Singer considered similar pullbacks from a combinatorial perspective, which they call *basketballs*.

Definition 6.1.9. A *basketball* is a pair of non-crossing matchings with the given compatibility condition: Every arc from the first non-crossing matching intersects exactly one arc in the other non-crossing matching and vice versa.

Proposition 6.1.10. *Let $p \in \mathbb{C}\text{-}\textsc{Poly}_d^{mc}(R)$. Every regular cross in R pulls back as a pair of non-crossing matchings satisfying the basketball criterion.*

Proof: Evidently, the preimage under polynomial maps of rectangle diagrams with crossing lines satisfy this condition so long as the crossing lines are regular (in the sense that they don't meet a critical value). Since, if they crossed multiple times in the preimage, the same would be true in R. Diagrams for the pullback of a cross resulting in basketballs are in Figure 6.14 and Figure 6.15. □

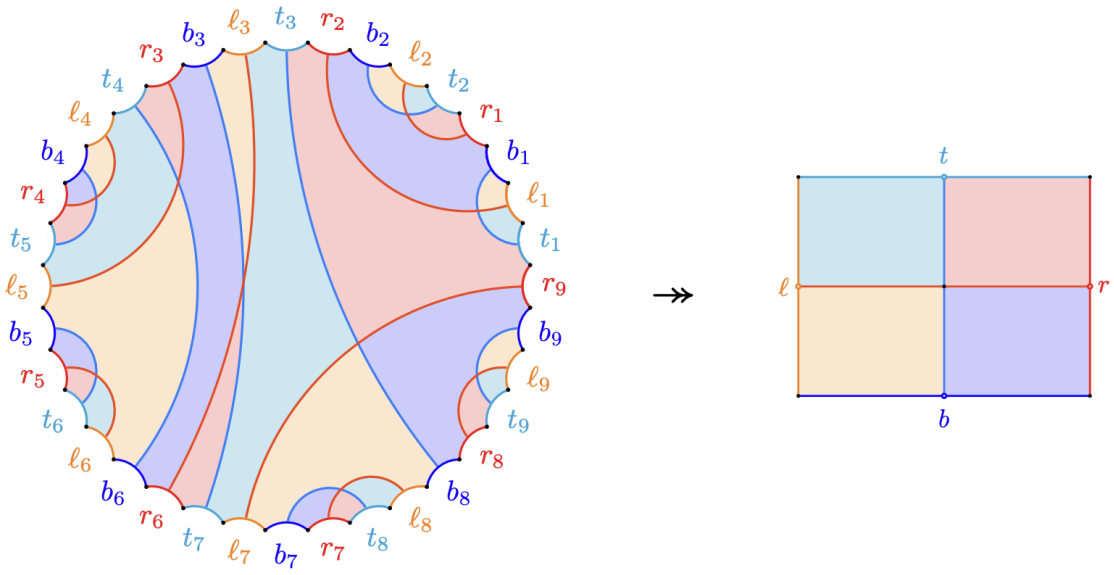

Figure 6.14: Crossing line preimages are basketballs.

Here is similar figure with respect to the example in the other figures.

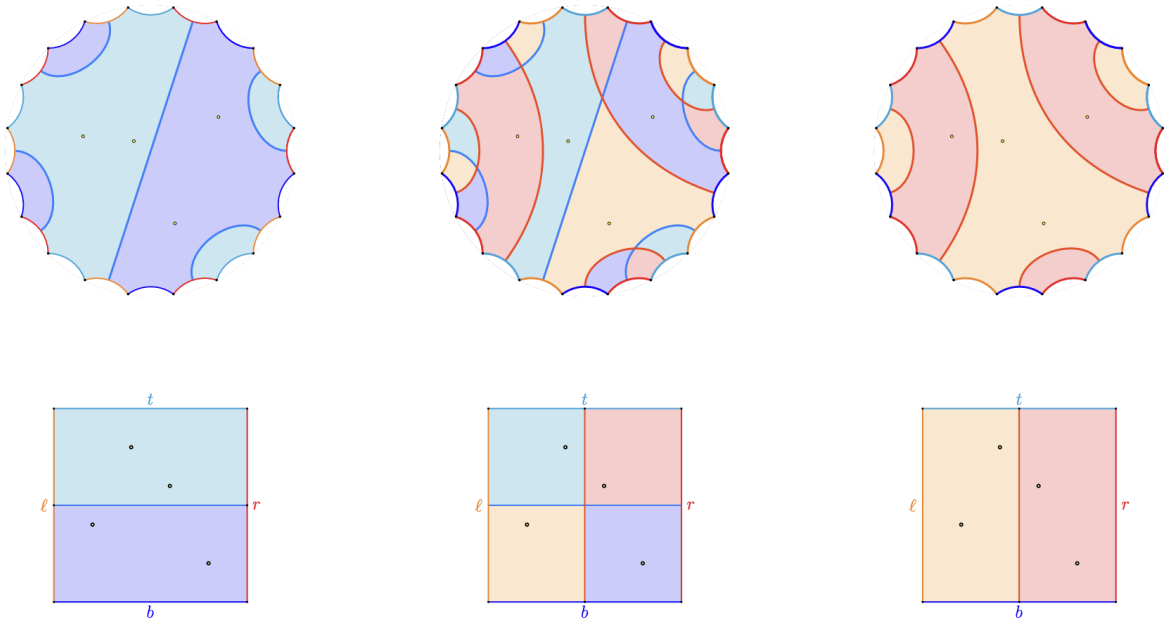

Figure 6.15: Basketball diagram associated to a specific polynomial.

Remark 6.1.11. If ever a "plus sign" can be drawn in the rectangle diagram avoiding any critical value latitudes or longitudes, they will pull back forming a basketball. The generic example we have been working with has 25 such "plus signs" pulling back to distinct basketballs. See below for the plus signs and their pullbacks in Figure 6.16 and Figure 6.17 that come from the 5 different horizontal separating lines and the 5 different vertical separating lines.

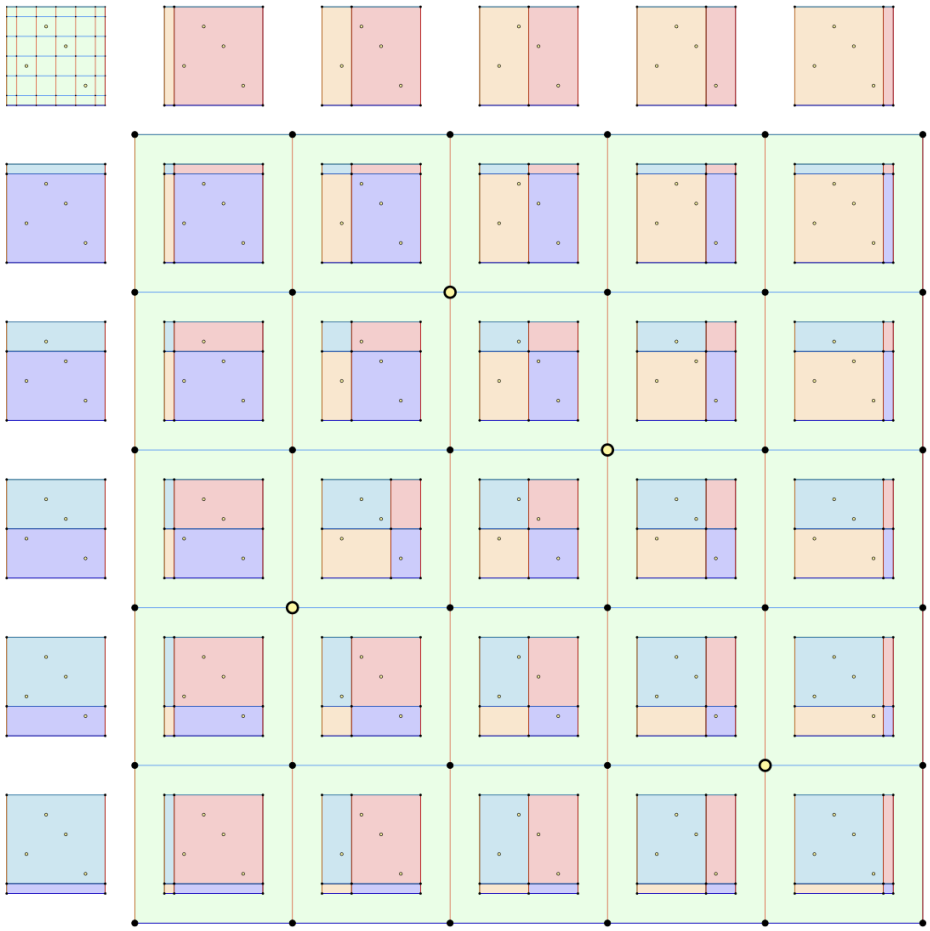

Figure 6.16: The 25 different plus signs avoiding all critical values.

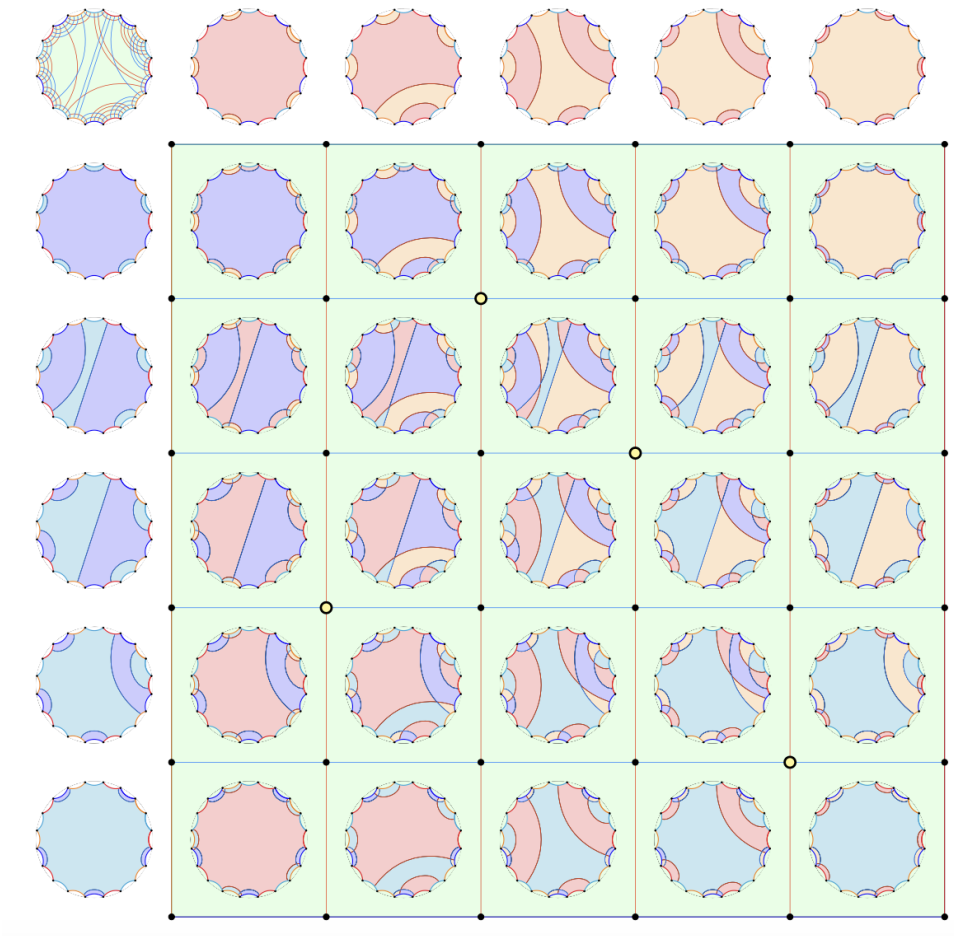

Figure 6.17: The 25 corresponding basketballs matching with Figure 6.16.

Chapter 7

Geometry of Monic Complex Polynomials

This chapter continues to highlight the recent work of Michael Dougherty and Jon McCammond. In particular, it illuminates the natural correspondences between three spaces:

- monic complex polynomials of degree d.
- d-sheeted branched covers of a Euclidean rectangle R.
- metric cell complexes built from non-crossing partitions called the (metric) Basketball Complex.

The third viewpoint leads to a new geometric combinatorial parametrization of the space of complex polynomials.

Garside Structures led to at least two different classifying spaces for the Braid Group. There was the Salvetti Complex, which could be thought of as a quotient of the permutohedron, and the Dual Braid Complex with the orthoscheme metric. The original construction of the Dual Braid Complex had nothing to do with complex polynomial space.

However, the (metric) Basketball Complex with side identifications, which corresponds as a metric cell complex to the space of monic complex polynomials with distinct roots, admits a deformation retraction onto the Dual Braid Complex as its spine.

7.1 Basketball Complex

As established in Chapter 6, there is a lot of combinatorial information that is appearing for a single polynomial. Each regular horizontal cut on a rectangle bounding the polynomial's critical values pulls back to give a non-crossing partition/matching and same for regular vertical cuts. Each pair pulls back in a compatible way to form basketballs.

The cell complex $|NCP_d| \times |NCP_d|$ has top-dimensional cells that are the product of two n-dimensional simplices (recall we have set $n = d - 1$) corresponding to maximal chains in the non-crossing partition lattice.

The vertices in the direct product are ordered pair of vertices, one from each factor. However, to identify the subcomplex that agrees with the combinatorics for polynomials we require the extra condition that the pair corresponds to a basketball.

Definition 7.1.1 (Basketball Vertices)**.** The vertices in $|NCP_d| \times |NCP_d|$ that satisfy the basketball criterion are called *basketball vertices*.

Definition 7.1.2 (Basketball Complex)**.** The *basketball complex* is the full subcomplex restricted to the basketball vertices. We also call this the *branched rectangle complex* $\textsc{BrRect}_d$.

Remark 7.1.3. Even though the order complex for the non-crossing partition lattice is not a manifold, and neither is the direct product with itself, restricting to the basketball vertices is topologically a $2n$-dimensional ball. This becomes apparent using results from this chapter.

So, for each polynomial with critical values in R we can determine a pair of chains in the non-crossing partition lattice that are compatible under the basketball criterion. Other polynomials may give the same pair of chains. All those with the same basketballs forming determine a cell in the basketball complex. The polynomial in Example 6.1.1 is a degree 5 polynomial with 4 critical values that each had distinct real and imaginary components and in $\textsc{BrRect}_d$ its combinatorics determines an 8-cell (the product of two 4-simplices) shared by any other monic degree 5 polynomial with critical values in R which admits the same pair of non-crossing partitions/matchings chains.

For a less generic distribution of 4 critical values in R, for example if some critical values have higher multiplicities or if they share a real or imaginary component, instead of getting maximal chains, we would get some shorter chains, and would place us into a lower dimensional cell. The cell structure of the basketball complex encodes coincidences between the real and imaginary parts of the critical values.

Now lets reinforce the metric information that we have been ignoring as of yet. To do this we invoke the following specific use of the pullback metric, which is well behaved everywhere the polynomial acts as a local homeomorphism.

The space $\textsc{Mult}_n(U)$ has a natural metric as inherited from the Euclidean metric on $\mathbb{C}^n$ under the quotient by the symmetric group action.

Definition 7.1.4. Given a polynomial $p \in \mathbb{C}\text{-}\textsc{Poly}_d^{mc}(U)$. For $z_1, z_2 \in \mathbb{C}$ such that $p(z_1), p(z_2) \in U \subset \mathbb{C}$. We define the *pullback metric for* p as follows: Let $\{H_\alpha\}_{\alpha \in J}$ be the set of all paths from z_1 to z_2 and define $d_p(z_1, z_2)$ to be the minimum length of the paths $\{p(H_\alpha)\}_{\alpha \in J}$.

The pullback metric on the polynomial space $\mathbb{C}\text{-}\textsc{Poly}_d^{mc}(U)$ is defined similarly.

Definition 7.1.5 (Pullback Metric on Polynomial Space)**.** Let $\{H_\alpha\}_{\alpha \in J}$ be the set of all paths in polynomial space from two polynomials $p_1, p_2 \in \mathbb{C}\text{-}\textsc{Poly}^{mc}(U)$ and define the

pullback metric on polynomials to be the minimum length of $\{\mathbf{cvl}(H_\alpha)\}_{\alpha\in J}$, where that length is with respect to the natural metric in $\textsc{Mult}_n(U)$.

Remark 7.1.6 (Coordinates)**.** The combinatorics of a branched rectangle determines a cell in the basketball complex. The specific metric information determines the specific point in the interior of this cell. In particular, the relative sizes of the width of the small rectangles give barycentric coordinates in one simplex and the relative sizes of the heights of the small rectangles give barycentric coordinates of the other simplex.

So, recovering the metric information gives the specific point in the simplicial complex. Other monic polynomials of the same degree with critical values in the same rectangle may determine the same combinatorics and land in the same cell, but with the metric information the point is uniquely determined by a polynomial up to precomposition with a translation, i.e. it uniquely determines a monic centered polynomial.

Theorem 7.1.7 (Basketballs and Branched Rectangles)**.** *The points of the basketball complex* $\textsc{BrRect}_d(R)$ *are in natural bijection with the space of all (based) planar d-sheeted metric branched covers of a metric rectangle R.*

Not only do we have the ability to associate a polynomial with a point in the basketball complex $\textsc{BrRect}_d$, we can also put a nice cell structure on the polynomial space that agrees with that of the basketball complex. That work from [11] and [10], is summarized here.

Given a generic polynomial, if you took the roots and moved them around, that determines a path in the space of polynomials. This would also determine a path of the critical values in the range. We want something like path-lifting so that if we move critical values, we would like to have that determine a path in the space of polynomials in a unique way given the start point. There are technical details to worry about because

the map from polynomials over to polynomials determined by critical values is not always a local homeomorphism, it exhibits branching. Bearden, Carney, and Ng proved in 2002 the following:

Theorem 7.1.8 (Bearden, Carney, Ng 2002)**.** *Every possible distinct set of n complex numbers are critical values for a monic complex polynomial up to translation.*

It boils down to the existence of a map from $\mathbb{C}^n \to \mathbb{C}^n$ such that if the determinant of the Jacobian is nonzero, it is a local homeomorphism. They were able to determine that the map is a local homeomorphism if the critical values are distinct. And as such, any path like this can be lifted back to the space of polynomials.

From this, we know that all the points in the interior of the top-dimensional cells (product of two orthoschemes) and all the paths in that interior can be lifted uniquely. To be clear, this is the scenario when all critical values are distinct. The ultimate goal is to continue this procedure to extend it to the facets of these cells when critical values have some multiplicities.

Concretely, given $p \in \mathbb{C}\text{-}\textsc{Poly}_d^{mc}$, we can factor $p'(z) = d(z - z_1)\dots(z - z_n)$ and record the vector $\vec{z} = (z_1, \dots, z_n) \in \mathbb{C}^n$. With the extra assumption that $p(0) = 0$ we can rebuild the polynomial

$$p(z) = \int_0^z d(w - z_1)\dots(w - z_n)dw.$$

So the map $\vec{z} \mapsto ((p(z_1), \dots, p(z_n))$ maps the tuple of critical points to the critical values which is a polynomial defined map. But the output is really a n-tuple of multivariable polynomials. The Jacobian is an $n \times n$ matrix with partial derivatives with respect to the variables. As long as $z_i's$ are distinct and nonzero, the determinant of this Jacobian is also nonzero according to Bearden, Carney, and Ng.

To allow for multiplicity, assume $p'(z) = d(z - z_1)^{m_1} \dots (z - z_k)^{m_k}$ where $\sum m_i = n$ with fixed $m_i's$. The $k \times k$ matrix corresponding to this setup had a Jacobian whose determinant admits a clean factorization into linear terms, established in [10].

Theorem 7.1.9. *Determinant of that Jacobian is*

$$\frac{1}{\binom{n}{m_1, \dots, m_k}} \prod_{j=1}^{m} (-z_j)^{a_j} \prod_{1 \le j \ne k < m} (z_k - z_j)^{a_j}.$$

Therefore,

Corollary 7.1.10. *If the critical points for the set of polynomials remain distinct and nonzero, we have a local homeomorphism.*

Essentially, via the unique lifting of paths in the polynomial space $\mathbb{C}\text{-}\textsc{Poly}_d^{mc}(R)$ established in the work of Dougherty and McCammond in [11], we get a cell structure on $\mathbb{C}\text{-}\textsc{Poly}_d^{mc}(R)$ coming from the basketball complex. By recognizing that the map from $\mathbb{C}\text{-}\textsc{Poly}_d^{mc}(R) \to \textsc{BrRect}_d(R)$ is a cellular map, and that the two complexes agree on the number $n!d^{d-2}$ of top dimensional cells, we have some indication that this map is injective. As a consequence of the fact that the braid group action on maximal chains is transitive on maximal chains in the non-crossing partition lattice, we can establish that the map is onto. So, since they agree on count and the map is onto, we also get injectivity.

Theorem 7.1.11. *There are homeomorphisms* $\textsc{BrRect}_d(R) \cong \mathbb{C}\text{-}\textsc{Poly}_d^{mc}(R) \cong \mathbb{D}^{2n}$ *which restrict to* $int(\textsc{BrRect}_d(R)) \cong \mathbb{C}\text{-}\textsc{Poly}_d^{mc}(int(R)) \cong int(\mathbb{D}^{2n})$.

7.2 Polynomials Topologically

The conversation in this section is designed to illustrate why the basketball complex discussed in Section 6.1 is flexible enough to describe as a metric object the entirety of $\mathbb{C}$-$\textsc{Poly}_d^m(\mathbb{C})$ regardless of the choice of rectangle, which in Section 6.1 was chosen simply to bound the critical values of the polynomial in Example 6.1.1. In particular,

Theorem 7.2.1. $\mathbb{C}$-$\textsc{Poly}_d^{mc}(\mathbb{C}) \cong \mathbb{C}$-$\textsc{Poly}_d^{mc}(int(R))$. *In particular, we get that the branched rectangle complex, built out of basketball vertices is a compactification of the monic centered complex polynomials.*

To establish Theorem 7.2.1, the main tool is the idea of a nonsplitting homotopy, which we will describe here, drawn from [12].

Definition 7.2.2 (Homotopies)**.** A *point homotopy* is a map $H : U \times I \to Y$ with $I = [0, 1]$. We write $H(u, t) = h_t(u) = h^u(t)$ for each $u \in U$ and $t \in I$. These refer to the time map $h_t : U \to Y$, and the path map $h^u : I \to Y$. We also write u_t for $H(u, t) = h^u(t)$ and U_t for $H(U, t) = h_t(U)$, so that h^u is a path from u_0 to u_1 and H is a homotopy from U_0 to U_1.

Whenever we have a homotopy on points in $\mathbb{C}$ it induces a homotopy of the tuples in $\mathbb{C}^n$ and a homotopy of multisets in $\textsc{Mult}_n(\mathbb{C})$ for any $n \in \mathbb{N}$.

Definition 7.2.3 (Induced Homotopies)**.** Let $H : U \times I \to \mathbb{C}$ be a point homotopy from U_0 to U_1 inside $\mathbb{C}$. There is a corresponding *tuple homotopy* $H^n : U^n \times I \to \mathbb{C}^n$ from $(U_0)^n$ to $(U_1)^n$ inside $\mathbb{C}^n$, defined by $H^n(\mathbf{z}, t) = (H(z_1, t), \ldots, H(z_n, t))$ for each $n \in \mathbb{N}$, with $\mathbf{z} = (z_1, \ldots, z_n) \in \mathbb{C}^n$ and $t \in I$. The multiset quotient $\textsc{Mult}(H^n(\mathbf{z}, t))$ is constant under the $\textsc{Sym}_n$-action of permuting coordinates. So we also have an induced homotopy $H_n : \textsc{Mult}_n(U) \times I \to \textsc{Mult}_n(C)$ from $\textsc{Mult}_n(U_0)$ to $\textsc{Mult}_n(U_1)$ inside $\textsc{Mult}_n(\mathbb{C})$, by taking the relevant multisets of each piece. In particular, if $M \in \textsc{Mult}_n(U)$ is an

n-element multiset in U and $\mathbf{z} \in U^n$ is any n-tuple with $M = \textsc{Mult}(\mathbf{z})$, then $H_n(M,t) = \textsc{Mult}(H^n(\mathbf{z},t))$.

The induced time maps are $(h^n)_t : U^n \to \mathbb{C}^n$ for H^n and $(h_n)_t : \textsc{Mult}_n(U) \to \textsc{Mult}_n(\mathbb{C})$ for H_n and the induced path maps defined as expected are $(h^n)^{\mathbf{z}}$ and $(h_n)^M$, respectively.

The key feature we want to record is whether the point paths in point homotopies merge or split.

Definition 7.2.4 (Splitting and Merging)**.** Let $H : U \times I \to \mathbb{C}$ be a point homotopy. We say that H *splits* points if there are distinct points $u, v \in U$ and distinct times $s < t \in I$ such that $u_s = v_s$ and $u_t \neq v_t$. Similarly, we say that H *merges* points if there are distinct points $u, v \in U$ and distinct times $s < t \in I$ such that $u_s \neq v_s$ and $u_t = v_t$. When H does not split points it is *nonsplitting* and when it does not merge points it is *nonmerging*. A point homotopy that is both nonsplitting and nonmerging, *preserves points*. In particular, for a point-preserving homotopy, $u_s = v_s$ at some time $s \in I$ if and only if $u_t = v_t$ for all $t \in I$.

Remark 7.2.5. When H is a nonsplitting point homotopy, points with $u_0 = v_0$ stay together throughout, so the entire homotopy H factors through the quotient map $h_0 \times \mathbf{1} : U \times I \twoheadrightarrow U_0 \times I$ to produce a simpler point homotopy $H' : U_0 \times I \to \mathbb{C}$. This allows us to assume without loss of generality, that all nonsplitting homotopies are injective at time $t = 0$ with $U = U_0$.

A nonsplitting point homotopy leads to multiset paths that are uniquely liftable.

Remark 7.2.6 (Nonsplitting)**.** Let $H : U \times I \to \mathbb{C}$ is a point homotopy and let H_n be the corresponding multiset homotopy. When H is nonsplitting, the points in a multiset path can merge but not split, which means that they have a weakly increasing shape. In

particular, multiset paths in H^n satisfy the necessary conditions to be uniquely liftable through the **cvl** map.

In particular, we can carry along these ideas into polynomials.

Definition 7.2.7 (Polynomial Homotopies)**.** Let $H : U \times I \to \mathbb{C}$ be a nonsplitting point homotopy with $U = U_0 \subset \mathbb{C}$. We can use the polynomial path lifting theorem to define a function $\mathbb{C}\text{-Poly}(H) : \mathbb{C}\text{-Poly}_d^{mc}(U) \times I \to \mathbb{C}\text{-Poly}_d^{mc}(\mathbb{C})$ as follows. Let p be a monic centered degree d polynomial and let $M = \mathbf{cvl}(p) \in \text{Mult}_n(U)$. There is a unique lift of $(h_n)^M$ to a path $P : I \to \mathbb{C}\text{-Poly}^{mc}(U)$ that starts at p. Finally, we define $\mathbb{C}\text{-Poly}(H)$ at the point $(p, t) \in \mathbb{C}\text{-Poly}_d^{mc}(U) \times I$ to be $P(t)$.

Remark 7.2.8. In particular, given a nonsplitting point homotopy $H : U \times I \to \mathbb{C}$ The function $\mathbb{C}\text{-Poly}(H)$ is continuous and a homotopy of polynomial spaces.

When the point homotopy preserves points, we get an even stronger condition for the induced polynomial homotopies

Lemma 7.2.9 (Homeomorphisms)**.** *If $H : U \times I \to \mathbb{C}$ is a point preserving homotopy, then all the $\mathbb{C}\text{-Poly}(H)$-induced maps $\mathbb{C}\text{-Poly}_d^{mc}(U_s) \to \mathbb{C}\text{-Poly}_d^{mc}(U_t)$ with $s < t \in I$ are homeomorphisms.*

Remark 7.2.10. This establishes most of Theorem 7.2.1 since we may easily construct point preserving homotopies from $\mathbb{C}$ to the interior of any rectangle in $\mathbb{C}$. The compactifications also can be shown to behave nicely. If we do have a merging homotopy, like in a homotopy that deforms a rectangle into an annulus, the result is a quotient. Since monic and centered polynomials with distinct roots are homeomorphic to monic, centered polynomials with critical values in an annulus, this implies that these polynomials can be compactified as the branched rectangle complex with side identifications. The induced map from the closed annulus to a circle induces through polynomials a map that realizes

the Dual Braid Complex as the spine of this side-identified branched rectangle complex. The idea is summarized in Theorem 7.2.11 and details can be found in [12].

Theorem 7.2.11. *Give a homotopy from a rectangle to an annulus in* $\mathbb{C}$*, the induced polynomial homotopy realizes that the space* $\mathbb{C}$-$\textsc{Poly}_d^{mc}(\mathbb{C}^*)$ *can be compactified as the branched rectangle complex with side identifications, called the branched annulus complex, which deformation retracts onto the Dual Braid Complex as its spine.*

Part II

Real Polynomials and their Underlying Combinatorics

The chapters in Part 2 focus on the real polynomial analogs of the Branched Rectangle Complex (also called the Basketball Complex) which compactifies monic, centered complex polynomials and the Branched Annulus Complex, with compactifies monic, centered polynomials with distinct roots. The first chapter highlights the special combinatorics that guide these discussions. The second and third deal with the cell complexes.

Chapter 8

Specialized Non-crossing Combinatorics

In the case of polynomials whose coefficients are real, the combinatorics discussed in Chapter 6 become more restrictive. Consider, for example the polynomial $p(z) = z^7 - 10.5z^6 + 48z^5 - 121z^4 + 1723z^3 - 131z^2$ and the corresponding preimage of a subdivided rectangle shown in Figure 8.1. There is an obvious reflection symmetry with respect to the x-axis, and this has a major impact on the combinatorics. In this chapter we investigate the structure of these more restrictive non-crossing features.

Within the literature on non-crossing partitions, there has been significant study of Type B non-crossing partitions. These arise by studying the dihedral group action on the set of non-crossing partitions, in particular those partitions fixed by rotations. This viewpoint is discussed in length in [24]. A similar study can be made for the stabilized non-crossing partitions of the reflections, which was started with varying levels of depth in [8] and especially by Ding in his dissertation [9]. A more pointed study of these non-crossing phenomenon is introduced here as a tool towards understanding (monic) polynomials with real coefficients. It should be noted that several of the similar results

from [9] that are presented here with updated proofs are being prepared for publication in joint work from Ziqian Ding and myself. Recall that the basketball complex concerns itself with chains in the non-crossing partition lattice and their products, subject to the basketball condition. In addition to the reflection symmetric non-crossing partitions, we also see a unique style of non-crossing partition chains when studying real polynomials which we call *palindromic* chains. Much less is known about these chains, which are being introduced here. We connect them with other combinatorial objects that may lend themselves to easier study.

The outline of this chapter is as follows: We start in Section 8.1 by introducing the relevant definitions for the specific subtype of non-crossing partitions that are the main focus of the chapter– reflection symmetric non-crossing partitions. This type of non-crossing partitions creates a sublattice of the regular non-crossing partition lattice, but the sublattice is neither graded nor self-dual as is the case in the larger poset. That said, the duality of the poset is well understood and is highlighted in Section 8.2 in Proposition 8.2.1 along with other basic facts about the poset's structure continued in Section 8.4 to understand the structure of intervals in the poset. These non-crossing partitions admit interesting recurrences, and in Section 8.3 we prove that they satisfy a Pascal-like recurrence relation which leads to myriad numerical results about these non-crossing partitions and the size within each rank (inherited as the subposet of the graded non-crossing partition lattice). In Section 8.5 we discuss the numbers and types of maximal chains that arise in this non-graded poset culminating in Theorem 8.5.6 and in Section 8.6 show the Moebius function for the poset depends on parity and is signed Catalan numbers in even cases or zero in odd cases. In Section 8.7, we provide an elegant direct proof about the size of the poset by shifting perspective to non-crossing matchings. In particular, although the poset structure is quite different these non-crossing partitions are equinumerous with Type B non-crossing partitions.

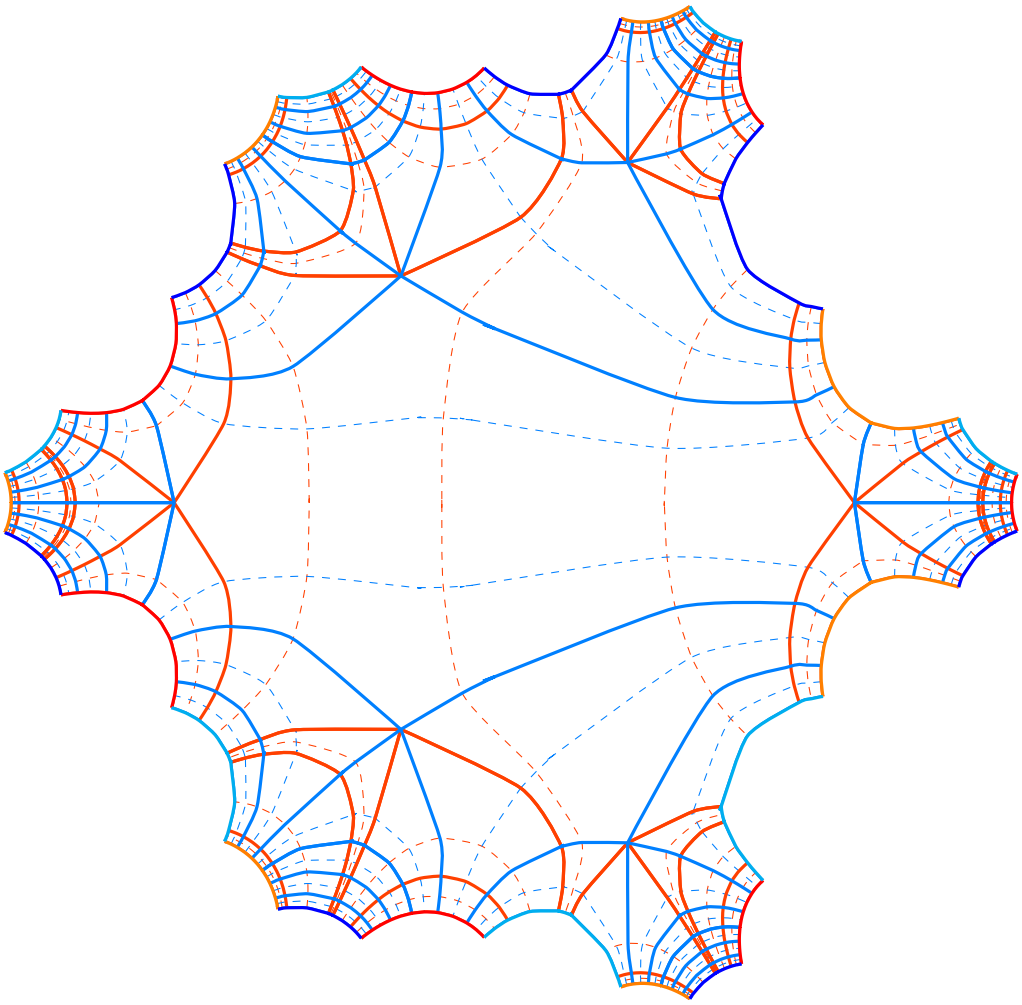

Figure 8.1: The branched rectangle diagram for a polynomial with real coefficients

The final section of this chapter turns attention towards the other type of non-crossing combinatorics that arises for real polynomials, the palindromic chains, defining them concretely and establishing a bijection from them to a family of labeled hypergraphs.

8.1 Reflection Symmetric Non-Crossing Partitions

In this section we define the first style of specialized non-crossing combinatorics that is covered in this chapter, reflection symmetric non-crossing partitions.

Definition 8.1.1. A non-crossing partition of vertices of a regular n-gon is *reflection symmetric* if it is invariant under a reflection that fixes a vertex or under a reflection that fixes the midpoint of an edge. To differentiate between these two types of symmetries, a reflection symmetric non-crossing partition fixing a vertex will be called *vertex reflection symmetric* and the ones fixing the midpoint of an edge will be called *edge reflection symmetric*

Remark 8.1.2. A useful convention to embed these reflection symmetric non-crossing partitions into $\mathbb{C}$ is consists of three sets of labels on the $4n$th roots of unity, $e^{\frac{ki\pi}{4n}}$.

- For $k \equiv 2 \mod 4$, label those roots of unity in a counter-clockwise way starting from the label 1 on $e^{\frac{2i\pi}{4n}}$ and ending at n.
- For $k \equiv 0 \mod 4$, label those roots of unity in a counter-clockwise way starting from the label 1 on $1 \in \mathbb{C}$ and ending at n.
- For odd k, label those roots of unity in a counter-clockwise way starting from the label 1 on $e^{\frac{i\pi}{4n}}$ and ending at $2n$.

With this convention, a edge reflection symmetric non-crossing partition on the $2 \mod 4$ roots (with respect to reflecting through the real axis—complex conjugation) induces both a vertex reflection symmetric non-crossing partition on the $0 \mod 4$ roots and a reflection symmetric non-crossing matching on the odd roots (which itself is an edge reflection symmetric non-crossing partition on $2n$ where each block is of size 2). This is visualized in Figure 8.2.

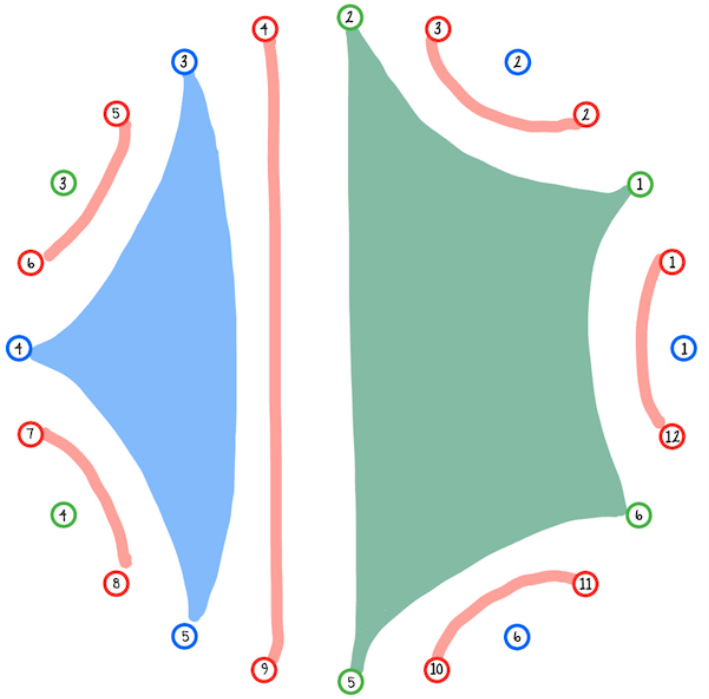

Figure 8.2: Superimposed reflection symmetric non-crossing partitions of edge type (in green), vertex type (in blue), and a reflection symmetric non-crossing matching (in red), with the established labelling convention from Remark 8.1.2 for $n = 6$.

Remark 8.1.3 (Complex conjugation as the reflection)**.** Throughout our study on reflection symmetric non-crossing partitions, we use the conventions from Remark 8.1.2 and consider the reflection symmetry across the real axis, which corresponds to complex conjugation. There is no difference in the combinatorics we present for any other reflective axis, but for clarity purposes we will only refer to reflection symmetry with respect to this particular reflective axis and particular arrangement of the labels. With that in mind, we can establish our particular reflection symmetric non-crossing partitions into purely combinatorial definitions.

Definition 8.1.4. A non-crossing partition τ is *edge reflection symmetric* if $a, b \in \tau_j$ implies $n - a + 1, n - b + 1 \in \tau_k$ for some j and k and $a, b \in [n]$.

Remark 8.1.5. The condition is most clear diagrammatically, wherein these non-crossing

partitions satisfy the condition that reflecting through the bisecting line between 1 and n results in the same diagram as diagrammed in Figure 8.3 for $n = 6$.

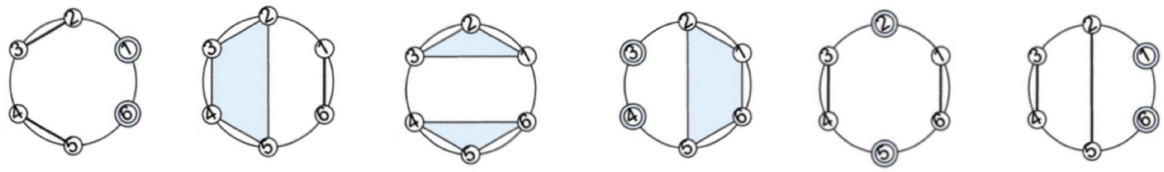

Figure 8.3: Examples of Edge Reflection Symmetric Non-crossing partitions for $n = 6$.

Definition 8.1.6. A non-crossing partition τ is *vertex reflection symmetric* if $a, b \in \tau_j$ implies $(-a + 2) \mod n, (-b + 2) \mod n \in \tau_k$ for some j and k and $a, b \in [n]$.

Remark 8.1.7. Like in edge version, these partitions are symmetric under reflection according to the labelling conventions establish, diagrammatically the reflection line strikes through 1 and bisects the diagram by striking through 1, visualized in Figure 8.4 for $n = 4$.

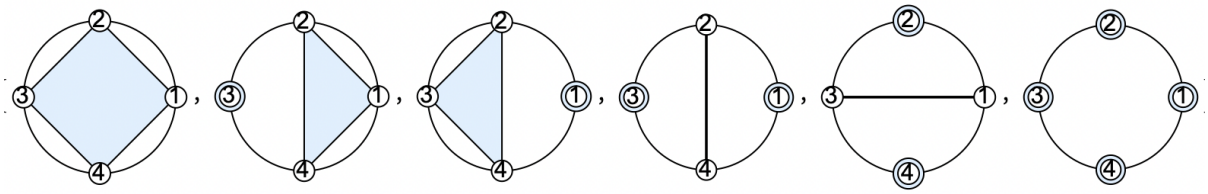

Figure 8.4: The Vertex Reflection Symmetric non-crossing Partitions for $n = 4$.

8.2 Poset Structure

As noted in 5.2, the non-crossing partition lattice has the structure of a graded lattice and enjoys many well known properties. It is self-dual and its maximal chains are in bijective correspondence with parking functions, etc. On the other hand the sublattice consisting of reflection symmetric non-crossing partitions is not graded, nor self-dual in general. In this section, we investigate the duality and establish some terminology for the covers and atoms/coatoms for the poset and consider some examples.

Terminology 1. As in previous chapters, we denote the usual poset of all non-crossing partitions of size n by $NCP(n)$, the subposet of edge reflection symmetric non-crossing partitions of size n by $RNCP_E(n)$, the subposet of vertex reflection symmetric non-crossing partitions of size n by $RNCP_V(n)$.

Proposition 8.2.1. *The posets $RNCP_E(n)$ and $RNCP_V(n)$ are dual. When n is odd, $RNCP_E(n) \cong RNCP_V(n)$ and thus, $RNCP_E(n)$ is self-dual when n is odd.*

Proof: The duality is easily seen by taking Kreweras compliments, evidenced in Figure 8.2. Evidently, when n is odd, vertex symmetry coincides with edge symmetry, since reflections that fix a vertex necessarily fix the midpoint of the edge on the opposite side as well. With our particular labels in mind, the map $x \mapsto x + \frac{n+1}{2} \mod n$ is an isomorphism from $RNCP_E(n)$ to $RNCP_V(n)$ for the odd case. □

Terminology 2 (Covering Relations)**.** In the standard non-crossing partition lattice, every covering relation adheres the same rule, namely $\tau \prec \pi$ is a minimal covering relation if and only if one block of π is the union of two blocks of τ, and all other blocks coincide.

However, due to the added restriction for symmetry in the the reflection symmetric non-crossing partitions, this is not the only minimal covering relation in $RNCP_E(n)$ or

$RNCP_V(n)$. Minimal covering relations like the ones described above for $NCP(n)$ still exist, but many of the covers in $NCP(n)$ do not preserve reflection symmetry. Moreover, there is a different minimal covering relation of height two. For convenience, we classify the minimal covering relations into two distinct types.

Recall our established context is that we are thinking of non-crossing partitions embedded into $\mathbb{C}$ as in Remark 8.1.2. Our convention is to call blocks that intersect the real axis *real blocks* and those that do not *complex blocks*. Note that in the reflection symmetric setting, complex blocks always appear in conjugate pairs. For completeness, we outline the types of covers that exist in the reflection symmetric case stratified by whether they are a 1-fold or 2-fold cover in the corresponding non-crossing partition lattice. In Figure 8.5, we show the diagrams for the corresponding covers.

1. The first kind of cover is itself a cover in the non-crossing partition lattice. An x-type covering relation is the minimal covering relation that does one of the following things: It could join into a single block a block elements of $[n]$ that are mirror images of each other with respect to the real axis. Said another way, these covering relations combine conjugate pairs of complex blocks into a real block. The other kind of x-type cover is when two real blocks merge into a single real block. These are covers in the non-crossing partition lattice as well because they relate, under refinement, two non-crossing partitions for which two blocks have joined to create a single block.

2. A y-type covering relation is a minimal covering relation in $RNCP_E$ and $RNCP_V$ but is a 2-fold covering relation from the perspective of the $NCP(n)$ and again pertains to two situations: Either two complex blocks in the same half space combine and simultaneously so do their conjugate blocks. or when a conjugate pair of complex blocks merge with a real block. In the latter situation, it is a cover

precisely when the convex hulls of the two conjugate blocks together non-trivially intersects the real block.

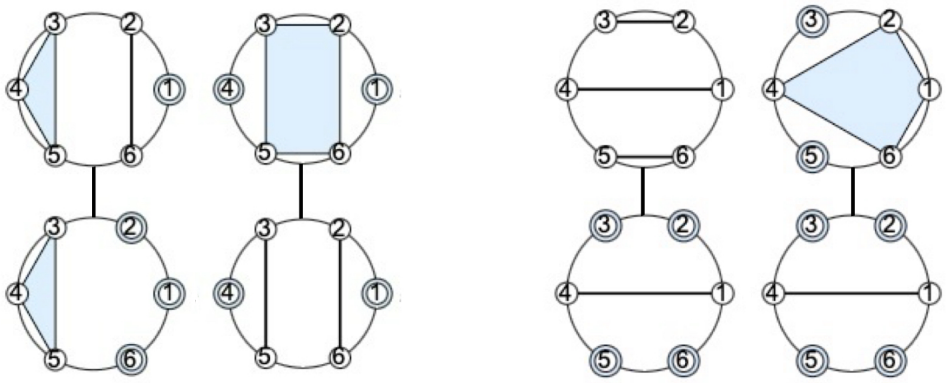

Figure 8.5: The left two columns describe the two styles of x-type covers, and the right two columns describe the two styles of y-type covers, as top-bottom pairs.

Remark 8.2.2. It is easily checked that under the dualization that goes between $RNCP_E$ and $RNCP_V$, these two types of covering relations types interchange in a predictable way. In particular, If $\tau \prec \pi$ via an x-type covering relation, then $\pi' \prec \tau'$ in the dual poset is again an x-type covering relation. Similarly, if the relation is a y-type covering, then the dual relationship is again a y-type covering.

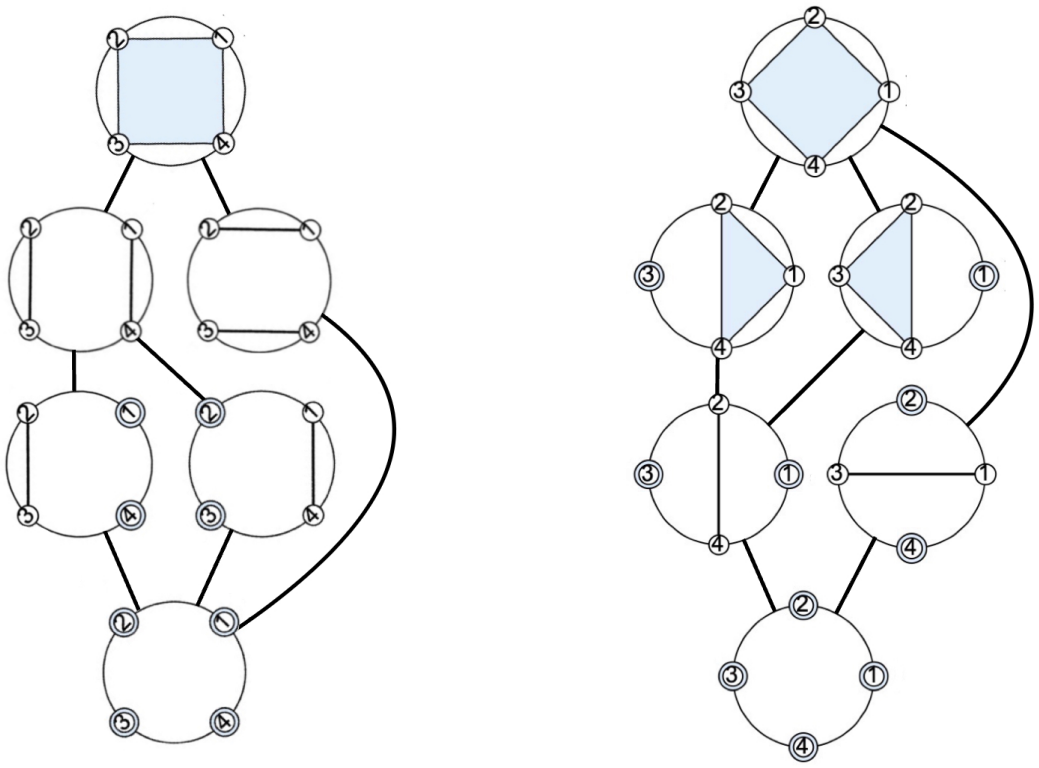

Figure 8.6: The posets $RNCP_E(4)$ and its dual $RNCP_V(4)$.

Remark 8.2.3 (Atoms and Coatoms)**.** We denote the specific symmetric non-crossing partition in which the only nontrivial block contains a label i for $1 \leq i \leq \lfloor \frac{n}{2} \rfloor$ and its reflected image label as π_i and notice that this is an atom for both $NCP(n)$ and $RNCP_E(n)$. In particular, π_i has as its only nontrivial block $\{i, (n+1)-i\}$.

The other sort of atom is not an atom of $NCP(n)$. We denote the symmetric non-crossing partition in which the nontrivial blocks are $\{i, j\}$ for $0 < i, j \leq \lfloor \frac{n}{2} \rfloor$ and the reflected version of that block $\{(n+1)-i, (n+1)-j\}$ as $\pi_{i,j}$ and notice that this is atomic in $RNCP_E(n)$ but not in $NCP(n)$.

These two types exhaust the list of atoms for $RNCP_E(n)$.

The coatoms of $RNCP_E(n)$ also have two distinct types: If the symmetric non-crossing partition consists of two blocks A and B then the partition is uniquely determined

by the maximum labeled vertex $m \in [1, \lfloor \frac{n}{2} \rfloor]$ within the block containing the labeled vertex 1. If $1 \leq m < \frac{n}{2}$, the coatom is the partition consisting of the block $\{\pm 1, \ldots, \pm m\}$ and $\{\pm(m+1), \ldots, \pm \lceil \frac{n}{2} \rceil\}$ whereas if $m = \frac{n}{2}$ the partition is $[1, \frac{n}{2}] \sqcup [-\frac{n}{2}, -1]$, where by abuse of notation we think of $-i$ as the labeled vertex $(n+1) - i$ (the reflected vertex of i). We denote these coatoms as $\pi^{1,m}$.

The other type of coatom is not a coatom of $NCP(n)$. The specific non-crossing partition in which all but i and $-i$ belong to a single nontrivial block for $1 < i < \lceil \frac{n}{2} \rceil$ is a coatom of $RNCP_E(n)$ we denote as π^i.

8.3 Pascal Like Recurrence

In this section I describe a recurrence relation to obtain the number of reflection symmetric non-crossing partitions of n with k blocks, denoted $RNCP_E(n, k)$.

In many instances, the recurrence which arises coincides with the Pascal Recurrence for binomial coefficients.

Remark 8.3.1. The exact recurrences below still work for both types of reflection symmetric non-crossing partitions, even though the proofs are only provided for Edge Type. Following the argument while passing through to the Kreweras complement gives a mirrored argument for the vertex reflective cases.

Lemma 8.3.2. *When n is even, $RNCP_E(n, k) = RNCP_E(n-1, k-1) + RNCP_E(n-1, k)$*

Proof: When k is odd, at least one of the blocks in any of the reflection symmetric non-crossing partitions with k blocks is a *real* block. Thus, the following operations are always well-defined.

Now consider any of the partitions in $RNCP_E(n-1, k-1)$. When n is even, the $\frac{n}{2}$th vertex is on the real axis for this partition of $n-1$. If this vertex is not in a block with

any other vertex, then shifting the labels past $\frac{n}{2}$ up by one followed by the replacement of $\frac{n}{2}$ with the disjoint pair of $\frac{n}{2}$ and $\frac{n}{2}+1$ gives a unique partition in $RNCP_E(n,k)$.

If $\frac{n}{2}$ is in an existing block, then the other entries in that block are conjugate pairs, because there are no other real vertices. To create a partition of $RNCP_E(n,k)$ from this, we can shift the labels past $\frac{n}{2}$ up by one and then divide the block containing $\frac{n}{2}$ into two blocks: one containing $\frac{n}{2}$ and the positive conjugates, the other containing $\frac{n}{2}+1$ and the negative conjugates.

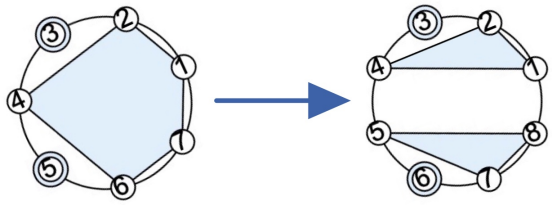

Figure 8.7: Demonstrating the injection of $RNCP_E(7,3)$ into $RNCP_E(8,4)$.

Thus, there is an injection under these operations from $RNCP_E(n-1,k-1)$ into $RNCP_E(n,k)$.

For a partition from $RNCP_E(n-1,k)$, we can obtain a partition from $RNCP_E(n,k)$ shifting the labels past $\frac{n}{2}$ up by one and adding the $\frac{n}{2}+1$ vertex into the same block as $\frac{n}{2}$.

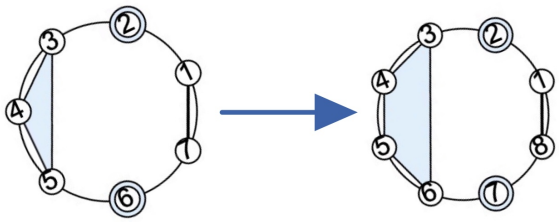

Figure 8.8: Demonstrating the injection of $RNCP_E(7,4)$ into $RNCP_E(8,4)$.

Thus, there is another injection of $RNCP_E(n-1,k)$ into $RNCP_E(n,k)$.

Clearly, the images under these injections are disjoint and their union equals all of $RNCP_E(n,k)$, since they partition the elements of $RNCP_E(n,k)$ into partitions containing a block that have both $\frac{n}{2}$ and $\frac{n}{2}+1$ and those that do not.

□

The situation when n is odd is more complicated since the choice of k affects the recursion.

Lemma 8.3.3. *When n is odd and k is odd, $RNCP_E(n,k) = RNCP_E(n-1,k-1) + RNCP_E(n-1,k)$.*

If k is even, $RNCP_E(n,k) = RNCP_E(n-1,k-1) + RNCP_E(n-1,k) - N(\frac{n-1}{2}, \frac{k}{2})$ where $N(n,k)$ is the Narayana number.

Proof: For odd k, the insertion of the $\lfloor \frac{n}{2} \rfloor + 1$ vertex after shifting all the entries past $\lfloor \frac{n}{2} \rfloor$ by one gives a well-defined injection from $RNCP_E(n-1,k-1)$ into $RNCP_E(n-1,k)$.

But when k is even, there is no guarantee that any real block exists for a partition from $RNCP_E(n-1,k)$. If a real block does exist, shifting all the entries past $\lfloor \frac{n}{2} \rfloor$ by one and then inserting a vertex $\lfloor \frac{n}{2} \rfloor + 1$ into the unique real block that preserves the non-crossing property will produce a unique element from $RNCP_E(n,k)$. When there is no real block, this process doesn't work. In this case the [even] blocks for the partition of $n-1$ are mirrored on top and bottom. It is easy to see that the number of such partitions coincides with the number of non-crossing partitions of $\lfloor \frac{n}{2} \rfloor$ with $\frac{k}{2}$ blocks. `https://oeis.org/A001263` Figure 8.9 describes the excluded partitions in $RNCP_E(8,4)$.

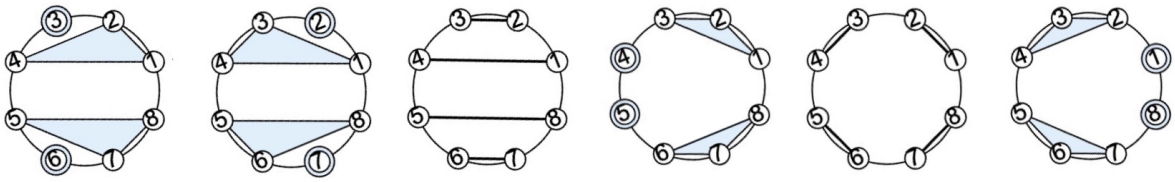

Figure 8.9: The partitions that must be excluded from the map of $RNCP_E(8,4)$ to $RNCP_E(9,4)$. The corresponding Narayana number is $N(4,2) = 6$.

Once again we partition all the elements of $RNCP_E(n,k)$, this time into those that have $\lfloor \frac{n}{2} \rfloor + 1$ in a nontrivial block, or not. □

Theorem 8.3.4. *When n is even, $|RNCP_E(n)| = 2|RNCP_E(n-1)|$. When n is odd, $|RNCP_E(n)| = 2|RNCP_E(n-1)| - C_{\frac{n-1}{2}}$, where C_k is the kth Catalan number.*

Proof: By Lemmas 8.3.2, when $n-1$ is odd, each reflection symmetric non-crossing partition gives rise to two reflection symmetric non-crossing partitions of size n, one in which a new central vertex is added in its own block, and one in which a new central vertex connects to a real block. Since $n-1$ is odd, there is always a real block or vertex. Thus, we recover $RNCP_E(n) = 2RNCP_E(n-1)$ when n is even. We can attempt the same in the case when $n-1$ is even, however as noted in the proof of the Lemma 8.3.3, there is not guarantee that any real block exists. In fact, when there are an even number of blocks, the reflection symmetric non-crossing partition may simply be a non-crossing partition on half as many, mirrored over the reflective axis. Thus, we exclude $N(\frac{n-1}{2}, k)$ the Narayana number corresponding to the number of non-crossing partitions of size $\frac{n-1}{2}$ with k blocks for any valid choice of k. Thus we exclude

$$\sum_{k=1}^{\frac{n-1}{2}} N\left(\frac{n-1}{2}, k\right) = C_{\frac{n-1}{2}}.$$

□

Proposition 8.3.5. *The number of reflection symmetric non-crossing partitions of size n with k blocks is*

$$|RNCP_E(n,k)| = \binom{\lfloor \frac{n-1}{2} \rfloor}{\lfloor \frac{k-1}{2} \rfloor} \binom{\lfloor \frac{n}{2} \rfloor}{\lfloor \frac{k}{2} \rfloor}$$

Proof: The result can be deduced by the recurrences in Lemmas 8.3.2 and 8.3.3 and is consistent with `https://oeis.org/A088855`. □

Remark 8.3.6. Using the recurrences, we can build a Pascal-like triangle where the kth entry of the nth row is the number of Reflection Symmetric non-crossing Partitions of n with k blocks.

$$\begin{array}{ccccccccccc}
 & & & & & 1 & & & & & \\
 & & & & 1 & & 1 & & & & \\
 & & & 1 & & 1 & & 1 & & & \\
 & & 1 & & 2 & & 2 & & 1 & & \\
 & 1 & & 2 & & 4 & & 2 & & 1 & \\
1 & & 3 & & 6 & & 6 & & 3 & & 1 \\
1 & & 3 & & 9 & & 9 & & 9 & & 3 & & 1 \\
1 & & 4 & & 12 & & 18 & & 18 & & 12 & & 4 & & 1 \\
1 & & 4 & & 16 & & 24 & & 36 & & 24 & & 16 & & 4 & & 1
\end{array}$$

The row sums of this triangle are central binomial coefficients, thus:

Corollary 8.3.7. *The size of $RNCP_E$ is*

$$|RNCP_E(n)| = \binom{n}{\lfloor \frac{n}{2} \rfloor}.$$

Proof: We observe that $\binom{n}{\lfloor \frac{n}{2} \rfloor}$ satisfy the same recurrence and initial conditions as $|RNCP_E(n)|$. □

8.4 Intervals

This section outlines the structure of intervals within the poset $RNCP_E$. As usual, the symbols $\widehat{0}$ and $\widehat{1}$ will denote the discrete partition and the trivial partition, respectively, which are the respective minimum and maximum partitions for both the lattices of non-crossing partitions and symmetric non-crossing partitions. In addition we will continue to use the abuse of notation by which we consider the vertex labeled $(n+1)-i$ as simply $-i$.

Remark 8.4.1. For a chain of reflection symmetric non-crossing partitions that consists of only y-type covers in the language of Terminology 2, the structure as a poset is very reminiscent of the original non-crossing partition lattice on about half as many vertices. Since there is mirroring happening on either side of the real axis, these are length 2 relations from the perspective of the non-crossing partition lattice. To describe this phenomenon which is important in understanding the intervals in $RNCP_E$, we use the notation $NCP^{(2)}(m)$ to signify the copy of the non-crossing partition lattice that appears in $NCP(2m)$ with some ignored middle steps. To illustrate this, $NCP^{(2)}(3)$ signifies the collection of non-crossing partitions (which are also reflection symmetric) $\{\widehat{0}, \pi_{1,2}, \pi_{1,3}, \pi_{2,3}, \widehat{1}\}$ inside $NCP(6)$ like in Figure 8.10. It is like a stretched copy of $NCP(3)$ where each cover now is a length 2 chain within the non-crossing partition lattice.

For any $\tau \in RNCP_E(n)$, the intervals $[\widehat{0}, \tau]$ are all straightforward to describe. It has the structure of a product of $RNCP_E$s and $NCP^{(2)}$s as follows: if a block of τ, say τ_i contains j and $-j$ for some j, then that contributes a factor of $RNCP_E(|\tau_i|)$. If not, that block and its mirror contributes a factor of $NCP^{(2)}(|\tau_i|)$.

In other words, we may partition the blocks of τ into two classes: real blocks denoted r_i (if they contain both $\pm j$ for all $j \in r_i$ which includes the case when $(n+1)-j = j$

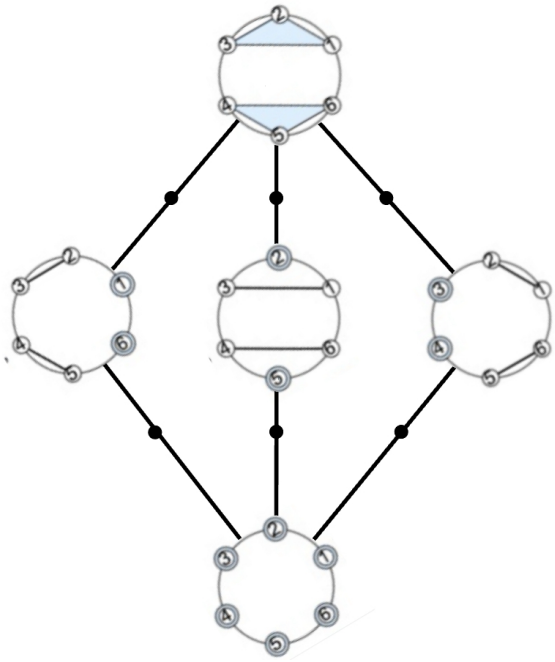

Figure 8.10: The "stretched" copy of $NCP(3)$ that sits inside $NCP(6)$.

for n odd) and complex blocks $c_i \sqcup \overline{c_i}$ (that come in pairs of all positive and all negative similar labels). So if $\pi = \{r_1, \ldots, r_k, c_1 \ldots, c_\ell, \overline{c}_1, \ldots, \overline{c}_\ell\}$ then

Proposition 8.4.2.

$$[\widehat{0}, \pi] = \prod_{j=1}^{k} RNCP_E(|r_j|) \times \prod_{i=1}^{\ell} NCP^{(2)}(|c_i|).$$

Proof: To establish the poset structure of real blocks, we recognize that in order to retain reflection symmetry, the covers must be of the form described in 2 and thus they contribute factors for the reflection symmetric poset of that size. For complex blocks, any non-crossing cover would need to be mirrored on the paired complex block. In that case, the covers we notice in the interval are two-fold covers from the point of view of the non-crossing partition lattice. Thus, they are all y-type covers in the language of 2. The result is a non-crossing partition lattice in which each cover is a height two cover.

Thus, each contributes the $NCP^{(2)}$ of the proper size. □

Example 8.4.3. For example, let

$$\pi = \{\{1,-1\},\{2,4\},\{3\},\{5,-5\},\{6\},\{-6\},\{-4,-2\},\{-3\}\}.$$

Via the proposition the interval $[\widehat{0},\pi]$ has the poset structure of $RNCP_E(2)\times RNCP_E(2)\times NCP^{(2)}(2)$, since there are two nontrivial *real* blocks both of size 2 and one pair of non-trivial *conjugate* blocks of size 2.

Now we direct our attention to intervals of the form $[\pi,\widehat{1}]$.

Remark 8.4.4. Given a reflection symmetric non-crossing partition π, viewed as diagram with labeled vertices on the unit circle, we may contract the partition along each block. For example, if there is an edge between i and j then the contraction will contract along that edge turning it into the point i/j. On a reflection symmetric non-crossing partition, after carrying out all possible contractions, we obtain a cellular cactus diagram in which some regions cross over the real axis (denoted *real* regions) and some do not cross the real axis and have a mirrored partner (denoted *complex* region). This is illustrated for an example in Figure 8.11. We can then determine the poset structure of $[\pi,\widehat{1}]$ to be the product of the admissible non-crossing posets in each region: for a real region R_i which looks like a circle with marked points bisected by the real axis, to retain the reflection symmetry we obtain a factor of $RNCP_V(|R_i|)$ where $|R_i|$ denotes the number of vertices on the circular region R_i. Notice the poset structure is that of the vertex reflection symmetric non-crossing partitions $RNCP_V$. That is because contracting a real block puts an identified vertex on the real axis, which happens in $RNCP_V$ for any n but not in $RNCP_E(n)$ when n is even. By Proposition 8.2.1, $RNCP_V$ is the correct catch-all whenever at least one real block exists.

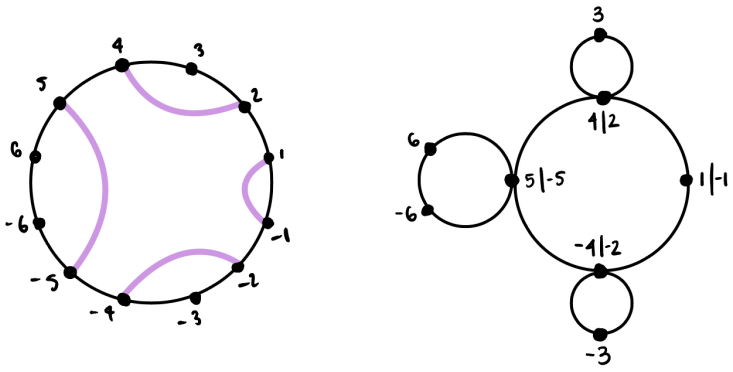

Figure 8.11: The symmetric non-crossing partition π along with the cellular cactus diagram obtained by contracting blocks.

For complex regions, we need only pay attention to the ones above the axis (since they are mirrored) and we may move along a chain to $\widehat{1}$ via any non-crossing partition in it so long as it is mirrored to its conjugate pair. Thus we obtain a factor of $NCP^{(2)}(|C_i|)$ following the same size convention as in the real regions.

Thus, if after carrying out the described contractions we obtain a cactus with *real* regions $R_1, \ldots, R_k$ and (upper) *complex* regions $C_1, \ldots, C_\ell$, then

Proposition 8.4.5.

$$[\pi, \widehat{1}] = \prod_{j=1}^{k} RNCP_V(|R_j|) \times \prod_{i=1}^{\ell} NCP^{(2)}(|C_i|),$$

or if π has no real blocks (which means it has one real region following contractions),

$$[\pi, \widehat{1}] = RNCP_E(|R_1|) \times \prod_{i=1}^{\ell} NCP^{(2)}(|C_i|)$$

Example 8.4.6. Returning to the example

$$\pi = \{1, -1\}, \{2, 4\}, \{3\}, \{5, -5\}, \{6\}, \{-6\}, \{-4, -2\}, \{-3\},$$

which is illustrate in Figure 8.11, the interval $[\pi, \widehat{1}]$ has the poset structure of $RNCP_V(3) \times RNCP_V(4) \times NCP^{(2)}(2)$. The subpartition of $\{6\}, \{-6\}$ and $\{5, -5\}$ contracts to the *real* region with vertices $6, -6$ and $5/-5$ which gives the factor of $RNCP_V(3)$, the collection $\{-5, 5\}, \{2, 4\}, \{1, -1\}, \{-4, -2\}$ contract to the *real* region with vertices $1/-1, 5/-5, 2/4, -4/-2$ give the $RNCP_V(4)$, and the $\{3\}$ with $\{2, 4\}$ gives a complex region with vertices 3 and $2/4$ contributing the $NCP(2)$, which is elongated to height 2 to capture the reflective symmetry on the blocks with $\{-3\}$ and $\{-4, -2\}$.

8.5 Maximal Chains

This section involves polynomials used for maximal chain enumeration, for which a neat closed form remains an open problem. In this section we establish an iterative process that can be used to generate a multivariable polynomial that encodes the number of maximal chains of any possible length.

Within the polynomial, any monomial in the variables x, y records as its leading term the number of maximal chains that involve that combination of covering relations.

Definition 8.5.1. Let $p_n^{\square}(x, y)$ be the polynomial described above for edge reflection symmetry, and $p_n^{\diamond}(x, y)$ be the same for the vertex style.

For example, we can generate the polynomial for $RNCP_E(4)$ by inspection of Figure 8.6, to produce

$$p_4^{\square}(x, y) = 2x^3 + yx,$$

which says that there are two maximal chains that involve three x-type covers and one maximal chain that involves a y-type cover and an x-type cover. Evaluating at $x = y = 1$ gives the total number of maximal chains, 3 in this case.

Remark 8.5.2. Outside of the question about the number of chains, the make up of

the chains is an interesting question. As in, how many covers in the chain are actually two-fold covers from the perspective of the ambient non-crossing partition lattice? Many of the maximal chains in the reflection symmetric poset are maximal chains in the non-crossing partition lattice, in particular the ones that only consist of x-type covers in the language of Terminology 2. The maximal chains that involve y-type covers are not themselves maximal chains in the non-crossing partition lattice. When we are not interested in discerning anything except the total length of the chain in the reflection symmetric poset, we will use a one variable variant polynomial in the variable z.

Our goal is to build up these polynomials iteratively, by collecting a database of the known polynomials for low values of n to use in producing the next polynomial. The key is Proposition 8.4.5, which highlights the structure of the intervals $[\pi, \widehat{1}]$ as the product of lower order reflection symmetric posets and a "stretched" version of the non-crossing partition lattice. By investigating the intervals above the atoms of the poset, the factors are all made up of pieces previously produced from the database, and we use that information to guide us in constructing the next polynomial. When we want to form chains from products of posets, the covers in the resultant chains can be any possible interweaving of the covers in each factor chain. To respect that feature we use the notation $p \boxtimes q$ to be the following operation on $p = \sum p_i$ and $q = \sum q_j$ (where p_i and q_j are the monomials that make up p and q respectively):

$$p \boxtimes q := \sum_{i,j} \binom{\deg(p_i) + \deg(q_j)}{\deg(p_i)} p_i q_j$$

where $\deg(p_i)$ and $\deg(q_j)$ are the multi-degrees of p_i and q_j as monomials.

Example 8.5.3. To see the process of building these polynomials in action for a more complicated example, we can work out what happens for $n = 6$ in the Edge Type: we

have three x-type minimal covers for the discrete partition going to the atoms π_1, π_2, π_3, respectively, and three y-type going from discrete to atoms $\pi_{1,2}, \pi_{1,3}$, and $\pi_{2,3}$. Thus,

$$p_6^{\square} = x(p_5^{\square}) + x(p_3^{\square} \boxtimes p_3^{\diamond}) + x(p_5^{\diamond}) + y(p_4^{\square}) + y(p_2^{\square} \boxtimes Np_2^{(2)}) + y(p_4^{\square}),$$

where $p_2^{\square} = x$, $Np_2^{(2)} = y$, $p_3^{\square} = p_3^{\diamond} = x^2$, $p_4^{\square} = p_4^{\diamond} = 2x^3 + yx$, $p_5^{\square} = p_5^{\diamond} = 2x^2y + 5x^4$. The interweaving required for $p_3^{\square} \boxtimes p_3^{\diamond}$ gives $\binom{4}{2}x^4$ and $p_2^{\square} \boxtimes Np_2^{(2)} = \binom{2}{1}xy$. Thus the final polynomial

$$p_6^{\square} = x(2x^2y + 5x^4) + x(6x^4) + x(2x^2y + 5x^4) + y(2x^3 + yx) + y(2xy) + y(2x^3 + yx)$$

$$= x^3y + x^3y + 5x^5 + 6x^5 + x^3y + x^3y + 5x^5 + 2x^3y + xy^2 + 2xy^2 + 2x^3y + xy^2$$

$$= 16x^5 + 8x^3y + 4xy^2.$$

In this two-variable version we can read off quite clearly how those chains behave with respect to the ambient non-crossing partition lattice. And, if we set all the variables to be equal we get a breakdown in terms of length of the maximal chain. In this example,

$$16z^5 + 8z^4 + 4z^3$$

tells us that of the 28 total maximal chains, there are sixteen chains of length 5, eight of length 4 and four of length 3.

Lemma 8.5.4. *The polynomials $p_n^{\square} = p_n^{\diamond}$ for all n.*

Proof: This was observable in Example 8.5.3, and is true as a general phenomenon by the duality between $RNCP_E$ and $RNCP_V$ outlined in 8.2.1. Indeed, the dual of a maximal chain is again a maximal chain. And, as noted in Remark 8.2.2, the same covers arise in the dual chain. □

Remark 8.5.5. With Lemma 8.5.4 in mind, we drop the qualifier for which type of reflection symmetry (edge reflective or vertex reflective) and simply use $p_n(x, y)$ or $p_n(z)$ to be the polynomial, in two or one variables, respectively, for maximal chain enumeration.

Thus, we obtain:

Theorem 8.5.6.

$$p_n = \sum_{odd\ k<n} x\,(p_{n-k} \boxtimes p_k) + \sum_{k=1}^{\lfloor \frac{n}{2} \rfloor - 1} \left(\left\lfloor \frac{n}{2} \right\rfloor - k \right) y \left(Np_k^{(2)} \boxtimes p_{n-2k} \right)$$

with $Np_n^{(2)} = n^{n-2}y^{n-1}$.

Proof: Here is a general algorithm to produce p_n for Edge Type, which we apply to the 2-variable version (the 1-variable version is recoverable from the 2-variable one):

Note that in Edge Type, for any n there are $\lfloor \frac{n}{2} \rfloor$ many vertices above the real axis. Thus, at the first level, there $\lfloor \frac{n}{2} \rfloor$ x-type covers, which we index using the odd numbers less than n. The $\binom{\lfloor \frac{n}{2} \rfloor}{2}$ y-type covers are grouped according to the size of the "stretched" non-crossing partition lattice factor that shows up and the complementary reflection symmetric piece, which depends on the size of the gap between i and j in the atom $\pi_{i,j}$. For example, above $\pi_{2,6}$ which has a gap of 4, there is a $NCP^{(2)}(4)$ factor in the interval $[\pi_{2,6}, \widehat{1}]$. From there, the validity of this formula for Edge Type and vertex reflection symmetry is a result of Remark 8.2.3 along with Proposition 8.4.5 and Lemma 8.5.4. □

Remark 8.5.7. Through this recursive definition, we can use computational tools to easily compute these polynomials and the evaluation at $x = y = z = 1$ to learn the number of maximal chains with remarkable efficiency advantages over direct chain counting algorithms for posets. Code to generate these polynomials is provided in the Appendix. Table 8.1 lists the relevant two variable polynomials for p_n and $Np_n^{(2)}$ which can be used

in Theorem 8.5.6. In Table 8.2 we list the corresponding one variable versions and the maximal chain counts for those values of n, which is the evaluation $p_n(1)$.

n	$p_n(x,y)$	$Np_n^{(2)}$
2	x	y
3	x^2	$3y^2$
4	$2x^3+xy$	$16y^3$
5	$5x^4+2x^2y$	$125y^4$
6	$16x^5+8x^3y+4xy^2$	$1296y^5$
7	$61x^6+32x^4y+11x^2y^2$	$16807y^6$
8	$272x^7+152x^5y+62x^3y^2+27xy^3$	$262144y^7$
9	$1385x^8+802x^6y+323x^4y^2+94x^2y^3$	$4782969y^8$
10	$7936x^9+4736x^7y+1952x^5y^2+676x^3y^3+256xy^4$	$100000000y^9$
11	$50521x^{10}+30832x^8y+12706x^6y^2+4288x^4y^3+1077x^2y^4$	$2357947691y^{10}$

Table 8.1: A table of iteratively computed polynomials for maximal chains.

Corollary 8.5.8. *The posets $RNCP_E$ and $RNCP_V$ are not graded. I.e. their maximal chains are not of consistent length.*

Proof: Some maximal chains in $RNCP_E$ consist only of x-type covers, which means they are also maximal chains in the ambient non-crossing partition lattice and so they

n	$p_n(z)$	$p_n(1) =$ #max chains
2	z	1
3	z^2	1
4	$2z^3 + z^2$	3
5	$5z^4 + 2z^3$	7
6	$16z^5 + 8z^4 + 4z^3$	28
7	$61z^6 + 32z^5 + 11z^4$	104
8	$272z^7 + 152z^6 + 62z^5 + 27z^4$	513
9	$1385z^8 + 802z^7 + 323z^6 + 94z^5$	2604
10	$7936z^9 + 4736z^8 + 1952z^7 + 676z^6 + 256z^5$	15556
11	$50521z^{10} + 30832z^9 + 12706z^8 + 4288z^7 + 1077z^6$	99424
12	$353792z^{11} + 219904z^{10} + 90752z^9 + 31104z^8 + 9382z^7 + 3125z^6$	708059

Table 8.2: The one-variable polynomials and the number of maximal chains for given n.

are length $n-1$. Since the monomials in Theorem 8.5.6 include those of degree less than $n-1$, not all maximal chains have the same length. This, of course, was clear from earlier observations as well. □

8.6 Moebius Function

An interesting invariant of posets is the Moebius function, and for the non-crossing partition lattice, it is well known to be signed Catalan numbers [5].

The following lemmas are used to compute the Moebius function of $RNCP_E(n)$. Both can be found with proof in [1].

Lemma 8.6.1 (Hall)**.** *For a finite lattice P, if the unique maximal element $\widehat{1}$ is not the join of the atoms of P or if the unique minimal element $\widehat{0}$ is not the meet of the coatoms*

of P, then $\mu_P = 0$.

The next Lemma requires the following definition.

Definition 8.6.2. For a poset $(P, \leq)$, a map $J : P \to P$ is called a *closure operator* if

- $x \leq J(x)$
- If $x \leq y$, then $J(x) \leq J(y)$
- $J^2(x) = J(x)$.

The image of this map $J(P) := \{J(x) \mid x \in P\}$ is called the *quotient* of P by J.

Lemma 8.6.3 (Rota)**.** *Let P be a locally finite poset and J a closure operator on P with quotient Q. Then, for all $x, y \in P$,*

$$\sum_{z \in P; J(z) = J(y)} \mu_P(x, z) = \begin{cases} \mu_Q(J(x), J(y)) & \text{if } x = J(x) \\ 0 & \text{if } x < J(x) \end{cases}$$

Now we come to the main theorem of this subsection. It was originally conceived in an unpublished manuscript of Montenegro. For posterity, we provide a proof inspired by his original argument.

Theorem 8.6.4. *The Moebius function for $RNCP_E(n)$ is $(-1)^{\frac{n}{2}} C_{\frac{n}{2}-1}$ when n is even and 0 when n is odd.*

Proof: If n is odd we observe that the atoms A of $RNCP_E(n)$ satisfy $\bigvee A < \widehat{1}$ since it has two blocks. Thus by Lemma 8.6.1, we have $\mu(RNCP_E(n)) = 0$ when n is odd.

When n is even we define the following closure operation J:

$$\widehat{0} \mapsto \widehat{0}$$

$$\pi \mapsto \pi \vee \pi_1$$

so that the quotient via this closure is $Q = \{x \in RNCP_E(n) \mid x \vee \pi_1 = x\}$. Observe that π_1 is the only atomic element in the quotient lattice and $\widehat{1} \in Q$. Thus, via Lemma 8.6.1, $\mu_Q = 0$ because $\pi_1 \neq \widehat{1}$.

Now consider the reflection symmetric non-crossing partition $\pi^{1,\frac{n}{2}}$ where the only two blocks are $[1, \frac{n}{2}]$ and its conjugate pair. Clearly, $\pi^{1,\frac{n}{2}} \vee \pi_1 = \widehat{1} \vee \pi_1 = \widehat{1}$, but if π is any other reflection symmetric non-crossing partition, $\pi \vee \pi_1 \neq \widehat{1}$. Indeed for such a π, the subpartition on $[1, \frac{n}{2}]$ contains at least 2 blocks and the same is true for its join with π_1.

Thus by Lemma 8.6.3 we have

$$0 = \mu_Q = \sum_{J(y)=\widehat{1}} \mu_{RNCP_E(n)}(\widehat{0}, y) = \mu_{RNCP_E(n)}(\widehat{0}, \pi') + \mu_{RNCP_E(n)}(\widehat{0}, \widehat{1}).$$

From the above we recover that $\mu_{RNCP_E(n)} = -\mu_{RNCP_E(n)}(\widehat{0}, \pi^{1,\frac{n}{2}})$. Finally we observe using Proposition 8.4.2 that the interval $[\widehat{0}, \pi^{1,\frac{n}{2}}]$ is isomorphic as a poset to $NCP(\frac{n}{2})$, so from [5] we see $\mu_{RNCP_E(n)}(\widehat{0}, \pi^{1,\frac{n}{2}}) = (-1)^{\frac{n}{2}-1} C_{\frac{n}{2}-1}$ and thus

$$\mu_{RNCP_E(n)} = (-1)^{\frac{n}{2}} C_{\frac{n}{2}-1}$$

as desired. □

8.7 Reflection Symmetric non-crossing Matchings

The goal of this section is provide a direct proof that the set of reflection symmetric non-crossing partitions of size n is equinumerous with the number of Type B non-crossing partitions. In other words, the goal is establish a bijection between these two combinatorial objects. In [8], the authors noted the surprising connection between reflection

symmetric non-crossing partitions and non-crossing partitions symmetric with respect to the π radian rotation (called Type B non-crossing partitions), that they are equinumerous. Though the result matches with Corollary 8.3.7 (proven based on enumerative techniques), their methods follow the map introduced in Simion and Ullman based on the Kreweras complement and pass through lattice paths in [26]. It was again noted by Ding in [9] in a parity-dependent way. Here we introduce a different proof that defines a direct bijection between non-crossing partitions fixed by rotation and reflection by utilizing non-crossing perfect matchings. There are two advantages to this approach: firstly, it provides a proof of the result which is independent of parity that doesn't obfuscate the relationship between the two objects, and secondly, the framing of reflection symmetry with non-crossing perfect matchings is integral for identifying basketballs which are important for Chapter 9.

Definition 8.7.1. A *non-crossing perfect matching* is a non-crossing partition of $[2n]$ in which every block has size 2.

Remark 8.7.2. A non-crossing matching is *reflection symmetric* precisely when the associated non-crossing partitions it induces are reflection symmetric. It is helpful to use the labelling convention of Remark 8.1.2 to recover those partitions, however reflection symmetry is quite apparent on diagrammatic realizations of the matching since it is itself a reflection symmetric non-crossing partition on $2n$ with all blocks of size 2 (of Edge Type using the label convention of Remark 8.1.2).

Similarly, a Type B non-crossing matching on $2n$ is a Type B non-crossing partition with blocks of size 2 which is equivalent to saying that it induces Type B non-crossing partitions on n via the same set of conventions as above.

See Figure 8.13 for an example of each.

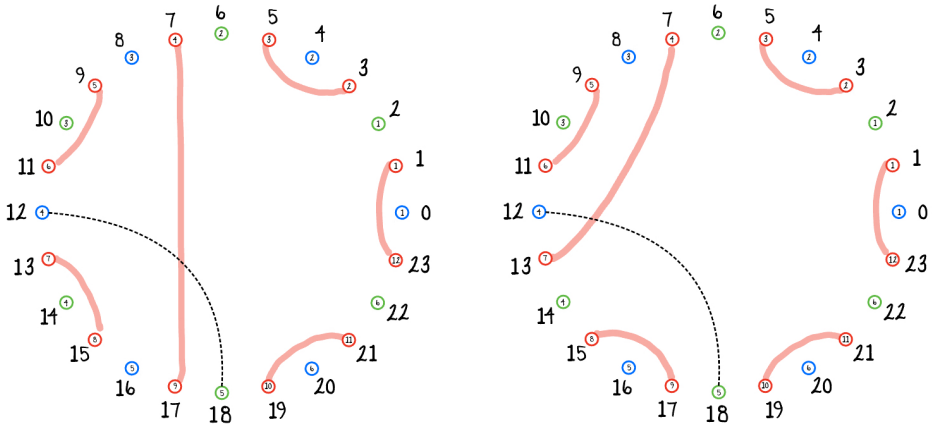

Figure 8.12: A non-crossing matching on $2n = 12$ and its image under the map $S_{12,18}$.

Definition 8.7.3. For a given n and even numbers $0 \leq i, j < 4n - 1$ let

$$S_{i,j} : NCM(2n) \to NCM(2n)$$

be defined as follows: Orient the non-crossing perfect matching according to the labelling convention from Remark 8.1.2, so that it is a matching on the odd powers of the $4n$th roots of unity. For the odd powers of the $4n$th root between i and j (where we allow cycling back around in case $i > j$), augment the matching according to these rules:

- if two odd powers are matched inside $[i, j]$ switch that pairing to be the opposite pairing inside $[i, j]$.
- if a node is matched with another outside of $[i, j]$, remove that matching and re-match with the *unique* node that retains the non-crossing property.

Remark 8.7.4. The map $S_{i,j}$ is an involution for any choice of even numbers $0 \leq i, j < 4n - 1$, i.e. $S^2_{i,j}(\tau) = \tau$ for any $\tau \in NCM(2n)$. In Figure 8.12 we see a visualization for the map $S_{12,18}$ on $NCM(12)$.

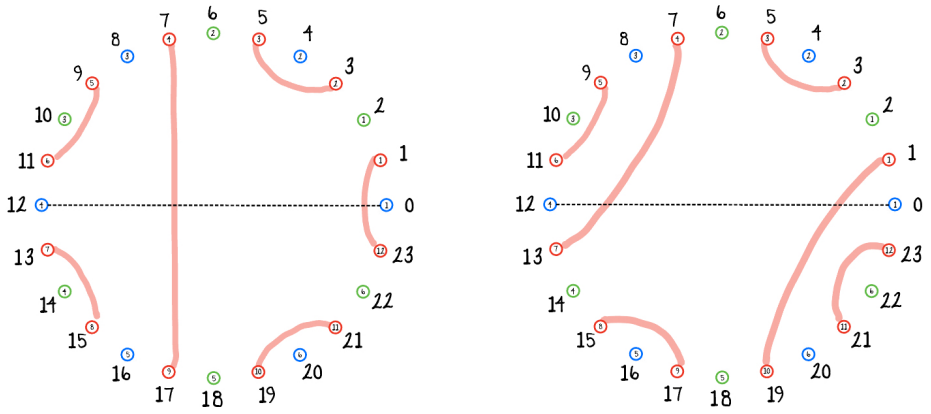

Figure 8.13: A reflection symmetric non-crossing matching and its image under $S_{12,0}$, a Type B non-crossing matching. This map establishes the bijection between reflection symmetric non-crossing matchings and Type B non-crossing matchings for $2n = 12$.

Theorem 8.7.5. *The set of reflection symmetric non-crossing matchings are in bijection with Type B non-crossing matchings for any given* $2n$.

Proof: For a given n, the map $S_{2n,0}$ restricts to a map from reflection symmetric non-crossing matchings to Type B non-crossing matchings and is easily checked to be a bijection, where the same map acts as the inverse. □

Remark 8.7.6. The map $S_{2n,0}$, visualized in Figure 8.13 is similar to the one discussed in [9] Theorem 2.1.5. But, from the point of view of non-crossing matchings, there are no special cases to verify. This defines, without obstruction, a map that is bijective between reflection symmetric non-crossing matchings and rotation symmetric non-crossing matchings. The underlying non-crossing partitions are also reflection symmetric and rotation symmetric, respectively, and so the bijection carries through.

8.8 Palindromic Non-Crossing Partition Chains

This section is devoted to describing a special collection of chains in the non-crossing partition lattice using three different but related points of view. There is the viewpoint

of non-crossing partitions, non-crossing matchings, and properly labeled hypertrees. The special collection we are interested in corresponds to the following situation.

Recall, for every non-crossing partition, the Kreweras complement maps a non-crossing partition of n with k parts into a non-crossing partition of n with $n-k$ parts. For a chain of non-crossing partitions, the Kreweras complement maps a chain to a chain. However, these chains are usually different, though they might be equivalent under some involution.

For clarity purposes, we will be using a particular Kreweras map, which we call the *flip Kreweras complement*, which we define as follows.

Definition 8.8.1. Arrange $2n$ nodes on the vertices of a regular $2n$-gon so that the $2n$-gon has antipodal edges bisected by the horizontal axis. Then alternate colors on the nodes to bicolor them. Starting above the horizontal axis in the first quadrant, consecutively label every other node (colored blue) with the labels 1 through n counterclockwise. Below the horizontal axis in the 4th quadrant, label every other node (colored green) with $1'$ to n' clockwise. A non-crossing partition on $\{1,\ldots,n\}$ induces a non-crossing partition on $\{1',\ldots,n'\}$ in the obvious way: form the convex hulls of nodes so long as that convex hull does not cross that for the original non-crossing partition's blocks. This particular version of the Kreweras complement will be called the *flip Kreweras complement*.

A nice aspect of this version of the Kreweras complement is that it is an involution, i.e. $(\pi^c)^c = \pi$.

Definition 8.8.2. If a given chain of non-crossing partitions is *flip Kreweras complementary* to the same partition chain but with 'prime' labels (for example if $\{1,5\}$ is the first nontrivial block in one then $\{1',5'\}$ is the first nontrivial block in the under the flip Kreweras map, and so on) these chains are the called *palindromic*.

We can set up the same idea from the perspective of non-crossing matchings as well.

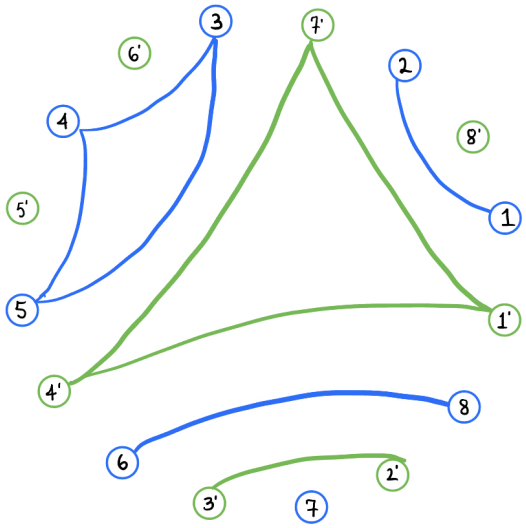

Figure 8.14: A visualization of the *flip Kreweras complement* taking the partition $\pi = \{\{1,2\},\{3,4,5\},\{6,8\},\{7\}\}$ to $\pi^c = \{\{1,4,7\},\{2,3\},\{5\},\{6\},\{8\}\}$.

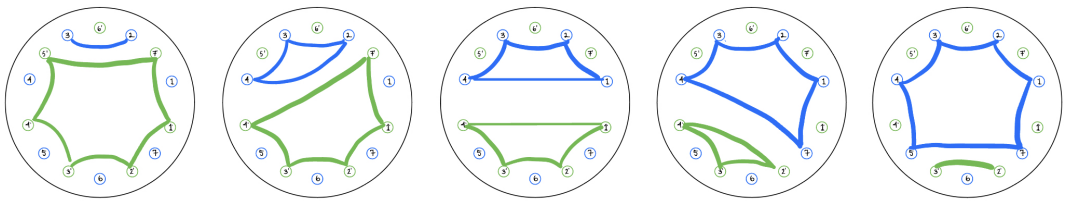

Figure 8.15: An example of a palindromic chain in the non-crossing partition lattice on $n = 7$, superimposed with its flip Kreweras complement in each diagram.

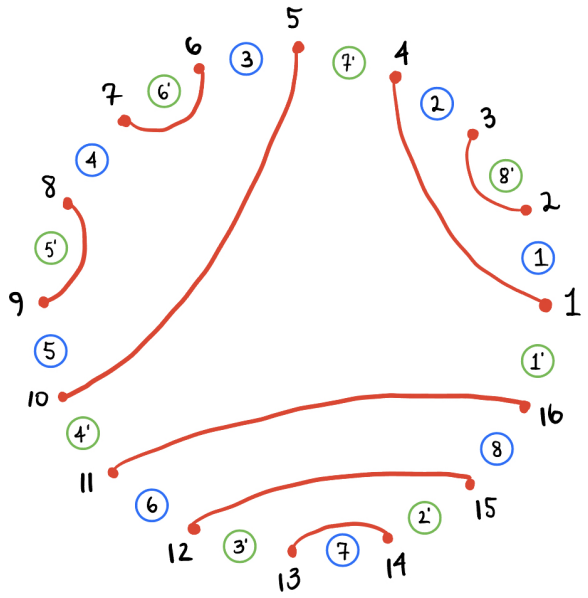

Figure 8.16: The induced non-crossing matching for the non-crossing partition (and its complement) from Figure 8.14.

Color the even powers of the $4n$th roots of unity red. For the odd powers, color them as blue if the power is $\cong 1 \mod 4$ and green if the power is $\cong 3 \mod 4$. Under this construction, the blue and green colors match exactly with the same colored nodes in the non-crossing partition point of view from above. From a non-crossing partition on the blue, we get an induced non-crossing matching on the red by thinking of those arcs as the boundary of the thickened convex hull of the nodes within each block. Similarly, a non-crossing partition on the green nodes induces a non-crossing matching on the red. If the induced non-crossing matching is the same for a blue non-crossing matching and a green one, then it is clear to see that these are flip Kreweras complementary non-crossing partitions. In particular we have the following lemma:

Lemma 8.8.3. *The effect of flipping this particular matching is that the pair of non-crossing partitions induced:*

$$(\pi, \pi^c) \mapsto (\pi^c, \pi)$$

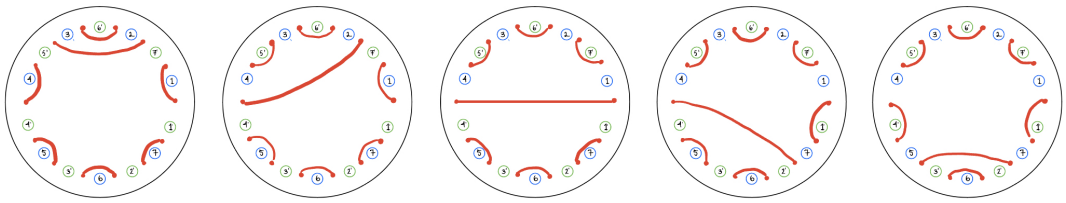

Figure 8.17: The same palindromic chain from Figure 8.15 from the point of view of non-crossing matchings.

And with this in mind, we can again define our palindromic condition:

Definition 8.8.4. A chain in the non-crossing matchings lattice on the $2n$ even powers of the $4n$th roots of unity in called *palindromic* if the π rotation of the chain is the same chain. Said another way, the flip over the real axis results in the same chain when read in the opposite order.

We can also view this condition through the lens of properly labeled non-crossing trees, using the language and conventions of [22].

Definition 8.8.5. A non-crossing (or planar) tree on the vertices of a regular n-gon is called *properly labeled* if for every vertex, the labels on the edge set that see that vertex are ordered so that they are strictly increasing in the clockwise sweep on the interior of the n-gon.

Remark 8.8.6. We can broaden this definition to include hypertrees, where instead of edges, we may also have labeled blocks of any size, and the same order convention still applies for the proper labelling.

In order to invoke similar symmetries to what we have been working with before, we will consider a particular embedding of the n-gon for this definition: position the regular n-gon in the complex plane so that the line $re(z) = 1$ is a defining hyperplane for the n-gon which lives in the halfspace $re(z) \leq 1$ scaled so that there are vertices at $1 + i$ and

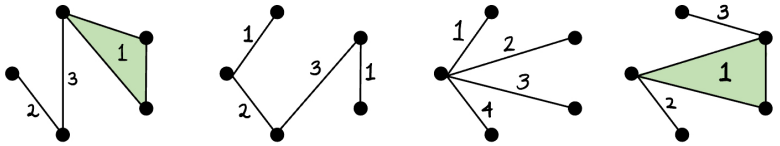

Figure 8.18: Several examples of properly labeled non-crossing hypertrees on the vertices of a regular 5-gon.

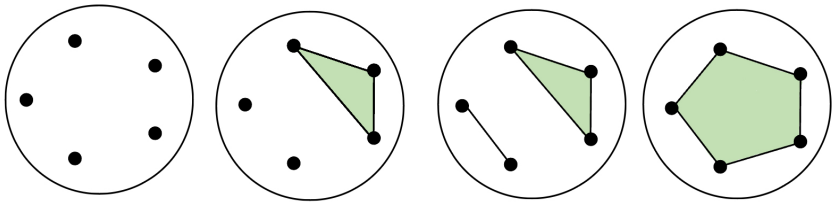

Figure 8.19: The chain in the non-crossing partition lattice for $n = 5$ corresponding to the 1st hypertree in Figure 8.18.

$1 - i$. The effect of this embedding is that the resulting n-gon is symmetric with respect to the flip over the real axis. Label the vertex at $1 + i$ by 1 and continue counterclockwise to the label n for the vertex at $1 - i$.

These properly labeled trees correspond to chains in the non-crossing partition lattice.

Lemma 8.8.7. *A chain in the non-crossing partition lattice can be represented by a properly labeled hypertree on the vertices of a regular n-gon. In particular, a properly labeled tree on these vertices without repeated labels corresponds to a maximal chain.*

Proof: Here is how we would obtain the corresponding chain from a properly labeled hypertree:

At step i, two or more blocks will be joining, the joining blocks are the ones connected by the hyperedge labeled i.

Since the hypertree was planar/non-crossing, the partition obtained at any step i is non-crossing.

Conversely, given a chain of non-crossing partitions, the properly labeled tree can be obtained iteratively first connecting via a hyperedge or block the first set up elements

of the n-gon corresponding to the partition, and so on. While there might be ambiguity when choosing how to connect blocks with a hyperedge, it is self-rectified in that only one choice would result in proper labeling.

This can be readily checked to be a bijection.

Another point of view passes through the factorization of an n-cycle with transpositions and its bijection with these chains. The element in each transposition (or cycle for hypertrees) identifies the vertices connected by edges or blocks. □

With the recognition that these properly labeled trees correspond to non-crossing partition chains, we can observe how certain manipulations of the tree affect the corresponding chain.

Of particular interest for our purposes, we want to highlight the effect of flipping the trees edge/block set vertically and inverting the label set. Both of these actions on their own change the orientation of the labeling from say, clockwise, to counterclockwise. The result of which results in a factorization of the inverse of the original n-cycle. From the point of view of the chain, doing both of these actions recovers a new properly labeled tree, however the chain that is recovered is a flip Kreweras complementary chain.

Lemma 8.8.8. *Under the bijection from properly labeled hypertrees to chains in the non-crossing partition lattice, the flip/invert labels action on the trees has the effect of producing the flip Kreweras complementary chain.*

Proof: The helpful viewpoint to understand how this works comes from viewing non-crossing perfect matching as coming from Morse theory on a branched rectangle map, which appeared in Chapter 7. In Figure 8.20 we can see that the flip complementary chain on the level of non-crossing matchings comes from reversing direction by which we analyze, from top to bottom or bottom to top of the associated rectangle. That direction change flips the order of the matchings that appear (signified by inverting the labels on

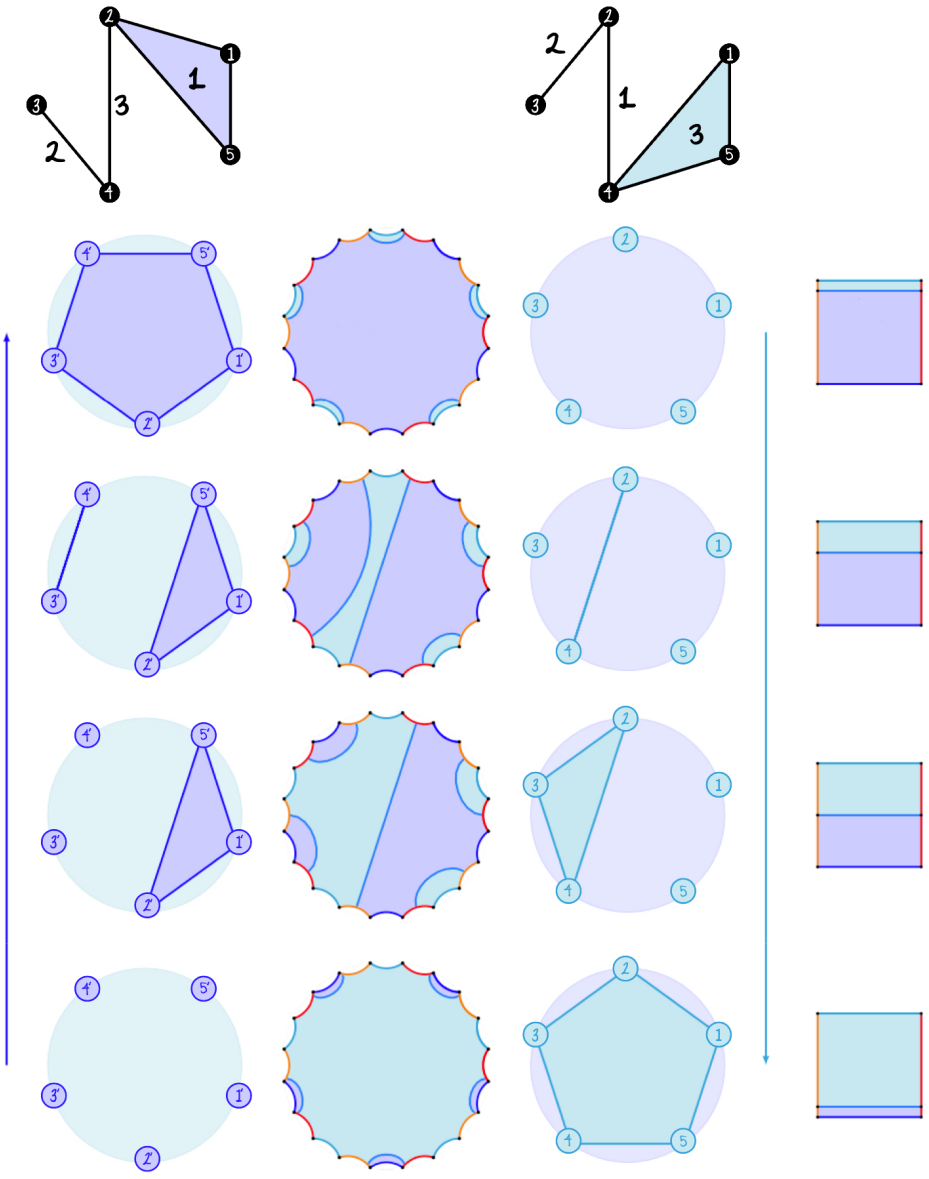

Figure 8.20: Visualizing flip complementary chains from different points of view.

the associated hypertree) for the chain that arises on the inverted set of vertices (signified by the flip of the hypertree vertically). It is clear that the correspondence carries past the specific example in the figure. □

This result offers justification for a third definition of the palindrome condition.

Definition 8.8.9. A properly labeled non-crossing hypertree is called *palindromic* if it is symmetric with respect to flipping vertically and inverting the labels.

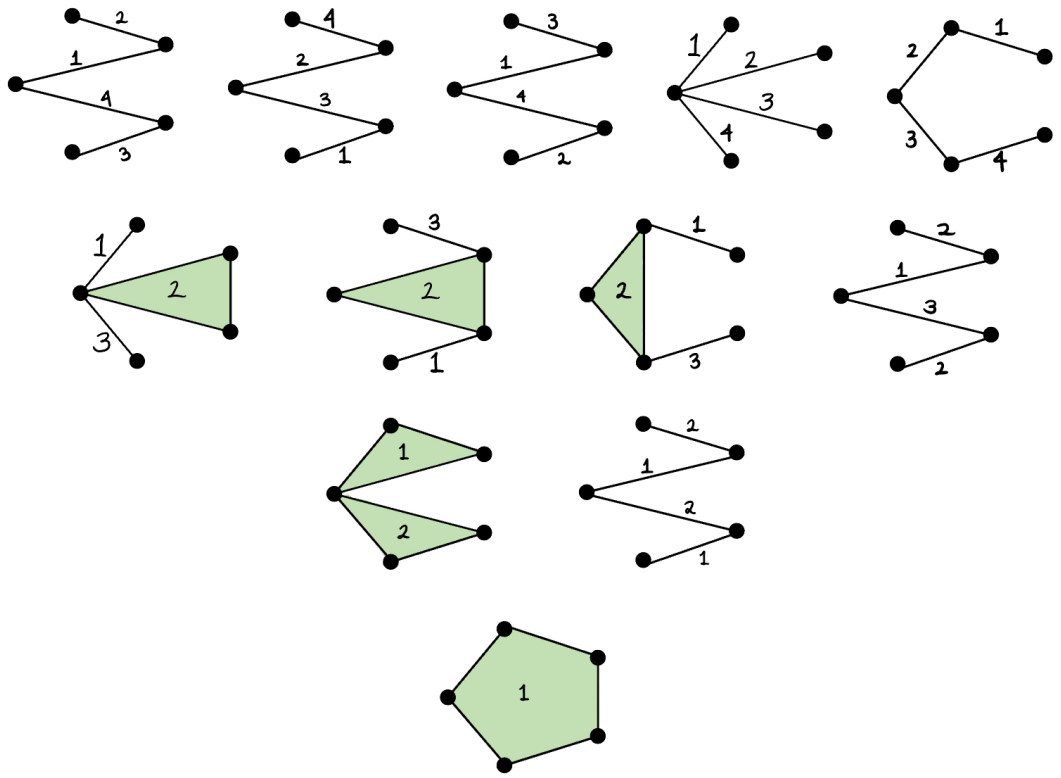

Figure 8.21: All of the palindromic properly labeled hypertrees on 5 vertices, stratified by length of the corresponding chain.

The main result in this section is that the three palindromic conditions correspond to the same general situation through bijective correspondences.

Proposition 8.8.10. *The following three sets are in bijective correspondence:*

1. *The set of palindromic chains in the non-crossing partition lattice of size n.*

2. *The set of palindromic chains in the non-crossing matching lattice of size $2n$.*

3. *The set of palindromic properly labeled hypertrees on the vertices of a regular n-gon.*

Proof: By Lemma 8.8.7, we know that the palindromic properly labeled hypertrees are associated bijectively with certain chains in the non-crossing partition lattice and by Lemma 8.8.8, we know that if the hypertree is invariant under the flip/invert labels, then the chain is flip complementary to itself. This establishes (1) $\iff$ (3). By Lemma 8.8.3 we see that the effect of flipping a chain of non-crossing matchings is that we obtain the flip complementary induced pairs of partitions in opposite order, due to the fact that the Kreweras complement is an anti-isomorphism. Thus, if the the chain recovers the same set of matchings in reverse order after the flip, then $\pi_i = \pi_{n-i}^c$ for all i, which establishes (1) $\iff$ (2). □

Remark 8.8.11. With reflection symmetric non-crossing partitions, we had two different duality conditions based on parity: For odd n, the poset was self dual since the two different styles of reflection symmetry were isomorphic. For even n, one reflection symmetry was dual to the other, due to the Kreweras map slightly changing the axis of symmetry.

One way around switching between these two different type of reflection symmetry was to pass to non-crossing matchings instead of partitions. Everything is perfectly translatable going to these matchings: reflection symmetric non-crossing partitions induce reflection symmetric non-crossing matchings but this version works slightly better under dualizing (which in the case of matchings is simply swapping the binary choice of side to distinguish the induced non-crossing partition. The reason this works is that, now, the non-crossing matching has no nodes on the reflective axis.

For palindromic chains, we again can pass to non-crossing matchings to clarify the palindrome condition as state above. However, the matching that perfectly captures this situation does have two antipodal nodes on the reflective axis, so it is a non-crossing matching for a slightly different embedding of $2n$ vertices along the unit circle in $\mathbb{C}$.

The advantage then to the non-crossing matching point of view is that it unifies with our vision of reflection symmetry and lend itself well towards the uses of these combinatorial objects in Chapter 9 when we superimpose matchings of both styles to create combinatorial basketballs. The major advantage of the properly labeled hypertree point of view, is that we can study these chains more directly and produce examples easily. In addition, we may apply enumerative techniques to the hypertrees, which are easier to study directly, though more detailed analysis is reserved for a future investigation.

Some preliminary numerical results are collected in Table 8.3.

n	palindromic maximal chains	palindromic chains
2	1	1
3	1	2
4	2	3
5	5	12
6	12	21
7	49	132
8	128	

Table 8.3: A table of enumerations for palindromic chains.

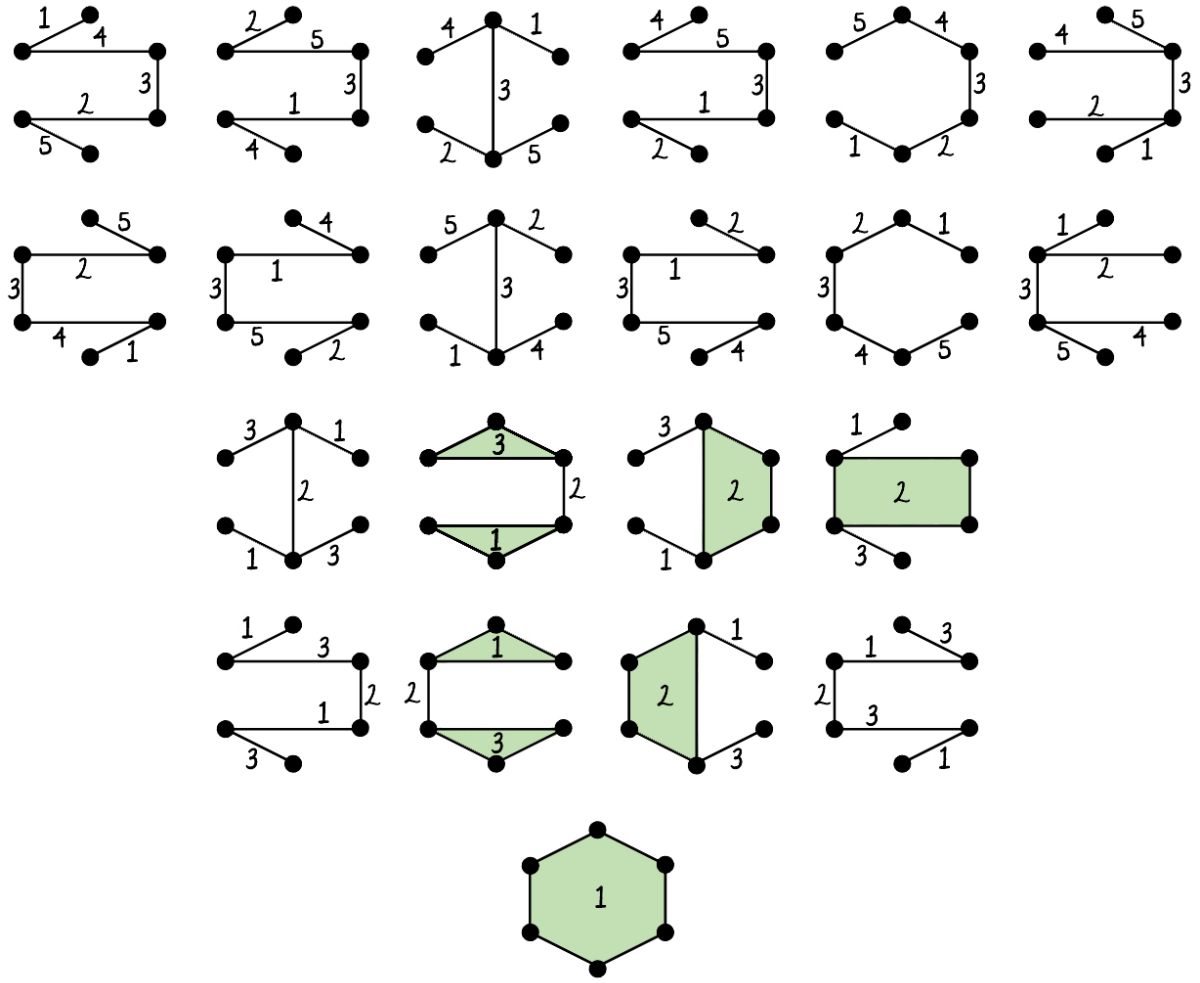

Figure 8.22: All of the palindromic properly labeled hypertrees on 6 vertices, stratified by the length of the corresponding chain.

Chapter 9

Real Polynomials from Metric Basketballs

9.1 Introduction

As discussed in Chapter 7, there is a connected cellular complex that represents the space of monic and centered complex polynomials. This metric object is the result of pulling back the metric on the rectangle of critical values. In our discussion on the combinatorics of complex polynomials we noted that its geometry was governed by the metric basketball complex, also called the Branched Rectangle Complex, BrRect, which is a subcomplex of the metric direct product of the order complex of the non-crossing partition lattice with itself, subject to the constraint that the product in each cell forms a metric basketball (a property that was especially evident from the perspective of non-crossing matchings). In this chapter, we apply these results for the subset of real polynomials in complex polynomial space. In particular, a portion of the metric basketball complex illuminates the geometry of real polynomials once we understand the specific metric basketballs that we may obtain from real polynomials. The main theorem in this chapter

outlines the method to construct the real metric basketball complex as a subcomplex of the basketball complex for complex polynomials. We also show how to concretely build it for degree 3.

9.2 Real Metric Basketball Complex

Any monic, centered polynomial with real coefficients behaves nicely with respect to complex conjugation. Its roots, critical points, and its critical values all are either real or come in conjugate pairs.

Proposition 9.2.1. *For any $p \in \mathbb{R}\text{-}\textsc{Poly}^{mc}(\mathbb{C})$, we have*

$$\mathbf{rts}(p) = \overline{\mathbf{rts}(p)} \quad \mathbf{cpt}(p) = \overline{\mathbf{cpt}(p)} \quad \mathbf{cvl}(p) = \overline{\mathbf{cvl}(p)}$$

where $\overline{A}$ is the set of complex conjugates of $A \in \textsc{Mult}_k(\mathbb{C})$.

Proof: This is evident from the basic facts $\overline{a} + \overline{b} = \overline{a+b}$ and $\overline{a^n} = (\overline{a})^n$ for any $a, b \in \mathbb{C}$ and $n \in \mathbb{Z}$. □

Thus, we may always choose a rectangle to bound the critical values for a real polynomials that is bisected by the real axis that would exhibit symmetry. And, it is immediately clear that the complex conjugate horizontal lines in the image, regular or not, will pull back as complex conjugate lines (or branched lines). In particular, this makes clear two general features about the combinatorics of non-crossing matchings that appear for real polynomials. As we are able to observe in Figure 8.1, the branched rectangle is symmetric with respect to flipping over the real axis. The output side (the rectangle) is also symmetric with respect to that flip, by virtue of being a real polynomial. This tells us two things: The pullback of a regular line vertical line is a reflection symmetric non-crossing matching on the preimages of top and bottom sides, and the pullback of

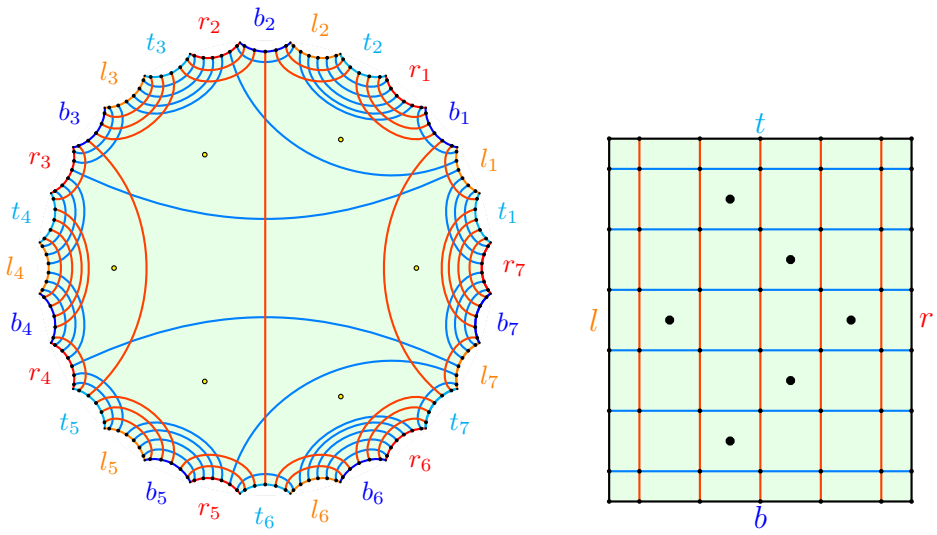

Figure 9.1: The stylized basketball 'court' from Figure 8.1 which is the preimage of the regular lines of the rectangle around its critical values.

horizontal regular lines determine a palindromic chain of non-crossing matchings on the preimages of left-right sides in the $4d$-gon.

Remark 9.2.2. A stylized version of the example illustrated in Figure 8.1 is in Figure 9.1, where we ignore the metric information and just consider the matching information we get by pulling back regular lines. The red lines pull back to a top-bottom matching that is reflection symmetric, and the blue lines pull back to left-right matchings that altogether form a palindromic chain. Each red matching forms a basketball with every blue matching. We refer to diagrams with all these matchings superimposed as a *basketball court* and it corresponds to a cell in the basketball complex that is obtained as the product of chains of the top-bottom matchings with the left-right matchings.

To highlight these features more clearly, we can clean the figure up by just considering the pullback of the vertical, red lines as in Figure 9.2. There we can see that all the matchings are symmetric with respect to flipping across the real axis.

We can also highlight the palindromic features by focusing on the pullback of one of the blue lines and its reflected pair. That is the content of Figure 9.4. It is clear that the

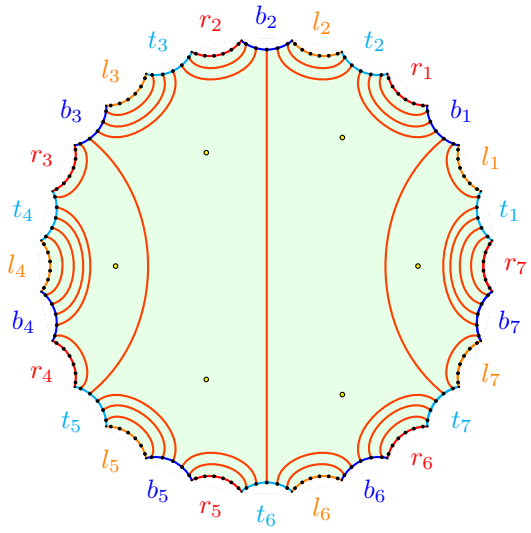

Figure 9.2: The pullback of just the vertical red lines of Figure 9.1. Each top-bottom matching (5 in total) is a reflection symmetric non-crossing matching.

condition of Definition 8.8.4 is satisfied by the pair of matchings. Also by superimposing all the matchings by taking the preimage of all the horizontal blue lines, as in Figure 9.3, we see that since the diagram is symmetric with respect to the real axis flip, we are obtaining a palindromic chain.

Clear immediately from examples like in Figure 9.1 are the features for the combinatorics discussed in Chapter 8. The rectangle diagram is reflection symmetric with respect to the flip across the real axis, and performing top-to-bottom Morse theory is mirrored in the bottom-to-top Morse theory on the preimage. The first observation recovers a reflection symmetric non-crossing matching as the pullback of any regular vertical line in the rectangle, and the second observation precisely translates to the palindromic condition for chains of non-crossing matchings that come from pulling back the regular horizontal lines of the rectangle.

Thus in this portion of the full (Metric) Basketball Complex, instead of simply looking at a chain times a chain in the product of two copies of the geometric realization of the non-crossing partition lattices (subject to the basketball condition), we are considering

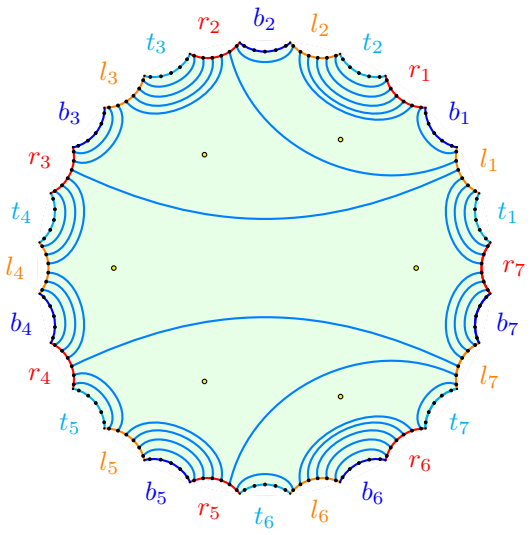

Figure 9.3: The pullback of all the horizontal blue lines at once. Since the diagram is reflection symmetric, this is a palindromic chain of left-right non-crossing matchings.

a chain in the reflection symmetric non-crossing partition lattice times a palindromic chain (still subject to the basketball constraint). We summarize this observation in the Theorem below, which is self-evident from the diagrams that arise for real polynomials and our discussion.

Theorem 9.2.3. *The portion of the (metric) basketball complex that comes from monic real polynomials consists of products that form* metric basketballs *of the form*

$$R \times K$$

where R is a chain of reflection symmetric non-crossing partitions and K is a palindromic chain.

With this in mind, we can describe the general features for this portion of the Metric Basketball Complex, which we refer to as the real metric basketball complex.

Remark 9.2.4 (Palindromic Barycentric Coordinates)**.** Geometrically realizing a palindromic chain results in a simplex as with any other chain. But generally, each subchain

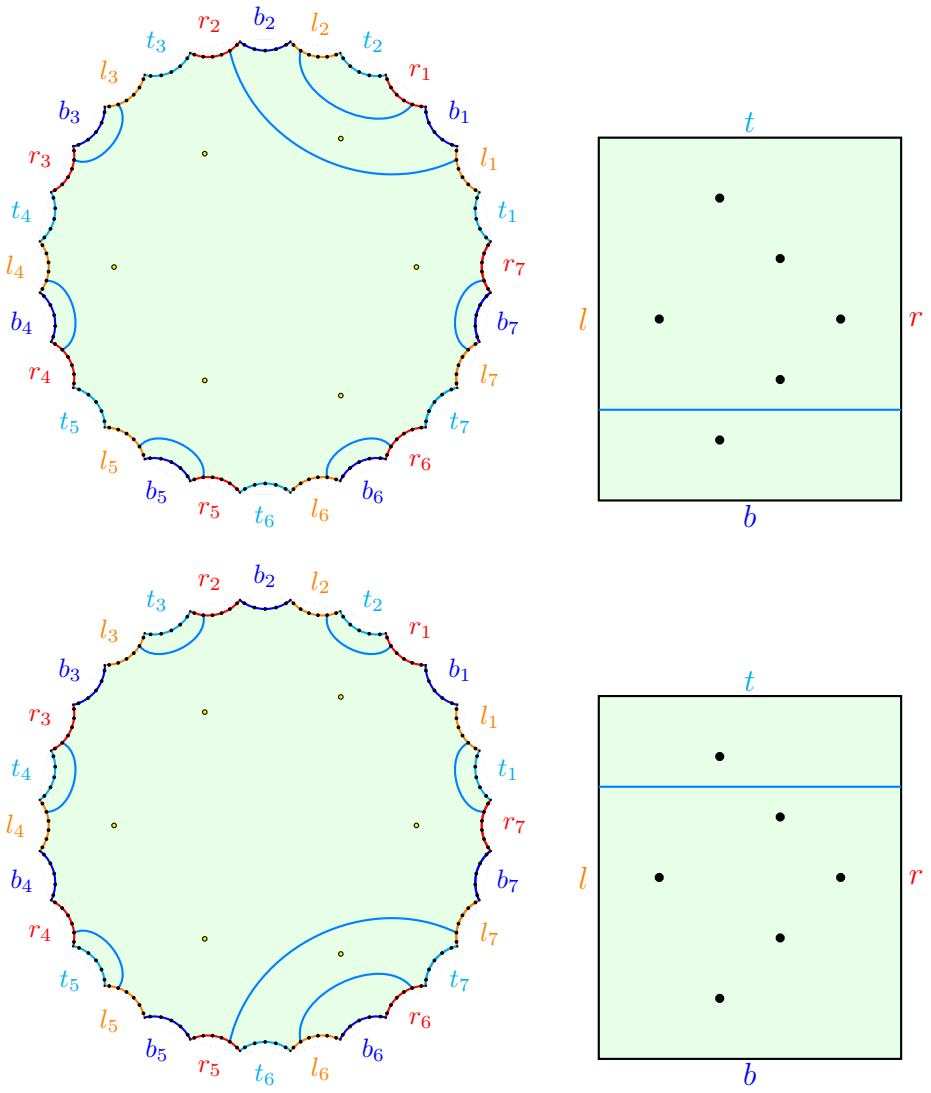

Figure 9.4: Pulling back the horizontal blue lines as pairs with its reflected copy recovers palindromicity.

would define a face of that simplex, whereas for palindromic chains not every subchain is a palindromic chain. To produce a subchain that is still palindromic, we need to consider the fix set of this simplex under the flip Kreweras map. Concretely, we have an orthoscheme defined on barycentric coordinates and there is a natural map that sends those barycentric coordinates to themselves, i.e for barycentric coordinates, $t_0, t_1, \ldots, t_{n-1}$ satisfying $\sum t_i = 1$ with all $t_i \geq 0$, we are interested in the fixed set under the map that sends $t_i \mapsto t_{n-1-i}$, which in particular is the intersection of the halfspaces defined by $t_i = t_{n-1-i}$. For clarity we consider this example, say we have barycentric coordinates defining the simplex in Figure 9.5:

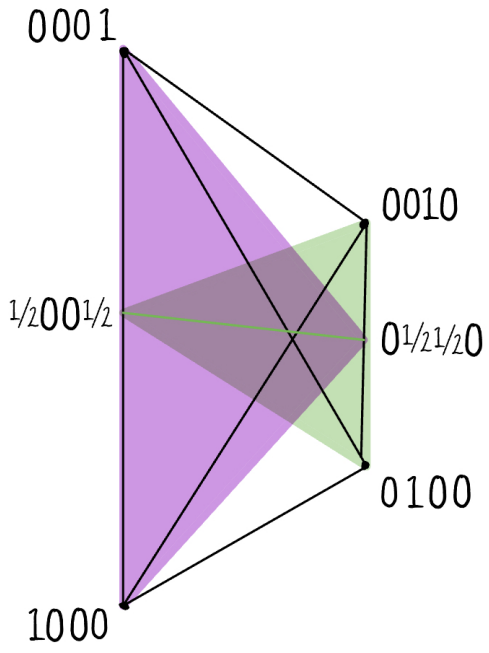

Figure 9.5: A 3-dimensional simplex with the highlight intersection corresponding to palindromic vertices.

So that the portion of this simplex that we really are interested in is simply the segment that is the convex hull of $\frac{1}{2}\,0\,0\,\frac{1}{2}$ and $0\,\frac{1}{2}\,\frac{1}{2}\,0$. Generally, for an n-dimensional simplex, the palindromic barycentric coordinates form a $\lfloor \frac{n}{2} \rfloor$-simplex.

Said another way, every palindromic chain corresponds to an orthoscheme, but rather than associating it to the full orthoscheme, wherein, some points don't exhibit palindromicity, we associate it to the barycenter. Palindromic subchains again would be barycenters of faces in that orthoscheme and moving around within the convex hull of these points retains the palindromicity throughout. So the palindromic chain gives a simplex of palindromic points of roughly half dimension. We summarize this remark in the Proposition 9.2.5

Proposition 9.2.5. *In the orthoscheme realization of a palindromic chain of length n, the portion in the real basketball complex is the convex hull of the palindromic barycentric points which is $\lfloor \frac{n}{2} \rfloor$-simplex.*

Remark 9.2.6. For the Reflection symmetric points, these match with every point in orthoschemes that are realizations of Reflection Symmetric Chains. So, the order complex of the Reflection Symmetric non-crossing Partition Lattice is entirely made up of admissible points.

Example 9.2.7. We can construct the real basketball complex concretely for degree 3 polynomials. There is a single palindromic tree on the vertices of the regular triangle, the geometric realization of the associated chain is itself a triangle, but the palindromic points are simply a segment with two palindromic vertices by Proposition 9.2.5. For the reflection symmetric non-crossing poset, again there is a single maximal chain, whose realization is again a triangle, but all these points and vertices are admissible. So, before passing through to the basketball criterion, we have the product of a segment with a triangle to form a triangular prism. Of the six vertices on this triangular prism, one vertex does not pass the basketball criterion, as we can check manually in Figure 9.6.

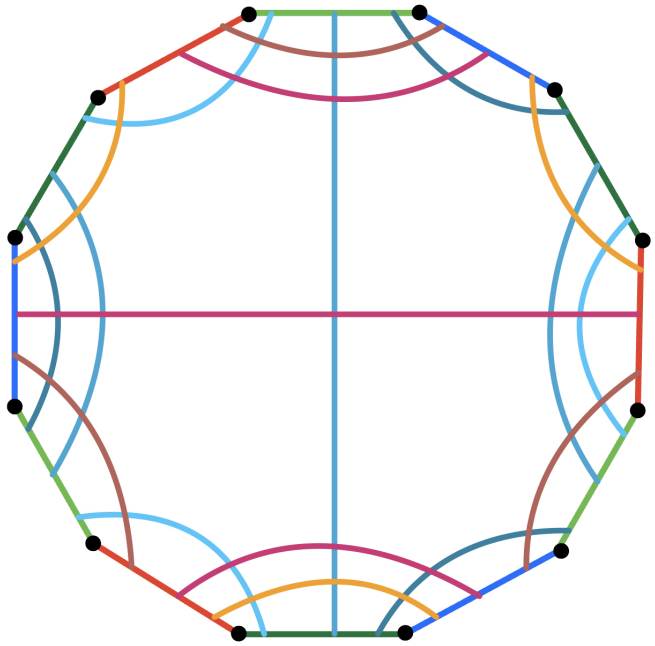

Figure 9.6: The superimposed non-crossing matchings for a reflection symmetric and palindromic chain that do not form a basketball.

So in particular, the full triangular prism is not the basketball complex we want. Instead we obtain the portion of that triangular prism highlighted in Figure 9.7. Metrically, this complex is a triangle times a point, glued to a product of two segments. I.e. it is a triangle glued to a square. This geometry comes from looking at the pairs of chains that do form basketballs, which for degree 3 are given in Figure 9.8. In the basketball on the left of the figure, the reflection symmetric chain is length 2, and as such is geometrically realized as a right triangle. The palindromic chain for that basketball is the trivial chain of length 1. Its geometric realization may be a segment, but the palindromic point is just the barycenter of the segment. That pair recovers the triangle times a point shaded in green in Figure 9.7. The right hand basketball in Figure 9.8 consists of the trivial chain in the reflection symmetric poset, which is a full segment, and a palindromic chain of length 2, which geometrically is the 1-simplex determined by the palindromic barycentric points

by Proposition 9.2.5. The two segments together form as their product the square shaded in blue in Figure 9.7. They are glued along another basketball (not pictured) which is the product of the trivial chain with itself producing an segment for the symmetric part and a point for the palindromic part, so an edge in total. As a look ahead, this matches the right hand portion for the distinct root case covered in Chapter 10 in Figure 10.6.

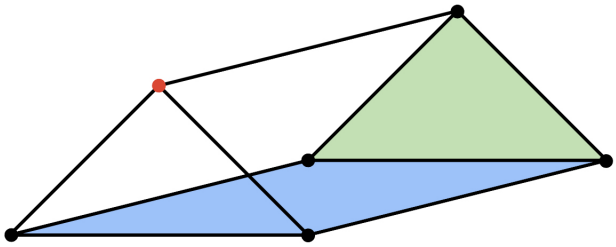

Figure 9.7: The portion of the triangular prism that forms the basketball complex for degree 3.

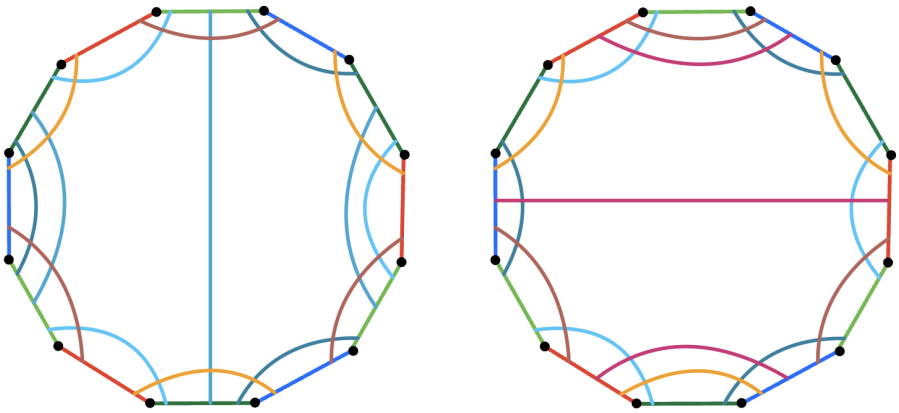

Figure 9.8: Two basketballs corresponding to top dimensional cells in the basketball complex for degree 3.

Remark 9.2.8. In the complex polynomials case, side identifications of the metric basketball complex produced the complex for monic centered polynomials with distinct roots

via the induced homotopy on polynomials coming from deforming a rectangle into an annulus, where the gluing described in [12] happened along the negative real axis. In the real polynomial case, since we are considering just the fixed set of the complex by the action of complex conjugation, the connection with distinct roots is harder to codify. Another impediment is that real polynomials often have negative critical values, so this manipulation will always leave out some information. Of course, we have the ability to carry out the same investigations if we glue the sides of the rectangle to become the positive real axis. In this case, no critical values are positive, but the diagrams and analysis is exactly analogous. For degree 3, we would again obtain a right triangle glued along its hypotenuse to a square. The triangle cell, as in the previous example describes polynomials with two real critical values because the symmetric chain is length 2, meaning the two critical values have different real parts, forcing them to be real. By identifying the square in each case under the natural map in which these are actually the same polynomials (since no critical values lie on either side of the real axis in this area) we obtain the full content of Figure 10.6, as we should expect. Our ability to recover the full picture relating to the distinct roots case of Chapter 10 is in some ways an artifact of the low degree in this example. For degree 4 and others, these analogous points of view (forming a version of the basketball complex avoiding the negative reals and another avoiding the positive reals and then gluing) will uncover more of, but not all of, the structure in the distinct roots case since there are also cases with distinct roots that have positive and negative real critical values.

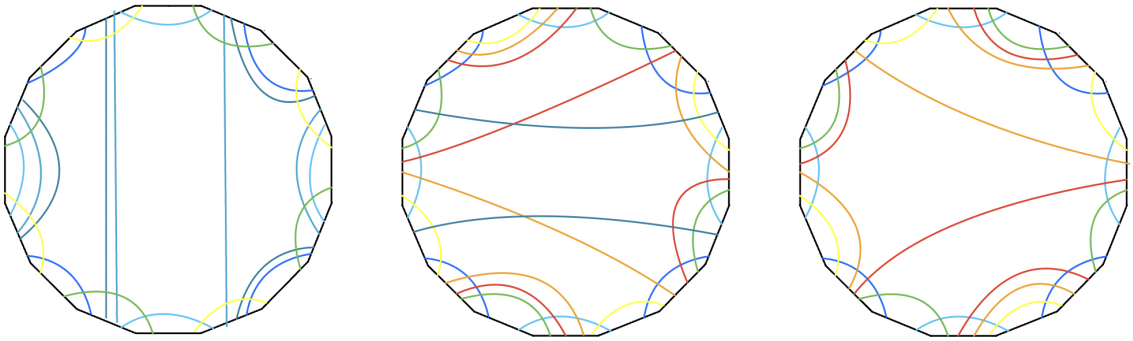

Figure 9.9: A non-exhaustive set of diagrams for basketballs in degree 4.

Remark 9.2.9. See Figure 9.9 for some of the basketball diagrams that appear for degree 4. We can describe the cells they contribute in the basketball complex by investigating the lengths of the chains. The leftmost basketball is the trivial palindromic chain matched with a length 3 reflection symmetric chain so geometrically it is a point times a tetrahedron. The middle basketball is a length 2 palindromic chain (so geometrically an edge by Proposition 9.2.5) and a length 2 symmetric chain, so geometrically it is an edge times a triangle... a triangular prism. The rightmost basketball has a length 2 palindromic chain and the trivial symmetric chain, so geometrically it is an edge times an edge... a square.

Chapter 10

Real Polynomials with Distinct Roots

Transitioning now to distinct roots, by way of Theorem 7.2.11, we devote this chapter to the subcomplex of the branched annulus complex corresponding to real polynomials with distinct roots. This still has many mysterious features especially in degrees larger than 5. However, we do know several interesting features that apply generally, and we have full understanding in low degrees.

Remark 10.0.1. In general the three important sets that we focus our attention on are roots, critical points, and critical values. The root point of view is helpful for understanding the underlying topology. The critical points must live in the convex hull of the roots. The critical values are what determines the metric information. Ideally, we want to meld these points of views together in order to obtain a full picture.

10.1 General Features

In this section we prove general features for the cell complex of monic and centered real polynomials with distinct roots. This is the fixed complex of the Branched Annulus complex under the action of complex conjugation.

Theorem 10.1.1 (Connected components)**.** *The subcomplex of real polynomials in the space of monic centered complex polynomials with distinct roots of a given degree with the pullback metric is disconnected. In particular, each connected component consists of all monic, centered real polynomials with distinct roots of that degree that share the same number of real roots.*

Proof: Real polynomials in this setting are exactly the ones fixed by the action of complex conjugation. Thus, complex roots appear in pairs that are mirrored across the real axis. Because of this restrictive symmetry, any path through real polynomials in which a complex pair of roots becomes two real roots, must go through a double real root before splitting into distinct real roots. Since that intermediate step is not within our space, it constitutes a disconnection.

Since the cell structure of the space is completely determined by the critical values, we also want to ensure that the pullback of a path of the critical values in the closed annulus is a path of real polynomials. If the range is symmetric with respect to complex conjugation, and you have a path in that closed annulus that is symmetric with respect to complex conjugation, you may still have a non-symmetric preimage. However, if the branched annulus begins as something symmetric with respect to complex conjugation, and then you have a path on the range side that respects complex conjugation, we know that has a unique lift. If the unique lift breaks complex conjugation, then we can apply conjugation to obtain a second lift, which violates the unique lifting of paths. Therefore, we may form a path between any two real polynomials via real polynomials so long as

they retain the same number of real roots. □

Corollary 10.1.2. *The number of connected components in the degree d space of monic square-free real polynomials is*

$$\left\lceil \frac{d+1}{2} \right\rceil$$

Proof: By Theorem 10.1.1, we need only count how many real roots are possible, with the only restriction coming from the fact that the number of other roots, the complex conjugate ones, must come in pairs, including the potential for zero pairs of conjugate complex roots. □

Example 10.1.3. For example, in degree 2, a polynomial could have no real roots or two real roots (the possibility of a single real root is excluded since it corresponds to the case in which there is a repeated root at the vertex). The critical value of the monic quadratic polynomial would be negative in the former case and positive in the latter. As such, the completion of the pullback metric gives rise to two disjoint segments– edges inside the two dimensional cellular complex of complex polynomials with distinct roots of degree 2.

Example 10.1.4. In degree 3, there are also two connected components corresponding to the case of a single real root and that of three real roots.

When the polynomial has three real roots, it necessarily has two critical values, with one of each parity. Any combination of values is acceptable, therefore the completed metric object corresponding to this case is the two-fold product of intervals, a square. when there is a single real root, the situation is a bit more complicated. The distribution of critical values could be: one or two negative, one or two positive, or one pair of complex conjugates. In the cases of the real critical values, the magnitudes of the values dictate the specific monic cubic. Metrically, these cases produce orthoschemes. To see this in the

positive value case, letting v_M and v_m be the local maximum and minimum (or saddle), respectively, we can assign any values inside $0 \leq v_m \leq v_M \leq 1$. The values satisfying these inequalities give a right-angled triangle, also known as a 2-orthoscheme. When $v_M = v_m$, there is a saddle point, and perturbing this value in the complex direction will split the value into the conjugate pair scenario. Since they are conjugate, we don't obtain any extra metric information by considering both points of the pair. We observe that the value with positive imaginary part can take any value in the upper half plane, so under the completed metric we have a square. The gluing of the two orthoscheme cells with the square happens on opposite side of the square and along the hypotenuse of each orthoscheme. Ultimately, this component is a hexagon with two right-triangular cells capping off opposite sides of a square as in Figure 10.6.

Example 10.1.5. For degree 4 polynomials, the case in which all roots are real follows a similar vein as in the previous degrees. Name the three critical values v_l, v_p, v_r for the left, positive, and right values under the normal viewpoint for the graph of the quartic. The values that are negative can be any combination of negative values, so that gives rise to a square. Cellularly, we have two 2-orthoschemes meeting along their hypotenuse, coming from whether $v_l \leq v_r$ or $v_r \leq v_l$. Then due to the positive critical value v_p having maximum choice along the positive axis, we take the product of this subdivided square with an interval. The result is a cube, formed by stacking two triangular prisms together in the obvious way.

Generalizing to any degree, the component in which all the roots are real gives the nice structure of a hypercube.

Theorem 10.1.6. *For a degree d polynomial, the subcomplex corresponding to the all real roots case will be a $(d-1)$-cube, the product of the $\lfloor \frac{d}{2} \rfloor$-cube of negative critical values and the $\lfloor \frac{d-1}{2} \rfloor$-cube of positive critical values (counting multiplicity).*

This $(d-1)$*-cube is divided into* $\lfloor \frac{d}{2} \rfloor ! \lfloor \frac{d-1}{2} \rfloor !$ *copies of* $\Theta_{\lfloor \frac{d}{2} \rfloor} \times \Theta_{\lfloor \frac{d-1}{2} \rfloor}$*, where* Θ_n *is an* n*-orthoscheme.*

Proof: In this component, since all roots are real, the same is true for all critical points (which are necessarily distinct) and their associated critical values (which need not be distinct). The structure of a $(d-1)$-cube comes from the freedom to choose any tuple of the $\lfloor \frac{d}{2} \rfloor$ negative critical values, and the $\lfloor \frac{d-1}{2} \rfloor$ positive critical values. Together, the product of the $\lfloor \frac{d}{2} \rfloor$-cube of negative values with the $\lfloor \frac{d-1}{2} \rfloor$-cube gives us the full $(d-1)$-cube since $\lfloor \frac{d}{2} \rfloor + \lfloor \frac{d-1}{2} \rfloor = d-1$.

Cellularly, any linear ordering is possible on the negative critical values and similarly on the positive critical values. Given a linear ordering of the negative critical values, we get a full orthoscheme worth of combinations as the values would be subject to inequalities $0 \leq v_1 \leq v_2 \leq \cdots \leq v_{\lfloor \frac{d}{2} \rfloor} \leq 1$.

Any linear ordering of the critical values is possible, so in total there are $\lfloor \frac{d}{2} \rfloor !$ many and the product would be taken with any of the $\lfloor \frac{d-1}{2} \rfloor !$ many copies of $\Theta_{\lfloor \frac{d-1}{2} \rfloor}$ arising from order the positive critical values. They glue along facets when equality arises like in the case of $v_1 \leq v_2 \leq v_3$ and $v_1 \leq v_3 \leq v_2$ we glue when these orthoschemes along the $v_1 \leq v_2 = v_3$ facet. □

Remark 10.1.7 (Branched Annuli and Lemniscates)**.** In the distinct roots case, all of our critical values lie in an annulus and have positive magnitude. The pullback of the positive levels of the modulus of a polynomial with distinct roots were referred to in [11] as *multipedal pairs of pants* which can be given a cell structure to produce what they call a *branched annulus* by pulling back critical level and direction sets (see [11] for details). This matches somewhat with the notion of a generalized lemniscate in the language of Arnol'd [2].

Definition 10.1.8. A line of positive level of the modulus of a polynomial is called a

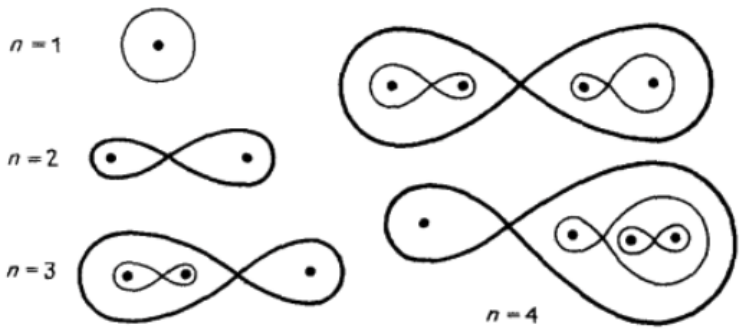

Figure 10.1: Some generalized lemniscates for different n.

generalized Cassini oval and if the level is critical, a *generalized lemniscate*.

In Figure 10.1 we see some lemniscates where the points can be thought of as the roots of the associated polynomial.

Remark 10.1.9. For our purposes, lemniscates will refer to the pulling back of all the critical levels, which produces in a Morse theoretic way a chain of non-crossing partitions of the roots of the associated polynomial. In [2], two generalized lemniscates are topologically equivalent if one can be deformed into the other. For real polynomials, this notion of equivalence is overly broad since it would equate lemniscates coming from different connected components of our cell complex or via homotopies that leave a particular connected component. Instead, we will refer to generalized lemniscates as being *similar* if they can be deformed to the other via a homotopy that stays within the same path component.

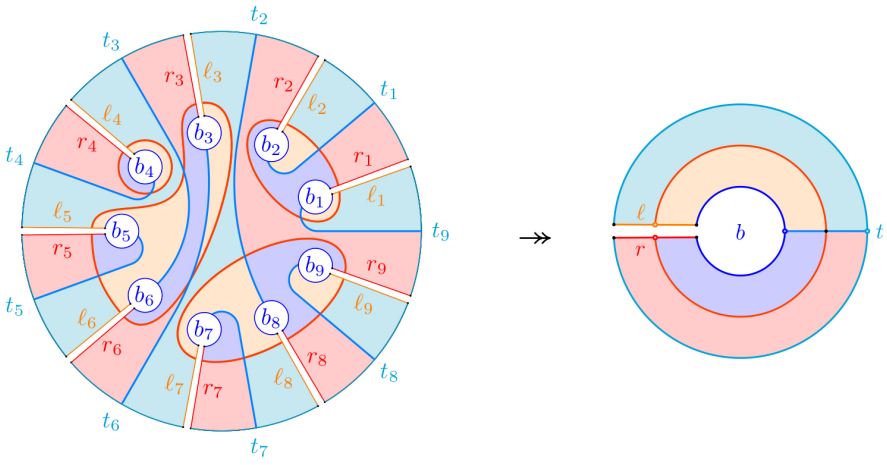

Figure 10.2: The annular version of a basketball formed by pulling pack a (regular) line of positive level of the modulus of a polynomial.

Remark 10.1.10. Regarding the similarity classes for the lemniscates in the case of all real roots, each gives rise to chain in the non-crossing partition lattice, which for the configuration of roots along the real axis is also a chain in the composition lattice (not necessarily maximal).

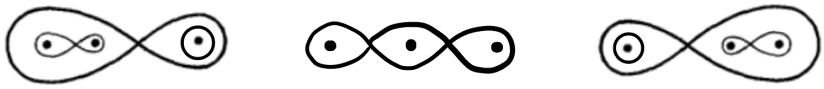

Figure 10.3: The three similarity classes for lemniscates in degree 3.

Theorem 10.1.11. *The number of similar lemniscates in the all real roots case is encoded by the Fubini Numbers.* `https://oeis.org/A000670`

Proof: A similarity class of a lemniscate for a polynomial with all real roots has to connect adjacent roots through the critical point between them. This means we have the following bijection from lemniscates to chains in the non-crossing partition lattice of points in a straight line, which is the composition lattice that go from the minimum

element to the maximum element: starting at $1+1+\cdots+1=d$, each critical level will correspond to collapsing some collection of the plus signs until none remain. Since the number of chains (not necessarily maximal) in the composition lattice that start at $1+\cdots+1=d$ and end at $d=d$ is enumerated by the Fubini numbers, the result follows. One way to see that Fubini numbers count these chains is to use the characterization of Fubini numbers as ordered set partitions. Label the $d-1$ plus signs in order $1,\ldots,d-1$. For an ordered set partition $\bigsqcup A_i=[d-1]$, evaluate the plus signs labeled by the entries in A_i at step i along the chain. □

Remark 10.1.12 (Euler Numbers)**.** Coming back to the cell complex, if a polynomial has no real roots, or a single real root in the odd degree case, and when the polynomial again has all real critical points, this portion of the complex also takes the form of orthoschemes that can be enumerated using ZigZag numbers, also known as Euler numbers `https://oeis.org/A000111` that count the number of up-down permutations on n letters The Zig numbers `https://oeis.org/A000364` count these type of permutations of even letters and the Zag numbers `https://oeis.org/A000182` count them for odd letters.

Theorem 10.1.13. *1. If the degree d is even, there are $Zag(\frac{d}{2})$ many $(d-1)$-orthoschemes in the cell complex of real degree d with no real roots corresponding to when all the critical **points** are real.*

2. If the degree d is odd and instead there is one real root, there are

$$(Z_{k-2i}\cdot Z_{2i}) \text{ many } \Theta_{k-2i}\times\Theta_{2i}$$

for $0\leq i\leq\frac{k}{2}$ where $k=d-1$ and $Z_n=Zig(\frac{n}{2}+1)$

Proof: When the degree is even, since the polynomial is monic, all the critical values must be positive. From left to right in the graph of the polynomial in the plane,

the critical values must satisfy $v_1 \leq v_2 \geq v_3 \leq \cdots \geq v_{d-1}$. This up-down correspondence means that a particular tuple of critical values may come from any of the valid up-down permutations on $d-1$ letters, which is encoded by the Zag numbers.

When the degree is odd, the single real root could lie before, between, or after the critical points. But once the parity of critical values changes, it does not change back. The sign must come in pairs since the 1st is a local maximum, then a local minimum, and so on. When the values have the same sign, they must follow down-up pattern such as $v_1 \geq v_2 \leq v_3 \geq \cdots \geq v_j$ (where j is necessarily even) which is encoded by the Zig numbers. □

A further generalization of the above theorem exists for an arbitrary number of real roots. Indeed, when all critical points are real, they can be linearly ordered and partitioned by the real roots of the polynomial. For example, a degree 7 polynomial with three real roots may have six real critical points where two occur before the first root, 3 between the first and second root and one after between the second and third root. The one extra caveat, is that there are restrictions on the number of critical points allowed within these gaps. If the critical points occur before or after all of the real roots, they must occur in groups of even size. If they occur between roots, they must occur in odd sized groups so that the real graph can change direction back towards the x-axis.

Theorem 10.1.14. *For a degree d polynomial with $m < d$ real roots, for any partition of $d-1$ with m parts like $p_1 + p_2 + \cdots + p_{m+1} = d-1$ satisfying the conditions: p_1, p_{m+1} are even (including possibly zero) and p_i is odd for all $i \neq 1, m+1$ we obtain*

$$Zig_{p_1} \cdot Zig_{p_{m+1}} \cdot \prod_{i=2}^{m} Zag_{p_i} \text{ many } \Theta_{p_1} \times \Theta_{p_{m+1}} \times \prod_{i=2}^{m} \Theta_{p_i}$$

orthoscheme products corresponding to when all critical points are real and linearly ordered within the real roots as determined by the partition.

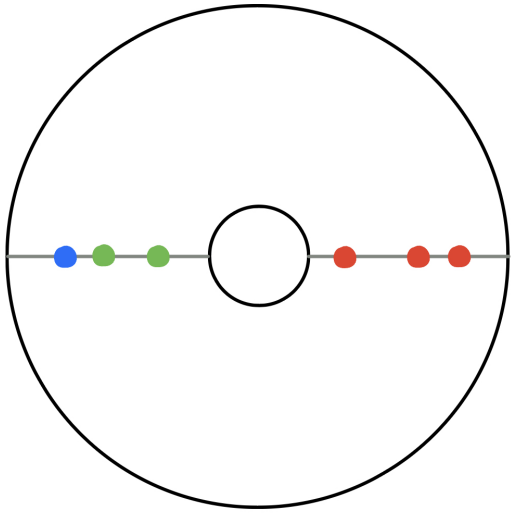

Figure 10.4: The annulus (output) view of a degree 7 polynomial agreeing with the partition $2+3+1+0$ in the language of Theorem 10.1.14.

For example, for the partition $2+3+1+0$ there are 2 copies of $\Theta_2 \times \Theta_3 \times \Theta_1$ corresponding to degree 7 polynomials with three real roots that have six real critical points where two occur before the first root, 3 between the first and second root and one after between the second and third root. They are glued along the $\Theta_2 \times \Theta_2 \times \Theta_1$ where the first and third critical point between the first and second root agree on their associated critical values. The Figure 10.4 shows an example polynomial output matching with this example. The points of the same color may be moved along the positive and negative real lines which traces out an orthoscheme. Different colored points don't depend on each other. In this figure, the green points are the first two critical values associated to the critical points prior to the first root (the 2 in the partition), the red are the positive values associated to the three critical points between the first and second roots (the 3 in the partition), and the blue point is the critical value associated with last critical value between the 2nd and 3rd roots (the 1 in the partition).

Theorem 10.1.15 (Topology of Components)**.** *The fundamental group of a connected*

component corresponding to n pairs of complex conjugate roots is the braid group on n strands.

Proof: Since real polynomials are fixed under complex conjugation, the preimage of $\mathbb{C}\backslash\{0\}$ (which compactifies to a punctured disk, punctured at the roots of the polynomial) has mirror symmetry with respect to the real axis, and therefore, we may understand the topology by understanding the upper half plane. In that upper half plane, roots may move freely so long as they do not collide, and so braiding is exhibited by these roots. The real roots do not contribute to the fundamental group. □

Corollary 10.1.16. *Components of degree d real polynomials with d or $d-2$ real roots are the only contractible components.*

10.2 Degrees up to 5

In this section we our knowledge of how the critical values of a real polynomial behave to concretely describe the components for the cell complex of monic and centered real polynomials with distinct roots in degrees 3, 4, and 5.

10.2.1 Degree 3

Since we know what the component corresponding to all real roots looks like for degree 3 by Theorem 10.1.6, we only have one other connected component to determine. The component in degree 3 corresponding to a single real root and a complex conjugate pair of roots is a subdivided hexagon.

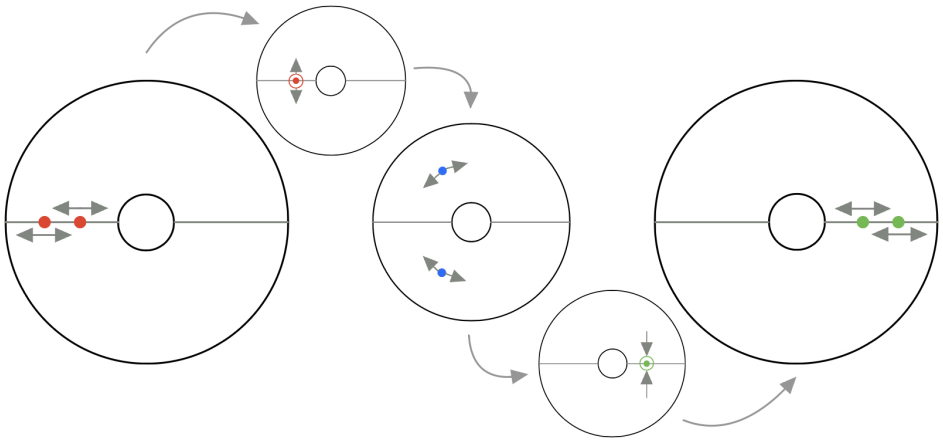

Figure 10.5: The degree 3 polynomial component corresponding to one real root.

In Figure 10.5 we consider how the critical values of such a polynomial might behave. From the critical values we are able to form the cell complex. We see that we obtain one triangle which is a 2-orthoscheme whose interior is characterized by distinct real negative critical values, thus it corresponds to the possible ways in which the red points can move along the interval in the leftmost diagram in Figure 10.5. On the hypotenuse, these critical values have become one of multiplicity 2. It is connected via an edge of a square which is the situation corresponding to complex critical values and depicted by the central diagram in Figure 10.5. The other end is a right-triangle (2-orthoscheme) that again corresponds to real critical values, though this time they are both positive which is depicted in the right-most diagram for the figure and is similarly glued up along its hypotenuse.

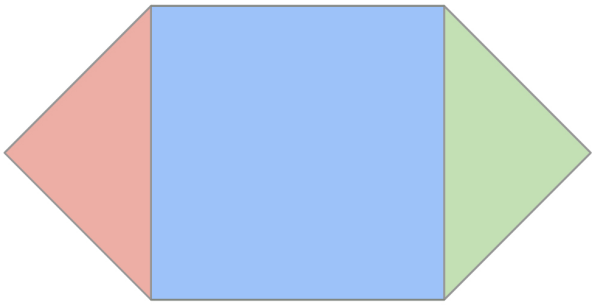

Figure 10.6: The subdivided hexagon obtained by investigated the metric information for degree 3 polynomials with one real root.

10.2.2 Degree 4

In degree 4, there are three connected components corresponding to the disjoint situations where we have (1) four real roots, (2) two real roots and a complex conjugate pair of roots, or (3) no real roots and two pairs of complex conjugate roots.

When there are four real roots, the case is completely understood in terms of Theorem 10.1.6 and as discussed in Example 10.1.5, it is a cube subdivided into two triangular prisms. In the rest of this section, we wish to concretely describe the other two connected components.

We begin with the case in which there is one pair of conjugate roots, and two real roots. One feature to keep in mind in this case and in other even degree cases, is that a real minimum of the function exists as a real critical value. In particular, when there are two real roots for the polynomial, the real minimum of the function is a negative critical value. For the other two not necessarily distinct critical values, they may both be negative, both positive, or form a complex conjugate pair. From the real graph it is clear we may have three distinct real critical points where either the first pair appear before the first root (when a local minimum and maximum occurs to the left of the first root), between the real roots (when 3 local minima/maxima occur between the real roots), or

we have a pair of real critical points after the roots (when there is a local max/min after the roots). We may also have two distinct real critical points, when one has higher multiplicity this time with 4 possibilities— we may have a saddle prior to the first root, a saddle to the left or right of the global minimum but between the two roots, or a saddle to the right of the roots. When there is one (necessarily real) critical point of multiplicity 3, the real graph appears as a wide-looking quadratic.

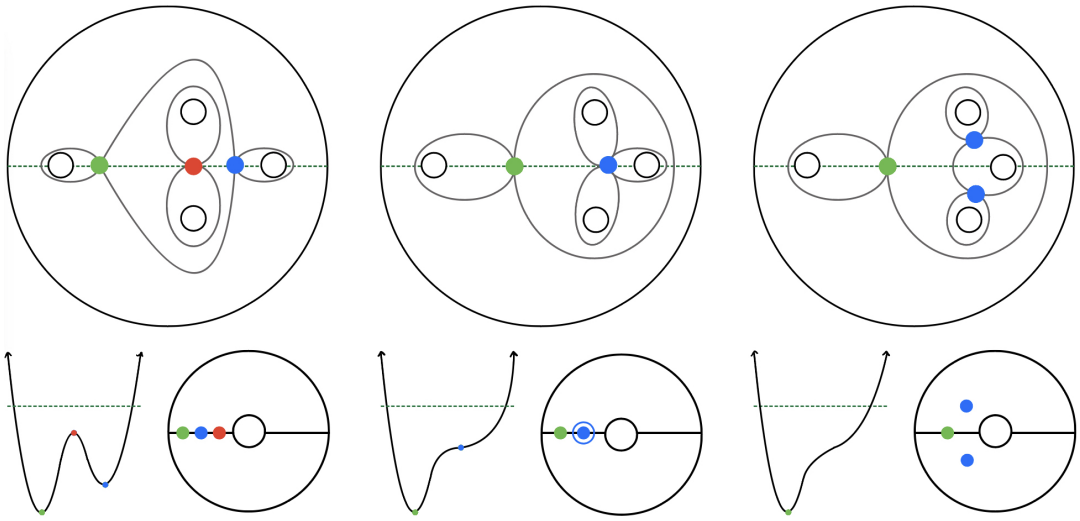

Figure 10.7: Sample polynomials from three perspectives tracing a path from all real critical points to one pair of complex conjugate critical points.

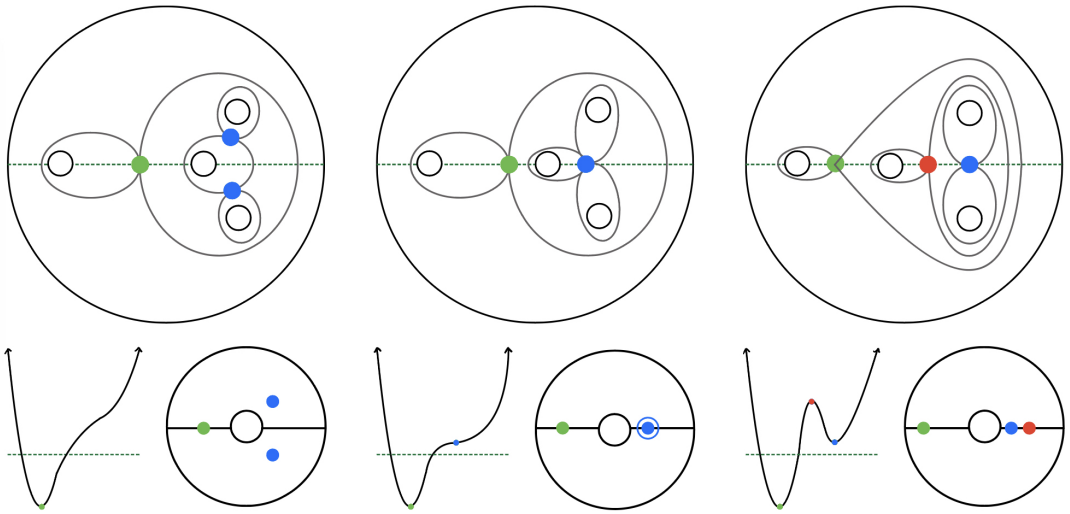

Figure 10.8: Sample polynomials from three perspectives for continuing the path from Figure 10.7 until real positive critical values appear.

Remark 10.2.1. In each cluster in Figure 10.7 (and the other similar figures) we balance three viewpoints simultaneously. In the bottom level is the real graph of the sample polynomial and the annulus containing its critical values. The graph is a key guide but doesn't show every bit of crucial information. The annulus of critical values, the output side, gives us the way to understand the cell structure on the complex via the pullback metric. The top level are the (reflection symmetric) lemniscates corresponding to those polynomials which captures where the roots (interior white circles) and the critical points (the colored points) are positioned. They are helpful to understand what is happening topologically.

When we have a conjugate pair of critical points, their effect may be perceptible on the real graph exhibiting a wiggle on the left or right of the real minimum (exhibited with a sample polynomial as the right cluster in Figure 10.7— in this situation the output side shows that their associated critical values are a conjugate pair of complex numbers, and regardless of the side the annular picture of the codomain may look exactly the

same. The difference is clear on the branched annulus viewpoint of the domain, where the wiggle corresponds to which real root the complex pair is closer to, and is position with respect to the real roots coincides with their orthogonally projected position within the real roots. In other words, taking the right diagram of Figure 10.7 and flipping the real graph through a vertical line would preserve the output diagram, but would also flip the lemniscate diagram through a vertical line.

However, there is one more situation in which a pair of critical points are complex conjugates but they both evaluate to a negative real critical value that has higher multiplicity less than the real minimum of the polynomial. This is basically invisible from the perspective of the real graph and this situation appears to like a quadratic on the real graph exhibited in the right-most diagrams of Figure 10.9.

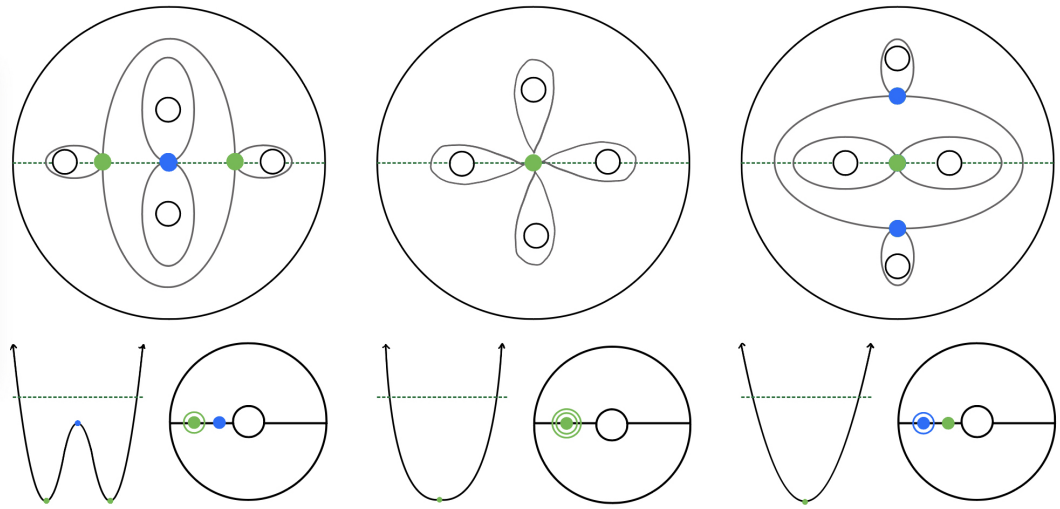

Figure 10.9: Sample polynomials from three perspectives of polynomials that trace the path pulling the complex pair of roots upwards.

With these ideas and guiding figures in mind, we can extract the metric information. In the case for which all the critical values are negative real numbers, we may also have real critical points, and in these cases we obtain two 3-orthoschemes. The left Θ_3 corresponds to when the real minimum value is the left-most in terms of the natural

linear order on the critical points, and the right Θ_3 corresponds to when the real minimum value is the right-most. They are glued along a 2-orthoscheme corresponding to when the real minimum is achieved by both the 1st and 3rd critical points (the situation in the left-most diagrams of Figure 10.9). This Θ_2 is actually part of a square, because glued along its hypotenuse is another Θ_2 corresponding to when there are three real negative critical values come from one critical point witnessing the real minimum, and two conjugate critical points corresponding to a negative critical value of multiplicity 2. This subdivided square comes from polynomials matching with all three examples of Figure 10.9, the perturbing of the left-most gives the interior of one right-triangular side, the middle diagrams represent the tracing out of the hypotenuse, which glues along the right-triangle obtained by perturbing polynomials like the one on the right-most side of the figure.

There is a subdivided left-cube made of of two $\Theta_2 \times \Theta_1$. The interior of this cube is characterized by polynomials having one real critical value and a conjugate pair of critical values. The graph of the polynomial over the real numbers has a wiggle on the right side of the critical point that witnesses the real minimum.

Similarly, another subdivided right-cube for the wiggle on the left side is glued to this one partially on the 2-orthoscheme with the critical value of multiplicity 2 coming from a conjugate pair of critical points. The other half is glued to the boundary of the right Θ_3 where the real graph shows a saddle to the left of the real minimum, i.e. a real critical point of multiplicity 2. Whereas, the other half of the left-cube glues to the face of the left Θ_3 which has a negative real saddle value on the right of the real minimum.

The subdivision of this cube happens along the rectangle where all the critical values have the same norm in the complex space.

Finally, there is a left triangular prism and a right triangular prism whose interiors are characterized with real graphs for a polynomial in which three distinct real critical

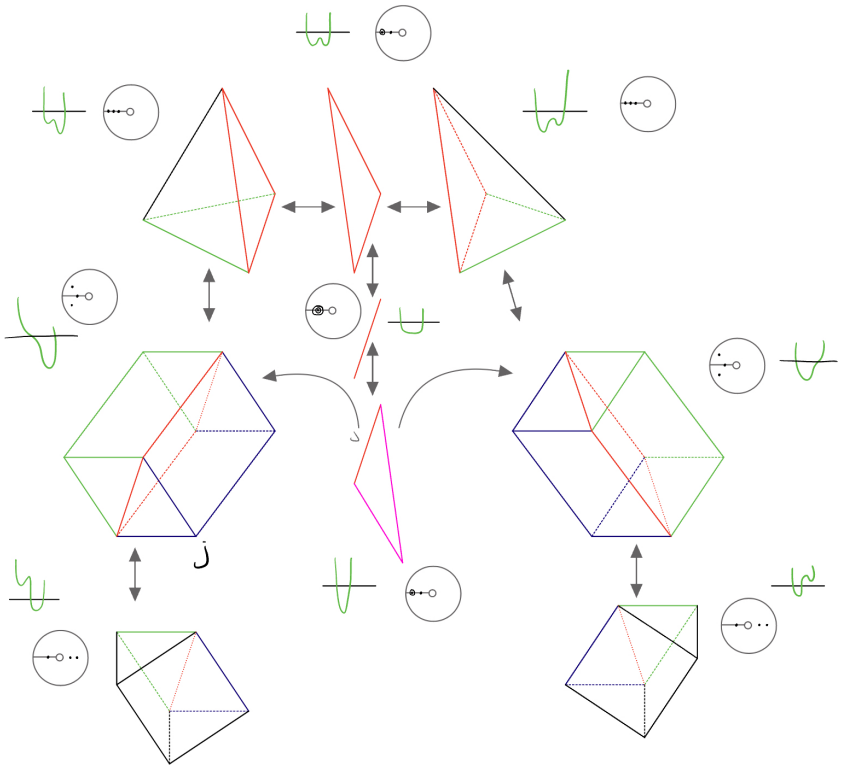

Figure 10.10: The cellular pieces of the component corresponding to two real roots in degree 4.

values arise, corresponding to three real critical points, with the real minimum critical point on the left or right, respectively, of the others in the natural linear order of the real critical points.

These prisms are glued along the square face of the left and right cubes, respectively along the boundary where the real graph exhibits a positive saddle.

Topologically (ignoring the cell structure), since we may precompose with a translation and normalize so that the roots appear fixed on the real axis, whilst the complex root (above the axis) can move freely in the upper half plane, we get a product of a disk with an interval, and so we have the topological type of a 3-ball, which is confirmed by the cellular description as well which is visualized in Figure 10.10. By labeling the vertices of each cell, we can see concretely how they would glue together. So, another

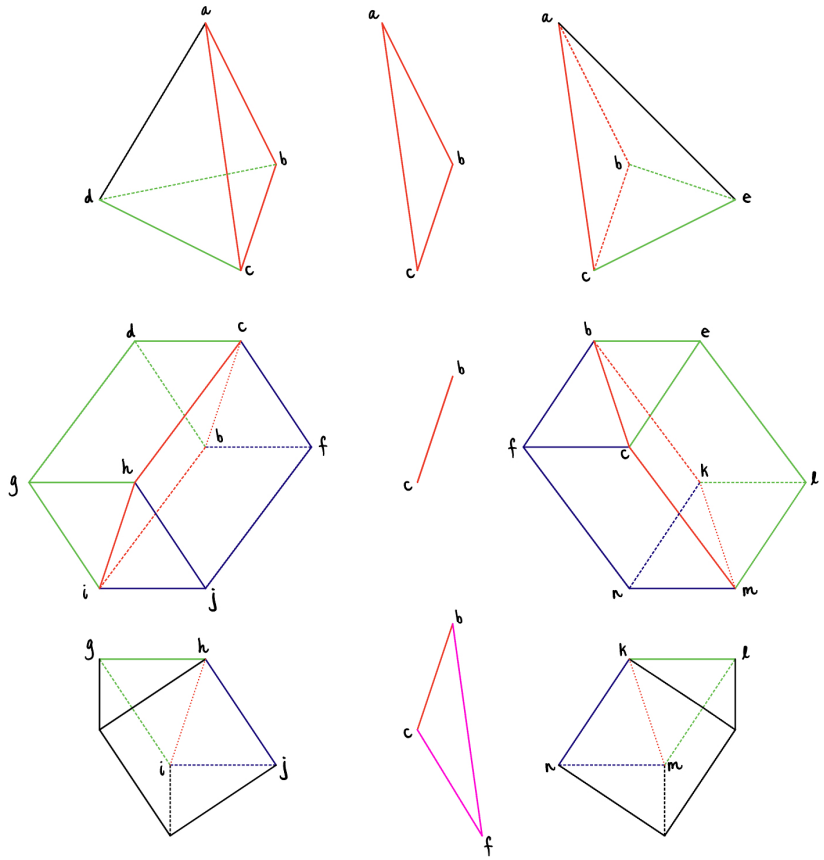

Figure 10.11: The cells with gluing information for the component corresponding to two real roots in degree 4.

way of describing the gluing instructions in 10.10 is shown in Figure 10.11.

The situation is not far off from the above description even when there are no real roots. In this case, the real minimum is a positive critical value, however, negative real critical values of multiplicity 2 may arise corresponding to a conjugate pair of critical points.

Recalling Remark 10.2.1, we want to consider three points of view simultaneously. We want to consider how each viewpoint contributes to our understanding. When no roots are real in degree 4, the real graph lies entirely above the x-axis and has either three distinct real critical points (when there are two local minima and a local maxima), two

distinct real critical points where one has higher multiplicity (when the graph exhibits the two local minima agreeing on the critical value, or when one local minimum coincides with the local maximum forming a saddle), or one real critical point of multiplicity 3.

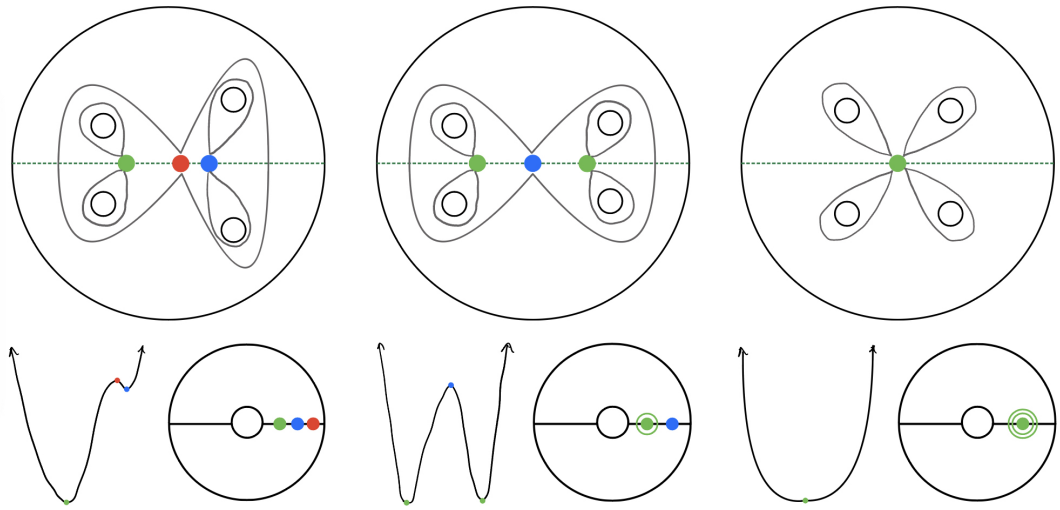

Figure 10.12: Sample polynomials from three perspectives for when all critical points are real.

However, there are other situations to consider, which may not be clear from the real graph, but are clearly born out of the analysis of specific polynomials. One critical point must be real, to witness the real minimum of the function. But, the others may be a conjugate pair of complex critical points. Whether their associated critical values are real or complex conjugates themselves are perceptible on the real graph in most cases, but that aspect is far clearer when using the combination of our three viewpoints.

Take for example the two polynomials $p(z) = (z+i)(z-i)(z-1-i)(z-1+i)$ and $q(z) = (z+i)(z-i)(z+2i)(z-2i)$ which are the left-most and right-most clusters in Figure 10.13. On the real graphs, these polynomial appear very similar, both appearing to resemble a quadratic. And indeed, both pairs of complex critical points for these polynomials correspond to a real critical value of multiplicity 2. The difference, is that

for $p(z)$, the real critical value associated to these critical points is positive, and for $q(z)$ it is negative. The general phenomenon is that if all the roots have the same real part (all the roots line up vertically), we obtain negative critical values imperceptible on the real graph because they come from a conjugate pair of complex critical values. Whereas if the upper half representatives of each pair of roots share the same imaginary part, and the difference in their real part is less than twice their imaginary part (i.e. when the roots form a tall rectangle in complex space) the associated critical value is positive but less than the real minimum.

Through this discussion in the previous paragraphs, we have exhausted all the ways in which a monic square-free real quartic with no real roots may have real critical values.

The other situation is, of course, when the complex pair of conjugate critical points evaluate to a complex pair of conjugate critical values. On the real graph, this is perceptible as a slight wiggle on either the left or right side of the real global minimum. Regardless of which side the wiggle appears, the annular picture of the codomain looks exactly the same. However, on the domain view of the branched annulus, the side of the wiggle corresponds to the side whose imaginary parts are greater as we can see in the middle diagrams of Figure 10.13.

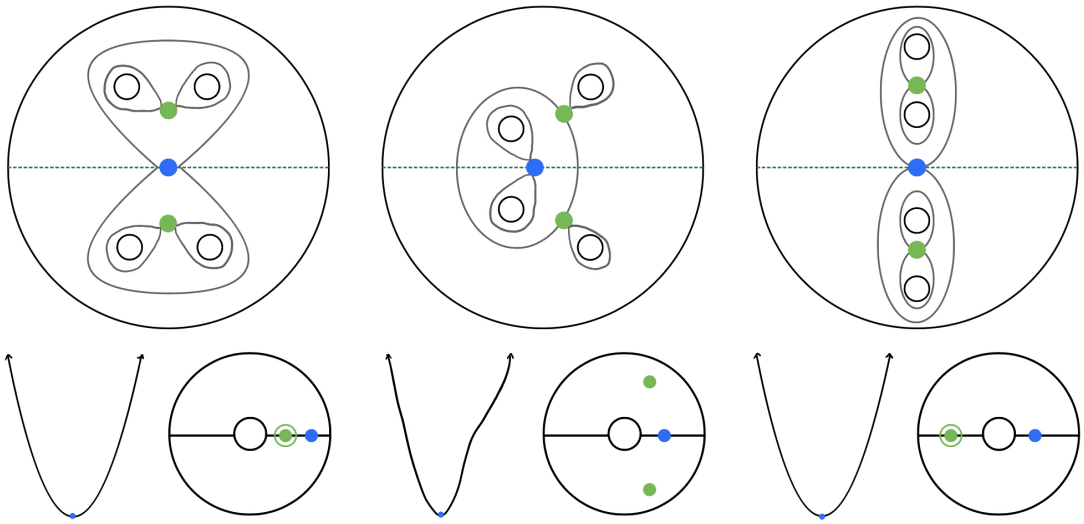

Figure 10.13: Sample polynomials from three perspectives for when a pair of critical points are complex conjugates.

Again there is a left and right 3-orthoscheme, glued along a 2-orthoscheme where the real minimum is achieved by the two outer real critical points which correspond to when all the critical points (and critical values) are real, like in Figure 10.12. As before there are 3 ways to travel with a critical value of higher multiplicity, it can go towards a real saddle on the right, the left, or a complex saddle. The left and right cubes also behave exactly as before, corresponding to a right or left wiggle gluing on the left/right Θ_3, respectively, and the complex saddle triangle shared as a portion of the square face on both cubes. The major difference is the lack of triangular prisms. In fact, whereas in the previous component there was no path between the cubes except for through the Θ_3's or the complex saddle Θ_2, in this component there is a shared boundary of the cubes, a square, corresponding to when negative real critical values of high multiplicity exist, like the situation on the right in Figure 10.13. The real graph of which looks like a sharp parabola.

This complex is visualized in Figure 10.14 with some sample polynomials. Topolog-

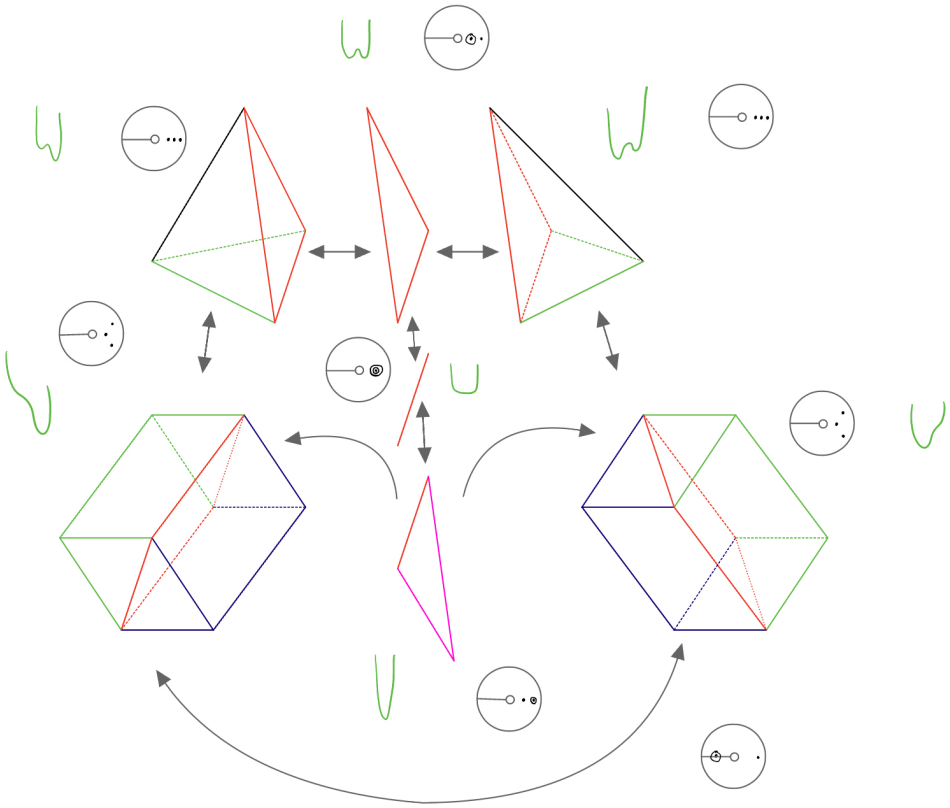

Figure 10.14: The cellular pieces of the no real roots case in degree 4.

ically, since the two roots in the upper half plane can move around each other, we have nontrivial fundamental group agreeing with the braid group on 2 strands, $\mathbb{Z}$. This is confirmed by the way the cells glue together in our complex, which is clarified in Figure 10.15

10.2.3 Degree 5

In degree 5, we have three connected components, like in degree 4, by Theorem 10.1.1. We may use our understanding of the 3-dimensional components in degree 4 to guide us in the case of the 4-dimensional components of degree 5.

Of course, by Theorem 10.1.6 the simplest component to describe corresponds to all

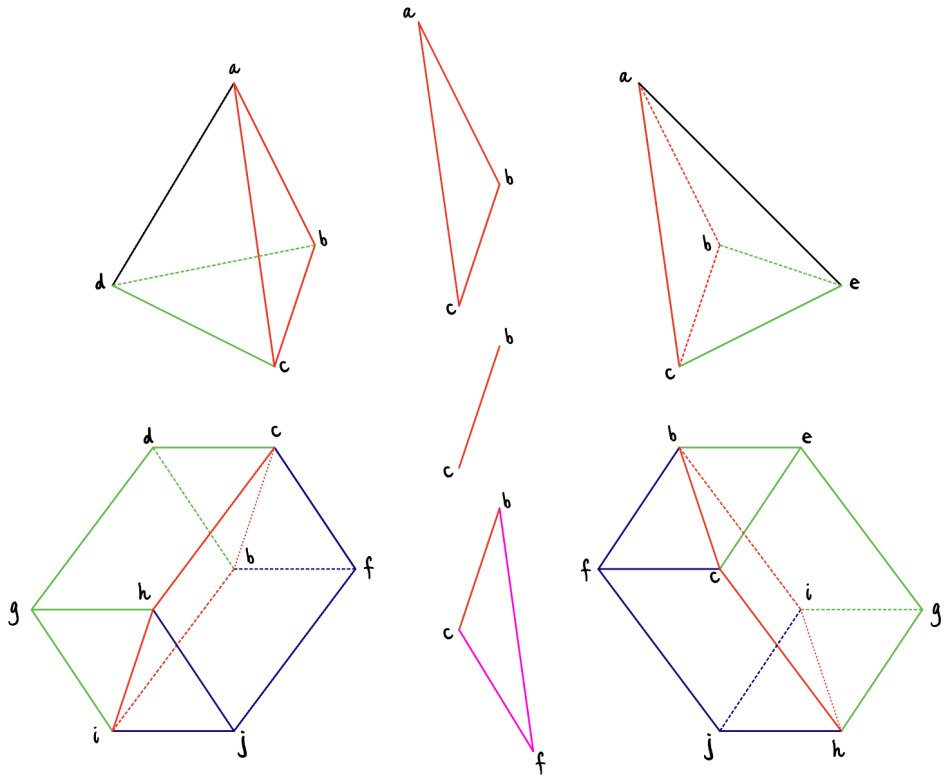

Figure 10.15: The cells with labeled vertices for the no real roots case in degree 4.

real roots, with no pairs of complex conjugate roots.

The other contractible component corresponds to three real roots, and a single pair of complex conjugate roots. The real graph of a polynomial within this component makes immediately clear that at least, we must have one positive and one negative real critical value and they must be positioned with the positive one's critical point between the 1st and 2nd root and the negative critical value's critical point between the 2nd and 3rd real root.

Summing up what happened in degree 4 when there were two real roots, essentially the complex is made up of a square pyramid with an extra triangle, and then two cubes branching out from the square plus triangle base, and then triangular prisms on the other ends of those cubes.

The pyramid is the place where the degree 4 polynomial with two real roots has all the interesting stuff (critical points, etc) happening between those real roots.

For degree 5, with three real roots, there are two hubs which appear like the situation described above for degree 4 with two real roots, except in 4 dimensions. They correspond to the two styles of degree 5 polynomials with three real roots wherein the interesting stuff happens between those roots. Either three real critical points (counting multiplicity) happen between the 1st and 2nd root, or they appear between the 2nd and 3rd root. They are bridged by a 4-cube and have two other 4-cubes heading off over towards 4-dimensional triangular prisms.

So it is like two copies of the degree 4 situation enhanced into a 4-dimensional shape and then superimposing them on each other on one of the cubular branches. This rough description is visualized (the best we can manage for 4 dimensional cells) in Figure 10.16. This is a contractible component and the cellular description confirms that.

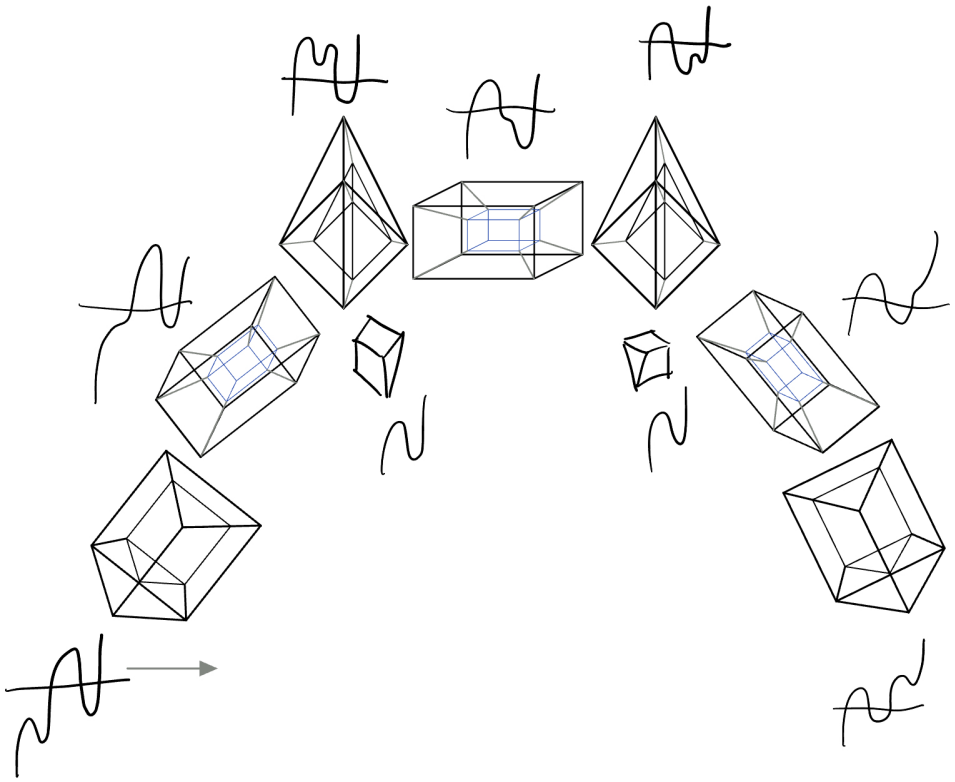

Figure 10.16: The component in degree 5 corresponding to three real roots.

When there is a single real root, we have a $\mathbb{Z}$ fundamental group that comes from the possible movements that two complex roots can rotate around each other in the upper half space. In this case, Theorem 10.1.14 tells us how some of the pieces behave. In particular, there are three hubs where all the critical points are real. One hub is when all the critical points are real and correspond to negative critical values, which by the theorem is five glued together copies of Θ_4. Another similar hub again looks like five glued together copies of Θ_4 for when the critical points are real and correspond to positive critical values. And the last hub corresponds to when the critical points are real and there are two positive and two negative critical values, which geometrically is $\Theta_2 \times \Theta_2$. Between these hubs there are either 4 dimensional triangular prisms: $\Theta_2 \times \Theta_1 \times \Theta_1$ or a 4-cube. Essentially this data is collected in a diagram in Figure 10.17, though in some

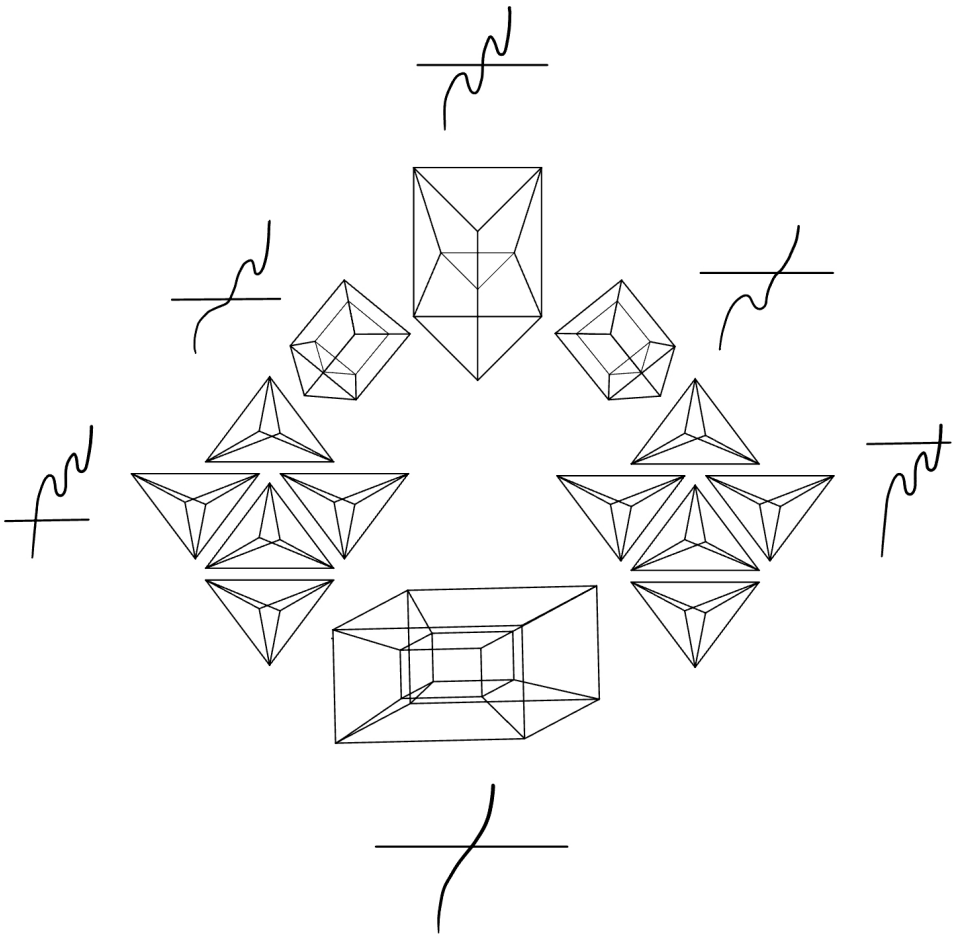

Figure 10.17: A diagram of the main cellular pieces for the degree 5 component with one real root.

ways, this component is still understudied.

Chapter 11

Future Directions

This short final chapter lists several direction for future investigation.

Remark 11.0.1. The known technique to understand the degree 5 components in a detailed way is to blend the three points of view of Remark 10.2.1 and analyze all the possibilities. This quickly becomes intractable as the degree increases, and new techniques will be required to push this type of work into higher degrees. So one further direction is to identify new techniques to understand each component of these cell complexes explicitly, in the style of the results from Section 10.1.

Remark 11.0.2. Palindromic chains are introduced in this dissertation, and much is still unknown about them. In particular, enumerations for general n is unknown, and no known closed formula exists to count them. Indeed, even the sequences of known values is unreported in the online encyclopedia for integer sequences. The counting techniques introduced in discussing palindromic chains, namely the bijection to properly labeled palindromic hypertrees, gives a possible direction lending itself to completing that counting problem.

In closing, it is worth highlighting an important feature of this (still mysterious)

cell complex that comes from its genesis as the fixed complex of the branched annulus complex under complex conjugation: its potential curvature.

Remark 11.0.3. Real polynomials are fixed point of complex conjugation involution. If you have a finite order 2 group acting on a CAT(0) space and you are looking at the fixed set, that is CAT(0). In particular, the branched annulus complex is conjecturally CAT(0), which is a property that would carry onto the real version. So another future direction is to investigate these curvature properties using tools from geometric group theory.

Appendix A

Appendix

A.1 Code for Reflection Symmetric Noncrossing Partitions

Remark A.1.1. Below are the tools added to CatalanObjects.wl to produce and study Reflection Symmetric Non-crossing Parititons (In Mathematica).

```
FlipGraph::usage = "FlipGraph[cg] flips the configuration.";
FlipGraph[CircularGraph[n_Integer, edges_List]] :=
  CircularGraph[n, Map[n - # + 1 &, edges, {1}]];

XFlipGraph::usage =
  "XFlipGraph[cg] flips the configuration throught the axis defined \
by the first point.";
XFlipGraph[CircularGraph[n_Integer, edges_List]] :=
 CircularGraph[n, Map[1 + Mod[n - # + 1, n] &, edges, {1}]]
```

```
RNonCrossingPartitions[n_Integer] :=
  RNonCrossingPartitions[n] = Select[
     NonCrossingPartitions[n], FlipGraph[#] == # &];

RXNonCrossingPartitions[n_Integer] :=
  RXNonCrossingPartitions[n] = Select[
     NonCrossingPartitions[n], XFlipGraph[#] == # &];

DiagramRNonCrossingPartitions[n_Integer] :=
 For[i = 1, i < n + 1, i++,
  Print[Select[RNonCrossingPartitions[n],
    Length[CircularGraphEdges[#]] == i &]]]

DiagramRXNonCrossingPartitions[n_Integer] :=
 For[i = 1, i < n + 1, i++,
  Print[Select[RXNonCrossingPartitions[n],
    Length[CircularGraphEdges[#]] == i &]]]

RXNCPRelationMatrix[n_Integer] :=
 Table[If[
   Combinatorica`CoarserSetPartitionQ[
    CircularGraphEdges[RXNonCrossingPartitions[n][[i]]],
    CircularGraphEdges[RXNonCrossingPartitions[n][[j]]]], 1, 0], {i,
   Length[RXNonCrossingPartitions[n]]}, {j,
   Length[RXNonCrossingPartitions[n]]}]
```

```
RNCPRelationMatrix[n_Integer] :=
 Table[If[
   Combinatorica`CoarserSetPartitionQ[
    CircularGraphEdges[RNonCrossingPartitions[n][[i]]],
    CircularGraphEdges[RNonCrossingPartitions[n][[j]]]], 1, 0], {i,
   Length[RNonCrossingPartitions[n]]}, {j,
   Length[RNonCrossingPartitions[n]]}]


RankSizeRNCP[n_Integer, k_Integer] :=
 Binomial[Quotient[n - 1, 2], Quotient[k - 1, 2]]*
  Binomial[ Quotient[n, 2], Quotient[k, 2]]


SizeRNCP[n_Integer] := Binomial[n, Quotient[n, 2]]
```

Remark A.1.2. Below is the code to to build the Reflection Symmetric Non-crossing Partition maximal chain enumerating polynomials (In Mathematica).

```
AlgebraicDegree[eqn_, vars_List] :=
 Max[Total[
   GroebnerBasis`DistributedTermsList[eqn /. Equal :> Subtract,
     vars][[1, All, 1]], {2}]]


AlgebraicDegree[eqn_] := AlgebraicDegree[eqn, Variables[eqn]]


Boxtimes[poly1_, poly2_] :=
 Total[Total[
```

```
   Table[ Binomial[
      AlgebraicDegree[MonomialList[poly1][[i]]] +
       AlgebraicDegree[MonomialList[poly2][[j]]],
      AlgebraicDegree[MonomialList[poly1][[i]]]*
     MonomialList[poly1][[i]]*MonomialList[poly2][[j]], {i,
     Length[MonomialList[poly1]]} , {j,
     Length[MonomialList[poly2]]} ]]]


dual[x] = z;
dual[y] = w;
dual[z] = x;
dual[w] = y;
var = {w, x, y, z};
var2 = {w, z}
rules = Table[
   var[[i]] -> dual[var[[i]]], {i,
    4}]; (* this set of rules dualizes the polynomial to switch from \
x<->z and y<->w, for square to diamond*)
rules1var =
  Table[var[[i]] -> x, {i,
    4}]; (* this set of rules makes all variables into 'x'*)
rules2var =
  Table[var2[[i]] -> dual[var2[[i]]], {i,
    2}];(*this set of rules makes w->y and z->x*)
Np[n_Integer] := n^(n - 2) y^(n - 1)
Npz[n_Integer] := n^(n - 2) y^(n - 2)*w
```

```
Psquare[1] = 1;

Pdiamond[1] = 1;

Psquare[2] = x;

Pdiamond[2] = z;

Psquare[3] = x*Boxtimes[Pdiamond[2], Psquare[1]];

Pdiamond[3] = Psquare[3] /. rules;


Psquare[n_] :=
 Expand[Sum[
    x*Boxtimes[Pdiamond[n - (2 i - 1)], Psquare[2 i - 1]], {i,
     Quotient[n, 2]}] +
   Sum[(Quotient[n, 2] - i)*y*Boxtimes[Np[i], Psquare[n - 2 i]], {i,
     Quotient[n, 2]}]]
Pdiamond[n_] := ReplaceAll[Psquare[n], rules]
```

Remark A.1.3. Code to build the poset of Reflection Symmetric Non-Crossing partitions in a more efficient way than sieving all non-crossing partitions (In SageMath).

```
    def ncp(n):
    "generates the noncrossing partition lattice as a poset"
    return posets.SetPartitions(n).subposet([x for x in posets.

    SetPartitions(n)
 if x.is_noncrossing()])

def vis(S):
```

```
    "finds the visible blocks of a noncrossing partition"
    vis=[max(S[0])]
    "The first visible block is always the first"
    for i in srange(1,len(S),1):
        test=[]
        "This test set will be used to determine which ones are visible"
        for j in srange(i):
            if max(S[j])>max(S[i]):
                test.append(1)
                "this means that block isn't visible"
            else:
                test.append(0)
                "this means it is visible"
        if sum(test)==0:
            vis.append(max(S[i]))
        else:
            vis
    return vis


def RNCP(n):
    "generates the data for reflection symmetric noncrossing

    partitions of type 1 as a ncp (n) plus a subset of the visible set"
    RNCP=[]
    for S in ncp(n):
        for y in subsets(vis(S)):
```

```
            RNCP.append((S,y))
    return RNCP


def neg(x):
    "negates a list"
    neg=[]
    for i in srange(0,len(x),1):
        neg.append(-x[i])
    return neg


def new_RNCP(n):
    "generates the reflection symmetric noncrossing partitions

    of size 2n with labels [n] and their negations"
    new_RNCP=[]
    for x in RNCP(n):
        part=[]
        for i in srange(len(x[0])):
            if x[1].count(max(x[0][i]))>0:
                part.append(list(x[0][i])+neg(list(x[0][i])))
            else: part.append(list(x[0][i]));part.append

            (neg(list(x[0][i])))
        new_RNCP.append(SetPartition(part))
    return new_RNCP
```

```
def refinement(A, B):
    "define the cover relation of refinement"
    #if len(A) != len(B)+1:
      #return False
    for a in A:
        if not any(set(a).issubset(b) for b in B):
            return False
    return True
```

A.2 Code for Palindromic Noncrossing Chains

Remark A.2.1. The below code was used for preliminary investigations into what became the study of palindromic chains of non-crossing partitions (In SageMath).

```
        def even_partition(partition):
    """
    Takes a set partition and returns a new partition where every element
    is replaced by twice that element.
    """
    return SetPartition([[2*x for x in block] for block in partition])


def odd_partition(partition):
    """
    Takes a set partition and returns a new partition where every element
    is replaced by twice that element minus 1.
    """
```

```
    return SetPartition([[2*x-1 for x in block] for block in partition])


def flip1(n):
    return Permutation(srange(n, 0, -1))
def flip2(n):
    return Permutation([1]+srange(n,1,-1))


def add_partitions(partition1, partition2):
    """
    Takes two set partitions and returns their union.
    """
    P1_list = list(partition1)
    P2_list = list(partition2)
    P_union_list = P1_list+P2_list
    return SetPartition(P_union_list)


def good_ncp(n): #this returns the set of noncrossing partitions


that if you superimpose with the flip its still noncrossing.
    good_ncp=[]
    for x in ncp(n):
            if add_partitions(even_partition(x.apply_permutation


            (flip1(n))),odd_partition(x)).is_noncrossing():
                good_ncp.append(x)
    return good_ncp
```

Bibliography

[1] M Aigner, *Combinatorial theory.— springer verlag, 1979, chap*, III et (1979), 201.

[2] Vladimir I Arnol'd, *The calculus of snakes and the combinatorics of bernoulli, euler and springer numbers of coxeter groups*, Russian Mathematical Surveys **47** (1992), no. 1, 1.

[3] David Bessis, *The dual braid monoid*, Annales scientifiques de l'Ecole normale supérieure, vol. 36, 2003, pp. 647–683.

[4] Joan Birman, Ki Hyoung Ko, and Sang Jin Lee, *A new approach to the word and conjugacy problems in the braid groups*, Advances in Mathematics **139** (1998), no. 2, 322–353.

[5] Andreas Blass and Bruce E Sagan, *Möbius functions of lattices*, advances in mathematics **127** (1997), no. 1, 94–123.

[6] Thomas Brady, *A partial order on the symmetric group and new $K(\pi, 1)$'s for the braid groups*, Adv. Math. **161** (2001), no. 1, 20–40. MR 1857934

[7] Tom Brady and Jon McCammond, *Braids, posets and orthoschemes*, Algebraic & Geometric Topology **10** (2010), no. 4, 2277–2314.

[8] David Callan and Len Smiley, *Noncrossing partitions under rotation and reflection*, arXiv preprint math/0510447 (2005), 1.

[9] Ziqian Ding, *Dihedral symmetries of non-crossing partition lattices*, University of Miami, 2016.

[10] Michael Dougherty and Jon McCammond, *Critical points, critical values, and a determinant identity for complex polynomials*, Proceedings of the American Mathematical Society **148** (2020), no. 12, 5277–5289.

[11] _____, *Geometric combinatorics of polynomials I: The case of a single polynomial*, Journal of Algebra **607** (2022), 106–138.

[12] _____, *Geometric combinatorics of polynomials II*, preprint 2024.

[13] Michael Joseph Dougherty, *The geometry and topology of the dual braid complex*, University of California, Santa Barbara, 2018.

[14] David BA Epstein, *Word processing in groups*, AK Peters/CRC Press, 1992.

[15] Edward Fadell and Lee Neuwirth, *Configuration spaces*, Math. Scand. **10** (1962), 111–118. MR 141126

[16] Thomas Haettel, Dawid Kielak, and Petra Schwer, *The 6-strand braid group is* CAT(0), Geom. Dedicata **182** (2016), 263–286. MR 3500387

[17] Allen Hatcher, *Algebraic topology*, Cambridge University Press, Cambridge, 2002. MR 1867354

[18] Seong Gu Jeong, *The seven-strand braid group is* CAT(0), Manuscripta Math. **171** (2023), no. 3-4, 563–581. MR 4597707

[19] Alan G. Konheim and Benjamin Weiss, *An occupancy discipline and applications*, SIAM Journal on Applied Mathematics **14** (1966), no. 6, 1266–1274.

[20] Germain Kreweras, *Sur les partitions non croisées d'un cycle*, Discrete mathematics **1** (1972), no. 4, 333–350.

[21] Jon McCammond, *The mysterious geometry of artin groups*, Winter Braids Lecture Notes **4** (2017), 1–30.

[22] ———, *Noncrossing hypertrees*, arXiv preprint arXiv:1707.06634 (2017).

[23] Luis Paris, $k(\pi, 1)$ *conjecture for artin groups*, Annales de la Faculté des sciences de Toulouse: Mathématiques, vol. 23, 2014, pp. 361–415.

[24] V. Reiner, *Noncrossing partitions for classical reflection groups*, Discrete Mathematics (1997), 1–10.

[25] Mario Salvetti, *The homotopy type of Artin groups*, Math. Res. Lett. **1** (1994), no. 5, 565–577. MR 1295551

[26] Rodica Simion and Daniel Ullman, *On the structure of the lattice of noncrossing partitions*, Discrete mathematics **98** (1991), no. 3, 193–206.

[27] Richard P. Stanley, *Catalan numbers*, Cambridge University Press, New York, 2015. MR 3467982